Molecular imprinting of polypyrrole for electrochemical sensing of clofibric acid

Dissertation

zur Erlangung des akademischen Grades eines
Doktors der Naturwissenschaften
– Dr. rer. nat. –

vorgelegt von

Bianca Schweiger

geboren in Preetz

Fakultät für Chemie
der
Universität Duisburg-Essen

2015

Die vorliegende Arbeit wurde im Zeitraum von Oktober 2010 bis April 2015 bei der KIST Europe Forschungsgesellschaft mbH in Saarbrücken und im Arbeitskreis von Prof. Dr. Mathias Ulbricht, Lehrstuhl für Technische Chemie II, an der Universität Duisburg-Essen durchgeführt.

Tag der Disputation: 19.01.2016

Gutachter:	Prof. Dr. Mathias Ulbricht
	Prof. Dr. Torsten C. Schmidt
Vorsitzende:	Prof. Dr. Elke Sumfleth

Content

Abstract

Molecularly imprinted polymers (MIPs) are artificial biomimetic receptors with applications in separation ranging from small molecules to whole cells. The combination of the MIP principle with conducting polymers allows the fabrication of specific and selective layers for sensing purposes. Not only the robustness of MIPs against environmental conditions and their low cost compared with natural receptors are advantages of MIPs, but also the possibility to prepare them for compounds which have no natural receptors.

In this work, piezoelectric quartz crystals and analogous gold substrates were electrochemically coated with molecularly imprinted conducting polypyrrole films for pulsed amperometric detection (PAD) of clofibric acid, a metabolite of the blood lipid regulator clofibrate. Usually clofibric acid is detected by using reversed-phase HPLC with spectrophotometric detection. This requires large instrumentation, ultrapure solvents, and suitable sample preparation. An electrochemical sensing method would be advantageous due to the simple setup and low cost, and the use of organic solvents for the detection could be avoided.

The films were prepared by cyclic voltammetry of an aqueous solution containing pyrrole as monomer, clofibric acid or, for feasibility studies, caffeine as template, and potassium chloride, potassium nitrate, or phosphate buffer solution as conducting salt. Non-imprinted polymers (NIPs) were prepared without template under the same conditions. The electrodeposition was monitored by a quartz crystal microbalance combined with an electrochemical cell. The deposition was influenced by the number of cycles and the applied potential, by the monomer concentration and the type of conducting salt, and also by the presence of the template. Cyclic voltammetry data obtained during polymerization and deposited weight estimations revealed a decrease of the polymerization rate with increasing clofibric acid concentration. Template entrapment and template removal were studied with X-ray photoelectron spectroscopy. The results indicated that clofibric acid could be removed after imprinting with an aqueous ethanol solution. Binding of caffeine and clofibric acid was studied with PAD. The results showed that optimizations of the washing procedure were needed. Washing procedures under stirring with frequent solvent change were tested with methanol, ethanol, and variation of the washing time, and were compared with washing by PAD measurements. In binding experiments, the highest sensor response to clofibric acid was obtained with sensors treated by PAD washing although the sensor response decreased gradually with repeated

washing/measurement cycles. MIP and NIP surfaces were studied with atomic force microscopy (AFM), ellipsometry, contact angle measurements, and zeta potential measurements. AFM measurements revealed smooth surfaces with roughnesses of 6–8 nm for imprinted and non-imprinted layers. Differences between MIP and NIP layers were revealed by contact angle and zeta potential measurements. The results showed that contact angles were higher for MIPs than for NIPs and that the isoelectric point was lower for MIPs than for NIPs.

Binding experiments with clofibric acid and other substances showed a pronounced selectivity of the MIP for clofibric acid *vs.* carbamazepine, but the response of MIP and NIP to the structurally related molecule 2,4-dichlorophenoxyacetic acid was higher than the response to clofibric acid. The smooth surface might be a reason for an excessively low density of specific binding sites for clofibric acid.

Additionally to cyclic voltammetry, the application of potential pulses during polymerization was tested. Compared with cyclic voltammetry, the use of potential pulses resulted in more adherent films, which allowed testing the application of a negative potential as washing method.

To introduce functional groups into the polymer, which could build more non-covalent bonds with the template during polymerization, pyrrole propionic acid and 2-(1H-pyrrole-1-yl)ethanamine were tested as monomers. Successful polymerization was obtained by copolymerization with pyrrole.

The feasibility of sensor fabrication with a combination of molecular imprinting and electrochemical deposition of polypyrrole for the detection of clofibric acid could be demonstrated, but the specificity (response for MIP *vs.* NIP) and selectivity were strongly dependent on preparation and washing conditions.

Zusammenfassung

Molekular geprägte Polymere (molecularly imprinted polymers, MIPs) sind künstliche biomimetische Rezeptoren, die zu Trennungszwecken für verschiedene Substanzen, von kleinen Molekülen bis hin zu ganzen Zellen, entwickelt werden können. Die Kombination des MIP-Prinzips mit leitfähigen Polymeren erlaubt die Entwicklung spezifischer und selektiver Schichten zu Messzwecken. Nicht nur die Widerstandsfähigkeit der MIPs gegen Umwelteinflüsse und ihre niedrigen Herstellungskosten im Vergleich zu natürlichen Rezeptoren gehören zu ihren Vorteilen, sondern auch die Möglichkeit, MIPs für Substanzen herzustellen, für die es keine natürlichen Rezeptoren gibt.

In dieser Arbeit wurden goldbeschichtete piezoelektrische Quarzkristalle und Glassubstrate elektrochemisch mit molekular geprägten leitfähigen Polypyrrolfilmen für die amperometrische Detektion von Clofibrinsäure, einem Metaboliten des Blutfettsenkers Clofibrat, beschichtet. Gewöhnlich wird Clofibrinsäure spektrophotometrisch mittels reversed-phase HPLC detektiert. Dies erfordert aufwändige Instrumentierung, hochreine Lösungsmittel und eine geeignete Probenvorbereitung. Der Vorteil einer elektrochemischen Methode wäre der mit niedrigen Kosten verbundene einfache Aufbau der Messanordnung und die Möglichkeit, den Einsatz organischer Lösungsmittel vermeiden zu können.

Die Filme wurden mittels Zyklovoltammetrie in wässriger Lösung bestehend aus Pyrrol als Monomer, Clofibrinsäure oder, für erste Machbarkeitsstudien, Koffein als Templat und Kaliumchlorid, Kaliumnitrat oder Phosphatpufferlösung als Leitsalz hergestellt. Nicht-geprägte Polymere (non-imprinted polymers, NIPs) wurden ohne Templatzusatz unter ansonsten gleichen Bedingungen hergestellt. Die elektrochemische Beschichtung der Sensoroberfläche wurde durch die Kombination der elektrochemischen Zelle mit einer Quarzkristallmikrowaage beobachtet. Die Abscheidung des Polymers wurde durch die Anzahl der Zyklen und das verwendete Potential, die Konzentration des Monomers und der Art des Leitsalzes sowie durch das Templat beeinflusst. Zyklovoltammetrische Messwerte, die während der Polymerisation erhalten wurden, und Abschätzungen der Polymermasse zeigten, dass mit steigender Konzentration an Clofibrinsäure die Polymerisationsrate sinkt. Der Einschluss und die Entfernung der Templatmoleküle wurden mit Röntgenphotonenspektroskopie untersucht. Die Ergebnisse deuteten darauf hin, dass Clofibrinsäure mit ethanolischer Lösung aus dem Polymer entfernt werden konnte. Bindungsversuche mit Koffein und Clofibrinsäure wurden mit gepulster

amperometrischer Detektion (pulsed amperometric detection, PAD) durchgeführt. Die Ergebnisse zeigten, dass das Vorgehen zur Templatentfernung optimiert werden sollte. Waschmethoden unter Rühren mit regelmäßigem Wechsel des Lösungsmittels wurden mit Methanol, Ethanol und Veränderung der Waschzeit getestet und mit Waschen durch PAD verglichen. Die höchste Sensorantwort auf Clofibrinsäure in Bindungsversuchen wurde mit Sensoren, die mittels PAD gewaschen worden waren, erreicht, doch die Sensorantwort nahm mit zunehmender Zahl an Wasch- und Bindungsversuchen ab.

Die Oberflächen der MIPs und NIPs wurden mit Rasterkraftmikroskopie (atomic force microscopy, AFM), Ellipsometrie, Kontaktwinkelmessungen und Zeta-Potentialmessungen untersucht. AMF-Messungen ergaben mit 6–8 nm eine geringe Rauigkeit der Oberflächen von MIPs und NIPs. Unterschiede zwischen MIPs und NIPs zeigten sich bei Kontaktwinkel- und Zeta-Potentialmessungen. Für MIPs wurden höhere Kontaktwinkel als für NIPs festgestellt. Weiterhin lag der isoelektrische Punkt von MIPs niedriger als der von NIPs.

Bindungsversuche mit Clofibrinsäure und anderen Substanzen zeigten eine höhere Selektivität der MIPs für Clofibrinsäure im Vergleich zu Carbamazepin, aber die Sensorantwort von MIPs und NIPs auf das strukturell ähnliche Molekül 2,4-Dichlorphenoxyessigsäure war höher als die Sensorantwort auf Clofibrinsäure.

Zusätzlich zur Zyklovoltammetrie wurde die Verwendung von Potentialpulsen als Polymerisationsmethode getestet. Im Vergleich zur Zyklovoltammetrie ergab die Verwendung von Potentialpulsen Filme, die stärker an der Goldoberfläche der Sensoren hafteten, was die Verwendung eines negativen Potentials als Waschmethode zur Entfernung des Templats erlaubte.

Zur Einführung funktioneller Gruppen in das Polymer, welche die Anzahl nicht-kovalenter Bindungen zwischen Templat und Polymer erhöhen könnten, wurden Pyrrolpropionsäure und 2-(1H-Pyrrol-1-yl)ethanamin als Monomere getestet. Eine Polymerisation wurde durch Copolymerisation mit Pyrrol erreicht.

Die Machbarkeit der Sensorherstellung mit einer Kombination aus molekularer Prägung und elektrochemischer Polymerisation von Polypyrrol zur Detektion von Clofibrinsäure konnte gezeigt werden, aber Spezifität und Selektivität hingen stark von den Herstellungs- und Waschbedingungen ab.

1 Introduction

Molecularly imprinted polymers are materials developed for the selective adsorption of molecules. The aim to adsorb specific molecules can be the removal of such substances from the surrounding media, the enrichment of specific substances followed later by desorption, or the detection of specific substances. These processes are beneficial for analytical applications and can be applied for instance in water treatment, for the evaluation of water quality and the occurrence of environmentally relevant substances, or in the pharmaceutical industry for quality control and health care applications. The combination of imprinted materials with electrochemical detection could meet the requirement for a simple experimental setup with low cost.

2 Theoretical background

2.1 Molecular imprinting

In nature, enzymes and receptors use molecular recognition for reactions with substrate molecules and ligand binding. As these recognition processes are highly specific and selective, researchers are interested in developing artificial biomimetic receptors. A promising area in this regard is molecular imprinting, where cross-linked synthetic polymers with specific binding sites are prepared in the presence of template molecules. Monomer and template molecules having complementary functional groups interact with each other through the formation of covalent or non-covalent bonds in the solvent, which acts as a porogen. After polymerization, the template is removed via washing steps leaving cavities that own the complementary geometrical and functional properties of the template. Template or similar molecules can bind again in these cavities (Fig. 1) [1].

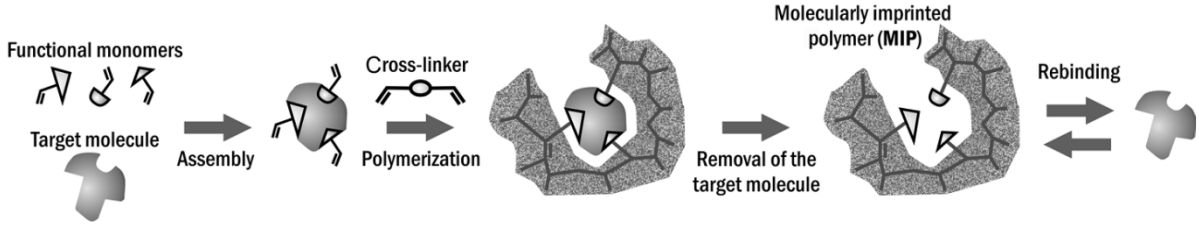

Fig. 1: Schematic representation of non-covalent molecular imprinting [2].

In 1894, Emil Fischer explained his observations of the selective reactions of yeast enzymes with glucosides with the “lock-and-key concept” depending on the molecular geometry [3]. In the 1930s, Linus Pauling proposed that antibodies and antigens have complementary shapes, where the attraction of the molecules is increased by the

complementary location of groups with electrical charges and hydrogen-bond forming groups [4]. A template effect of aromatic hydrocarbons on silica gel was discovered by Poljakov in 1931 [5]. Further research in the following years concentrated on the imprinting of silica gels with organic molecules and the resulting adsorption properties [5]. In the 1970s, vinylphenylic organic monomers were used by Wulff to create “enzyme-analogue built polymers”, where the template (e.g., D-mannitol) was bound covalently to the polymer [6]. A non-covalent approach was introduced 1981 by Mosbach, who polymerized acrylic based monomers with dyes as template molecules [7]. Compared to silica gels, the use of organic monomers provided a larger range of functional groups and resulted in polymers with more stable cavities [8].

2.1.1 Covalent and non-covalent approach

In the covalent approach, a polymerizable derivative of the desired species is used as template, which is integrated into the polymer by covalent bonds during polymerization. To remove the template, the bonds are cleaved, e.g., by acid hydrolysis [9]. This approach produces well defined and stable cavities, but the choice of functional monomers which can be linked to the template, e.g., by carboxylic or boronic esters, ketal bonds, or imine bonds, is limited [10].

In the non-covalent approach, interactions between functional groups of monomer and template molecules such as ionic interactions, hydrogen bonds, π-π-interactions, and hydrophobic interactions are utilized by simply mixing the template with the functional monomers. Subsequent crosslinking polymerization stabilizes the template-monomer complex. This approach is more versatile than the covalent approach because a wider range of monomers can be used and different monomers can be used at the same time, so that several interactions between template and monomer are possible. Popular monomers for the non-covalent approach are acrylates (acidic), acrylamides (neutral), vinylpyridine (basic), styrenes (hydrophobic), and imidazoles, which are polymerized in the presence of crosslinkers such as ethylene glycol dimethacrylate and p-divinyl benzene [1] (Fig. 2).

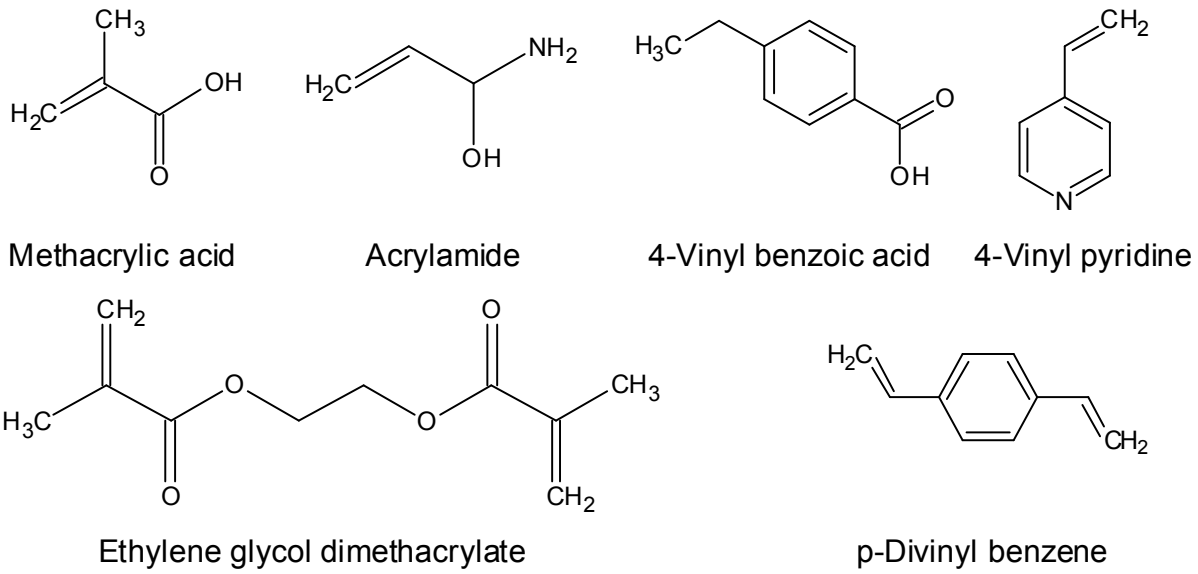

Fig. 2: Examples of monomers and crosslinkers.

The template molecules are extracted by washing with appropriate solvents, e.g., Soxhlet extraction with organic solvents, aqueous organic solvents, or acidic or basic aqueous solvents. For example, this is suitable for polymers synthesized from acidic monomers, where carboxyl groups in acidic monomers act as hydrogen donor and acceptor at the same time [11]. About 1–10% of the template molecules remain in the polymer in highly crosslinked areas [1]. Where template bleeding is critical, the use of a structural related molecule as template should be considered [12].

A third approach, which combines covalent and non-covalent approach, was investigated by Whitcombe, where cholesterol was covalently bound during polymerization. After template removal, cholesterol could bind again non-covalently via a hydrogen bond to a hydroxyl group [13].

The kind and size of covalent interactions between monomer and template molecules is influenced by the solvent. Commonly, MIPs are prepared in aprotic organic solvents because hydrogen bonds and electrostatic interactions would be disturbed by water molecules [13]. The solvent also acts as a porogen, which increases the porosity and surface area. Examples for imprinting in mixtures of water and organic solvent include 2,4-dichlorophenoxyacetic acid [14] and 1-naphthalene sulfonic acid [15], where ionic and π-π-interactions were strong enough to develop in polar solvents.

2.1.2 Bulk synthesis and other physical forms of MIPs

MIPs are often synthesized as bulk polymers, which are grinded and sieved after polymerization to small particles in the micrometer range to make the imprinted sites accessible. Drawbacks of this method are the inhomogeneous shapes and the broad

size range of the particles and that binding sites might be destroyed by the also time-consuming grinding. For applications with stationary phases such as liquid chromatography and solid phase extraction, where an evenly distributed flow is needed, spherical beads with narrow size distribution are preferable [16]. This can be done by covering preformed silica particles with MIPs [17], by two-step swelling procedures on polystyrene particles [18], or by suspension polymerization [19].
Monoliths are also used for separation applications due to their higher permeability compared with packed particles and can be prepared by in situ polymerization [20,21], by grafting of MIPs on monolithic matrices [22,23], or by non-hydrolytic sol-gel processes [24]. Other forms of MIPs include membranes [25] for adsorption [26] or perm-selective separation [27], thin layers for sensor applications, nanoparticles, and gels. Thin films can be prepared by various methods, e.g., by spin coating, evaporation of solvent, surface grafting, soft lithography, and electropolymerization [28]. Compared with bulk polymers, the template removal should be more efficient, and the binding should be faster, while the amount of binding sites might be lower depending on the surface area.

2.1.3 Applications

Besides as separation material and recognition elements for sensors, MIP materials are used for enzymatic catalysis, e.g., for mimicking the active center of the digestive enzyme chymotrypsin [29,30], stereoselective reactions, and drug release vehicles [10].
The replacement of natural receptors with MIPs could be advantageous for sensing purposes because natural receptors are sensitive to environmental conditions (temperature, pressure, and pH). Acrylic MIPs imprinted with theophylline were found to be stable up to 150 °C, to be stable in acidic and basic solution, as well as in organic solvents, and they could be autoclaved without loss of affinity properties. Samples stored for 8 years at ambient temperatures did not lose their binding affinities [31]. Also MIPs can be used for substances which have no natural receptor. Small organic molecules such as pharmaceuticals, pesticides, dyes, amino acids, steroids and sugars, as well as larger organic compounds such as proteins, enzymes, viruses, and even cells are examples for templates used for molecular imprinting [1,10].
Solid phase extraction cartridges with MIP material are commercially available from Biotage (AFFINILUTE, SupelMIP) and AFFINISEP (AFFINIMIP) for extraction of

pharmaceuticals (non-steroidal anti-inflammatory drugs, pesticides, herbicides) from waste water, for food safety tests (e.g., nitroimidazoles, fluoroquinolones, chloramphenicol, mycotoxins), and for health related examinations (tobacco-specific nitrosamines, bisphenol A, β-agonists, amphetamines) [32–34].

2.2 Conducting polymers

First reports about the electrochemical synthesis of organic polymers date back to 1862 when Letheby synthesized polyaniline on a platinum electrode [35]. Polymers of pyrrole, thiophene and other heterocycles were synthesized in the 19th and early 20th century, but their characterization was limited and their properties were poorly understood [36]. Significant progress was made in the 1970s by Heeger, MacDiarmid, and Shirawaka when the intrinsic conductivity of polyacetylene was increased seven orders of magnitude to 38 S cm^{-1} by doping with iodine [37]. The insolubility of polyacetylene and its instability in ambient air limited the applicability, so that soon research concentrated on other monomers such as pyrrole, thiophene, aniline, and their derivatives (Fig. 3). Nowadays, applications of conducting polymers include supercapacitors, light emitting diodes, solar cells, field effect transistors, rechargeable batteries, textile coatings, corrosion resisting coatings, antistatic coatings, and usage as transducers in chemical sensors and biosensors [38–41]. Also the use of conducting polymers as biocompatible and biodegradable materials for cell and tissue cultures, neural implants, and drug delivery devices is investigated [42].

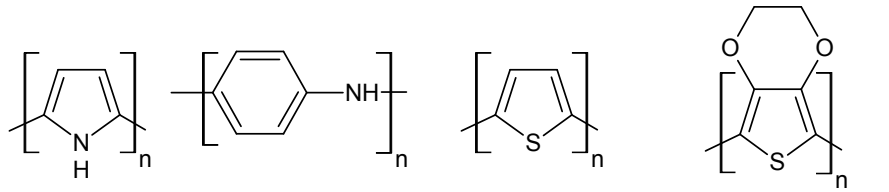

Fig. 3: Examples of conducting polymers.

In electronically conducting polymers, the polymer backbone is conducting in its charged state through conjugated double bonds, e.g., in conjugated polymers such as polyacetylene, aromatic polymers such as poly(p-phenylene) and polyanilin, and in heterocyclic polymers such as polypyrrole and polythiophene. The conductivity can change 10–12 orders of magnitude from the uncharged state to 1–1000 S cm^{-1} (Fig. 4) [43]. Table 1 lists conductivity values for some of the conducting polymers.

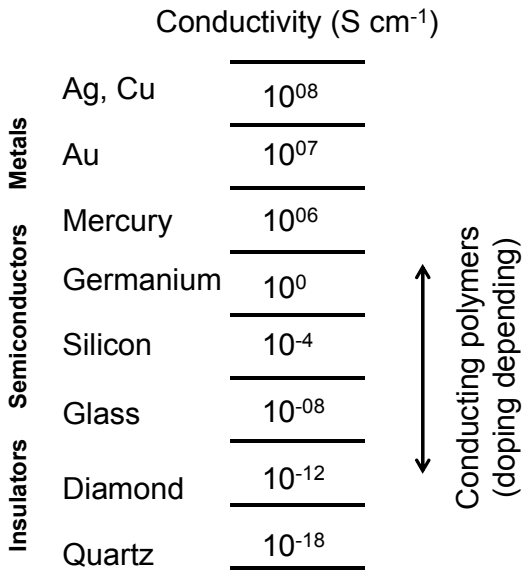

Fig. 4: Conductivity values of different materials (modified from [43]).

Table 1: Conductivity values of conductive polymers [44]

Polymer	Conductivity (S cm^{-1})
Polyaniline	30–200
Polyacetylene	10^3–1.7×10^5
Poly(p-phenylene)	10^2–10^3
Poly(p-phenylenevinylene)	3–5×10^3
Polypyrrole	10^2–7.5×10^3
Polythiophene	10–10^3

Charging is achieved by doping, which means in the case of conducting polymers a partial oxidation (p-doping) or reduction (n-doping) in an electrochemical cell or by redox reagents. To preserve electroneutrality, counterions from the solution diffuse into the polymer [43,45]. The mechanism of charge transport in the polymer can be explained by the formation of polarons (radical cation) at low oxidation levels and bipolarons (dication) at high oxidation levels. Additionally, electron-hopping can occur between polymer chains [43]. In band theory, conductivity of metals arises from an overlapping of valence and conduction band. Semi-conductors are characterized by a small gap between valence and conduction band. By input of energy, electrons can be excited into the conduction band. In insulators, the band gap is so large that thermal energy is not enough to excite electrons into the conduction band. For conducting polymers, polaron and bipolaron levels are generated in the band gap by doping. Polarons in organic polymers are localized charges which have a

lattice distortion around them because the geometry relaxation is energetically favorable. The removal of a second electron leads to the formation of a bipolaron when the energy gained by the lattice distortion is bigger than the Coulomb repulsion [46].

The monomers can be polymerized chemically by oxidants such as $FeCl_3$ [47] or electrochemically by galvanostatic, potentiostatic, or potentiodynamic methods [45]. The polymerization can be done in organic solvents or aqueous solutions at room temperature, which would be advantageous for the imprinting of biomolecules because denaturation and conformational changes could be avoided [48]. Besides pyrrole, only few other monomers with oxidation potentials lower than the oxidation potential of water can be polymerized in aqueous solution, e.g., aniline and ethylenedioxythiophene [45,49]. Electrodes of every form and shape can be used and the thickness of the polymer can be controlled by the polymerization parameters.

By copolymerization with monomeric derivates it is possible to incorporate into the polymer functional groups, which could increase the non-covalent binding between polymer and template. For example, carboxylic acid groups in a thiophene polymer (poly(3,4-ethylenedioxythiophene-co-thiophene-acetic acid) build hydrogen bonds with nitrogen atoms and amino groups of atrazin as template molecule [50].

2.2.1 Polypyrrole

Polypyrrole belongs to the first routinely electrochemically synthesized polymers [51]. It can be polymerized by anodic oxidation on the working electrode. During the initial step, pyrrole monomers are oxidized to radical cations, which couple subsequently to dimer cations (Fig. 5). Proton elimination leads to neutral dimers. Early research proposed a propagation mechanism, where oxidized dimers couple with monomeric radical cations to build oligomers, which themselves couple with radical cations. Later research proposes that coupling of monomeric radical cations with each other is dominating due to high rate constants [45]. Oxidized dimers couple then again with each other leading to tetramers and then to octamers. Additional coupling reactions resulting in trimers or hexamers, may occur with increasing monomer concentration [45].

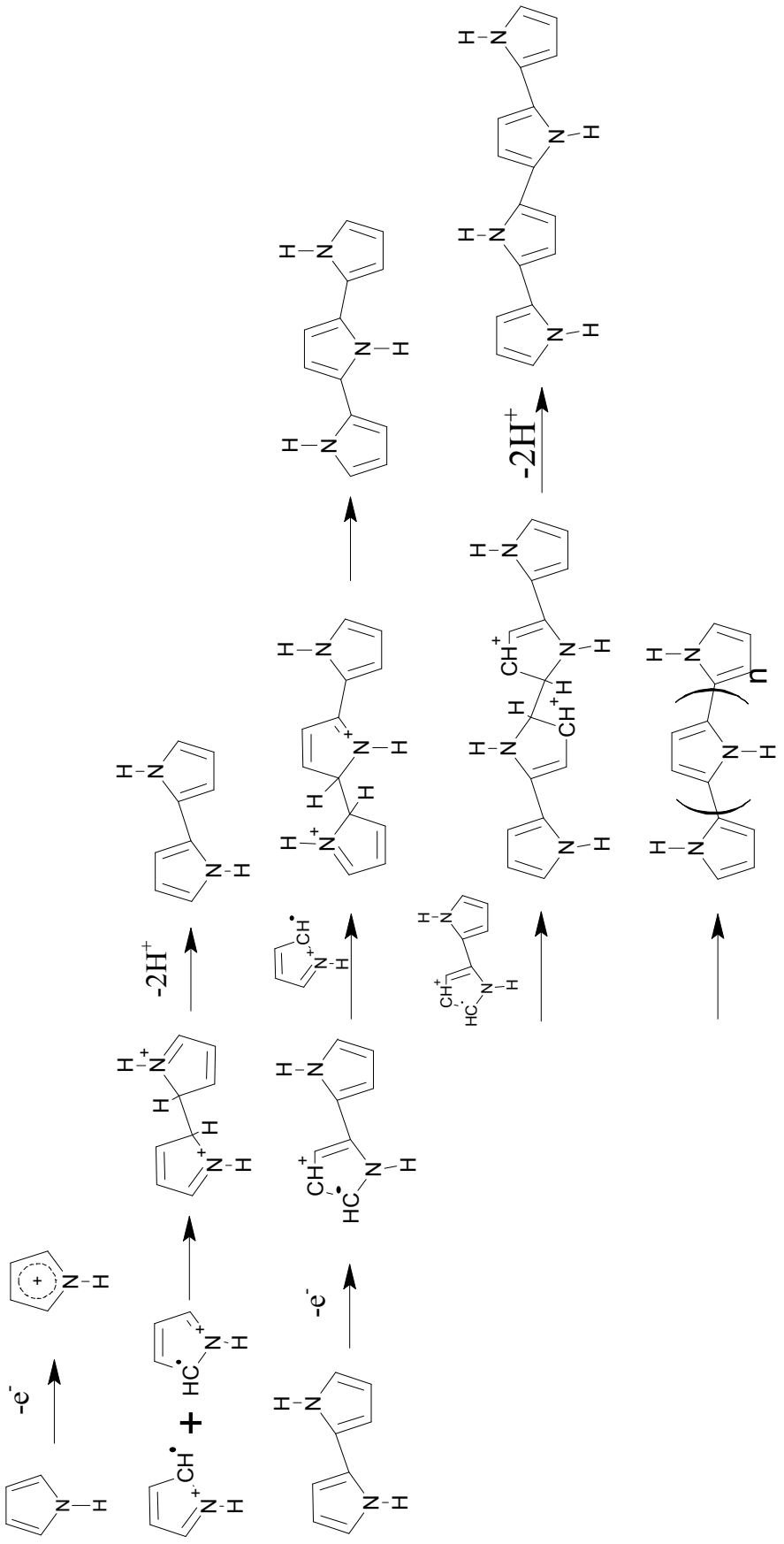

Fig. 5: Polymerization scheme of pyrrole (modified from [45]).

In ground state, the aromatic structure of polypyrrole has the lowest energy (Fig. 6). When polarons and bipolarons are formed during doping, the geometry changes around the lattice distortions to the quinoid structure, which has a higher energy than the aromatic structure, but a lower ionization energy and a larger electron affinity [46] (Fig. 6b-d).

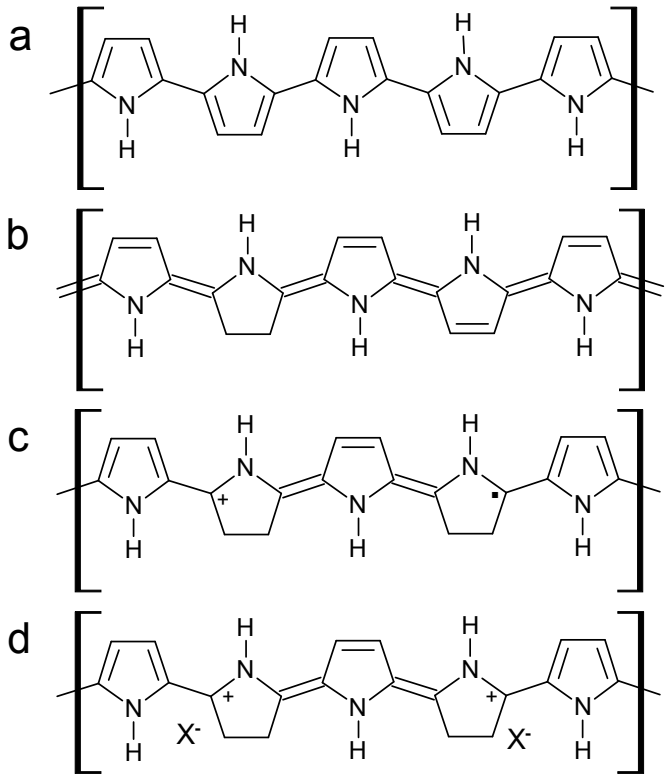

Fig. 6: Polypyrrole structures. (a) aromatic; (b) quinoid; (c) polaron structure; (d) bipolaron structure [52].

2.2.2 Parameters influencing polymerization

The polymerization process of pyrrole and the resulting properties of the polymer are influenced by several parameters: monomer concentration and purity, concentration and choice of the electrolyte, type of solvent, electrochemical parameters (chosen method and potential or current values), temperature, pH, and other factors such as cell geometry, surface treatment, *etc.* [53].

Galvanostatic and potentiostatic methods result often in nonadhesive films with low homogeneity. Scanning electron microscopy (SEM) pictures of polypyrrole films grown potentiostatically in acetonitrile showed dendritic, inhomogeneous structures [54]. A smoother surface was obtained by a potential step method in acetonitrile, which was investigated with atomic force microscopy (AFM) [55]. In contrast, films obtained by cyclic voltammetry, a potentiodynamic method, were adhesive, smooth, and homogeneous [54]. It was assumed that potentiodynamic methods provide more

nucleation sites for homogeneous growth, which also might promote the displacement of solvent molecules from the substrate surface [56].

Counterions or dopants can range in size from chlorine anions to polystyrene sulfonate and influence the structure and porosity. Examples for counterions used for polymerization of pyrrole in aqueous solution include chloride, sulfate, perchlorate, and dodecylsulfate [57], p-toluenesulfonate (pTS) [58], hyaluronic acid (HA), dextran sulfate, chondroitin sulfate A (CS), and poly(2-methoxyaniline-5-sulfonic acid) (PMAS) [59], naphthalene disulfonate, tetrafluoroborate [60], dodecylbenzene-sulfonate (DBS), and 10-camphorsulfonate [61]. Polypyrrole films doped with pTS were more stable after 55 days than films doped with perchlorate, tetrafluorborate, or nitrate [62]. At elevated temperatures up to 150 °C, polypyrroles doped with pTS and p-chlorobenzene maintained their conductivity and remained more stable than polypyrrole doped with dodecyl sulphate [63]. Kuwabata *et al.* reported a decreasing conductivity with increasing pK_a of carboxylic acids used as dopants for pK_a values between 0.3 (trifluoroacetic acid, [64]) and 4.75 (acetic acid). Limited growth was obtained for a pK_a >3.40. It was assumed that the affinity of the carboxylate anions to the positive charges of the polymer increased with the pK_a values of the conjugated acid [65].

The temperature during polymerization also influences the properties of the polymer. Higher conductivities are often obtained with lower synthesis temperatures. A polypyrrole film made from aqueous solution with pTS showed a conductivity of 500 S cm^{-1} with a synthesis temperature of 10 °C. Lower and higher temperatures lowered the conductivity, which was explained by shorter chain lengths due to the activation energy needed for each polymerization step at lower temperatures, and side reactions and the formation of defects at higher temperatures [66]. Maddison *et al.* reported a optimal synthesis temperature of 20 °C for highest conductivity of polypyrrole films (60 S cm^{-1}) made from aqueous solution with pTS [67]. A polypyrrole film with a conductivity of 1360 S cm^{-1} was obtained in propylene carbonate with a synthesis temperature of -30 °C. The potential during the potentiostatic growth was also varied, which showed that a lower potential resulted in lower chain lengths, but also in higher conductivity, presumably due to an increased local ordering of oligomers [68].

Solvents used for polymerization should have a high polarity to reduce Coulombic repulsion of cations during coupling reactions and a low nucleophilicity. A common solvent for polymerization of pyrrole is acetonitrile, although the addition of

water (1%) is necessary for successful polymerization. Polymers prepared in aqueous solutions have a lower conductivity and a more porous structure than those prepared in organic solvents due to the nucleophilic attack of water molecules on the intermediate cations [45].

Fig. 7 shows SEM images of polypyrrole films containing different dopants [69]. The polymer films were prepared in aqueous solution with $LiClO_4$ by cyclic voltammetry. The morphology of the films changed with the used dopants. In the presence of borate ions large aggregates were formed, while in the presence of bigger tosylate ions the surface was much smoother with small globules. With nitrate ions, tangled rods were observed. Galvanostatically grown polypyrrole (Ppy) films containing different dopants also showed various morphologies with nodules of submicron to 20 μm sizes (Fig. 8) [70]. The molecular weight of the dopants ranged from ~200 Da to 10 MDa. The polymers containing pTS, DBS, and poly(4-styrenesulfonate) (PSS), prepared with a current density of 2 mA cm^{-2}, had a rougher surface than the polymers containing PMAS, HA, and CS, prepared with a current density of 0.25 mA cm^{-2}, indicating also the influence of the electrochemical conditions.

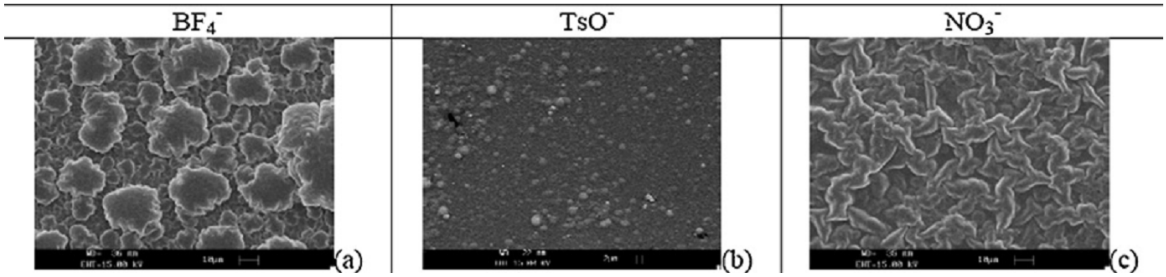

Fig. 7: Influence of the counter-ions on the surface morphology of polypyrrole films obtained from (a–c) SEM (magnification: 500×) [69].

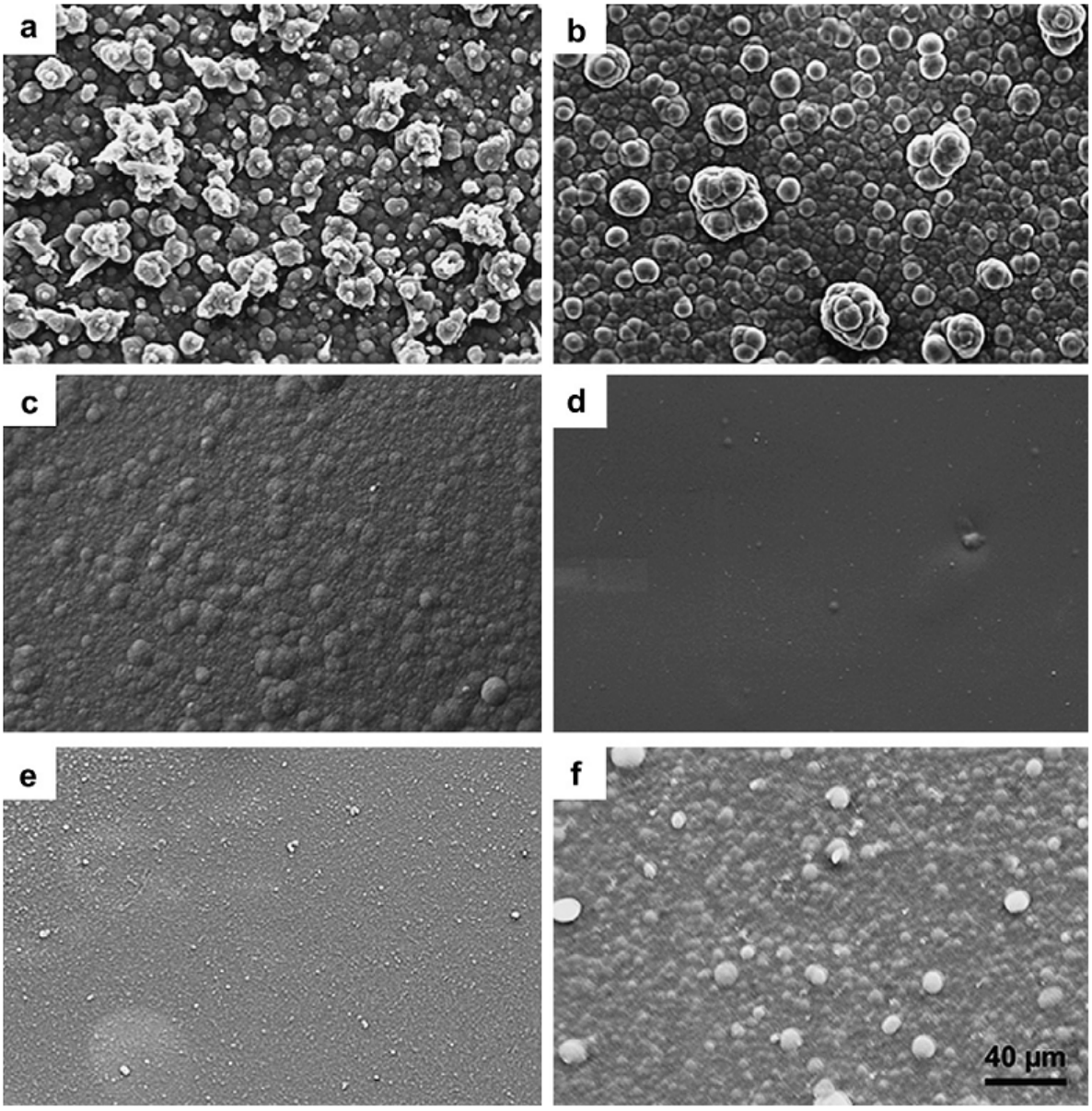

Fig. 8: SEM images of polypyrrole synthesized with different dopants. (a) PPy/pTS; (b) PPy/DBS; (c) PPy/PSS; (d) PPy/PMAS; (e) PPy/HA; (f) PPy/CS [70].

2.2.3 Imprinted polypyrrole

The first examples for the combination of imprinted polymers with electropolymerized polypyrrole were described in 1996 by Spurlock *et al.* [71], where adenosine, inosine, and adenosine 5-triphosphate were used as templates. The analyte signal was obtained with cyclic voltammetry. Template molecules were removed after polymerization by overoxidation of the polymer. By applying a certain potential the positive charge of the backbone is removed and oxygen containing groups such as carbonyl and carboxyl groups are introduced into the polymer.

This leads to release of the anionic template and loss of conductivity [72,73]. Several other examples of imprinted polypyrrole show the applicability of a washing procedure without overoxidation for template removal [72].

Examples of templates used for polypyrrole imprinting include caffeine [74–76], glutamic acid [77], sodium taurocholate [78], L-aspartic acid [79], adenosine, inosine and adenosine triphosphate [71], deoxynivalenol [80], dopamine [81,82], quercetin [83], clopidol [84], gliclazide [85], sulfanilamide [86], and sulfadimethoxine [87].

For the preparation of conducting imprinted polymer films, electrochemistry techniques such as galvanostatic, potentiostatic, and potentiodynamic methods were used, which allow the control of the film thickness. In combination with piezoelectric quartz crystals as working electrodes the observation of the mass deposition is possible [74,88].

2.3 Sensor integration

The recognition elements in biosensors usually consist of enzymes, antibodies, or other biological receptors, which are immobilized on the sensor surface. When an analyte binds to the recognition element, the resulting physical change is transduced into a recognizable signal, which can be monitored. This can be a heat change (calorimetric), a change of optical properties (e.g., absorbance, fluorescence, chemiluminescence), a mass change (piezoelectric), or electrochemical change. Electrochemical biosensors measure current (amperometric), voltage (potentiometric), conductance (conductiometric), or impedance changes (impedimetric). For instance, enzymatic biosensors are usually based on oxidoreductase enzymes coupled with amperometric detection, where a change of current as a result of electrochemical oxidation or reduction is detected, e.g., the electron transfer when glucose binds with glucose oxidase [89].

For usage in biosensors, two approaches to integrate the MIP material into the sensor surface are possible. Either the polymer is prepared before the integration with the transducer or it is prepared directly on the sensor surface. With the first method, the MIP particles are entrapped in a matrix such as agarose gel, poly(epichlorohydrin), or polyvinyl chloride. The matrix can also be an electrosynthesized polymer, often mixed with graphite to provide conductivity. Another possibility is the preparation of carbon-MIP nanocomposites, where the imprinted polymer is grafted by covalent binding or non-covalent adsorption onto graphene or carbon nanotubes. The composite is integrated with the transducer by drop or spin coating [90].
With the second method, MIP is prepared directly on the transducer surface via radical polymerization, sol-gel process, surface grafting, or layer-by-layer deposition. To control the thickness of the imprinted layer, electropolymerization of conductive polymers on graphite, glassy carbon and gold electrodes can be advantageous. To increase the surface area, and to facilitate the diffusion of analyte to binding sites, the polymer can be shaped as nanowires or prepared on carbon nanotubes or gold nanoparticles [72,90].

2.4 Pulsed amperometric detection

Pulsed amperometric detection (PAD) can be used to detect electroinactive anionic molecules with flow injection analysis. When a positive potential is applied to the polymer, it is oxidized and negatively charged molecules from the solution penetrate into the polymer, which gives an anodic current peak in the flow system. A following lower potential reduces the polymer and the negative ions are expelled from the polymer, which results in cathodic current [91,92]. This method was used for neutral molecules by Ramanaviciene *et al.* in combination with conducting imprinted polymers for the detection of caffeine and bovine leukemia virus glycoproteine (gp51) [93,94]. Pyrrole was polymerized on a platinum electrode in the presence of caffeine or gp51 in aqueous solution by applying 20 potential pulses between 950 and 350 mV. After template removal, the binding of the target molecule to the imprinted sites was detected by application of several potential steps and the sensor response was obtained by the peak difference of the current response (Fig. 9, see also Fig. 16, section 4.5.2). When neutral target molecules bind to the imprinted sites, the electron flow is reduced until saturation. PAD was also used for the detection of caffeine with an array of carbon nanotubes grafted with imprinted polypyrrole [75] and on gold

electrodes [76] . The advantage of this method is the possibility to detect the binding of electroinactive substances to imprinted sites.

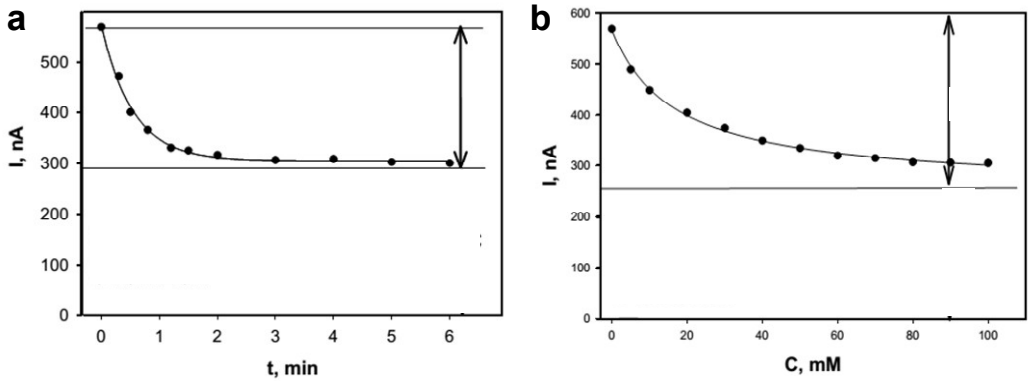

Fig. 9: (a) PAD current response of MIP imprinted with caffeine to 100 mM caffeine; (b) calibration curve [93].

2.5 Quartz crystal microbalance

With a quartz crystal microbalance (QCM), mass changes on the surface of a piezoelectric quartz crystal can be monitored in air, vacuum, or liquid. In 1959, Sauerbrey found a linear relationship between the absorbed mass on the sensor surface and the resonant frequency [95] (Equation 1).

$$f = \frac{2f_0^2}{A\sqrt{\rho\mu}}\Delta m \qquad (1)$$

f_o: resonant frequency of the quartz resonator

A: active crystal area

ρ: quartz density

μ: shear modulus

Δm: mass load

Δf: frequency change

The equation is valid for thin, rigid layers which fully couple to the oscillation of the crystal. In contrast, viscoelastic or soft layers dampen the oscillation. Information about the viscoelasticity can be obtained from the dampening or dissipation of the oscillation, which is defined as the ratio of the dissipated energy and the energy stored in the oscillator [96]. QCM can be used to characterize interfaces of materials, the deposition of polymer films, surface wetting processes, and biological interactions. In combination with electrochemistry, where the crystal is the working electrode, the progress of electropolymerization can be followed or ion and solvent transport can be studied [97]. MIP layers on QCM sensors have been studied for biomolecules, cells, and viruses, for ions, and for small molecules, which are, for instance, important in environmental monitoring [98].

2.6 Caffeine and clofibric acid

In this project, caffeine and clofibric acid (Fig. 10) were used as template molecules.

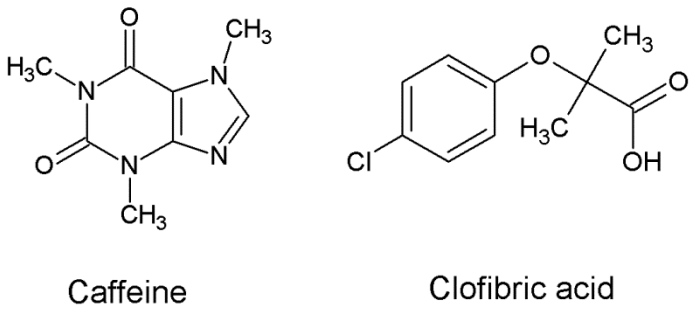

Fig. 10: Molecular structure of caffeine and clofibric acid.

Caffeine is a xanthine alkaloid naturally occurring in coffee plants, tea leaves, and many other plants. Products containing caffeine such as coffee, tea, soft drinks, or energy drinks are consumed worldwide in high amounts. Caffeine stimulates the central nervous system and acts as a diuretic. It is often added to pain relieving medicines as adjuvant, as it increases the analgesic effect of, for example, aspirin, ibuprofen, and paracetamol [99]. Caffeine has been detected in waste waters, surface waters, and ground water, and can be used as an indicator for untreated waste water sources in natural water bodies [100,101]. Various analytical methods for the detection and quantification in different media have been developed. Detection methods for caffeine include chromatographic methods, often coupled with mass spectrometry, and electrochemical methods [102]. Numerous MIPs for caffeine have been developed, e.g., for solid phase extraction [103,104], as imprinted membrane [105], for mass sensitive sensors [74,76,106], or for electrochemical sensors such as carbon paste electrodes with incorporated MIP [107] or imprinted polypyrrole on platinum electrodes [93].

Fig. 11 shows a scheme of possible hydrogen-bond- and π-π-interactions between polypyrrole and caffeine.

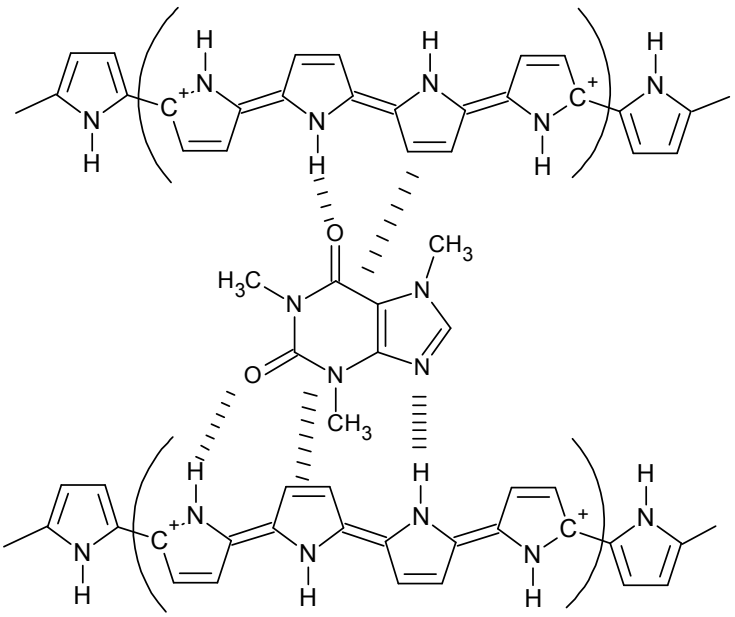

Fig. 11: Non-covalent interactions of caffeine with polypyrrole.

Clofibric acid, which was increasingly found during the last 30 years in waste waters, ground water, surface waters, and tap water, is the pharmacological active metabolite of the blood lipid regulators clofibrate, etofyllinclofibrate, and etofibrate [108]. In the North Sea it was detected in amounts between 0.01 ng L^{-1} and 1.35 ng L^{-1}, while in the Elbe river 18.6 ng L^{-1} were found [109]. Caffeine was detected at every station with concentrations between 2.0 and 16.1 ng L^{-1}. A more recent example is the finding of clofibric acid in the sediments of a wastewater receiving river in Shanghai in 2011, where 1.72–1.96 ng g^{-1} have been found [110]. Clofibric acid is highly persistent in the environment compared to other acidic pharmaceuticals such as diclofenac and ibuprofen, which have higher annual inputs into the hydrological cycle, but were not detected in the North Sea. While about 2% of the original doses of clofibrate or clofibric acid were found to leave the body unchanged after 24 h [111], clofibric acid is mainly excreted as gluconoride from the body (Fig. 12).

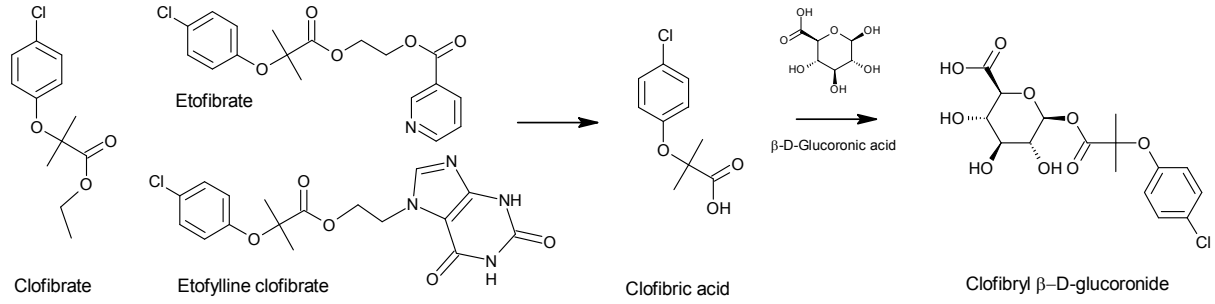

Fig. 12: Precursors and metabolic product of clofibric acid.

A cleavage of this molecule, which could additionally lead to the detectable amounts of clofibric acid in surface waters, might occur at waste water treatment plants [108].

For the effective removal of chemical pollutants from waste water, adsorption processes are studied. With graphene oxide nanosheets, over 90% of clofibric acid were removed from acidic aqueous solutions [112]. Also MIPs are explored for extraction and the following analytical determination of pollutants, but also for their selective adsorption, and for catalytic degradation [113]. Vinylpyridine-based imprinted polymers for the removal of clofibric acid from environmental water samples have been developed [114–116]. Also a commercially available imprinted polymer for solid phase extraction of non-steroidal anti-inflammatory drugs was tested with clofibric acid [117].

Clofibric acid is usually detected by liquid chromatography or also by gas chromatography coupled with mass spectrometry. Only a small number of references could be found which deal with the electrochemical detection of clofibric acid. Ambrosi *et al.* studied the electrochemical behavior of 4 pharmaceutically active compounds with voltammetric methods. Cyclic voltammetry graphs showed a reduction peak of clofibric acid at -1500 mV. Differential pulse polarograms showed a peak at ~-1300 mV [118]. The same group compared voltammetric and spectrophotometric measurements of 6 pharmaceutical active compounds and used differential pulse voltammetry (DPV), linear scanning polarography (LSP), and cyclic voltammetry (CYV) in the potential range between -1000 and -1700 mV for the detection of clofibric acid [119] (Fig. 13).

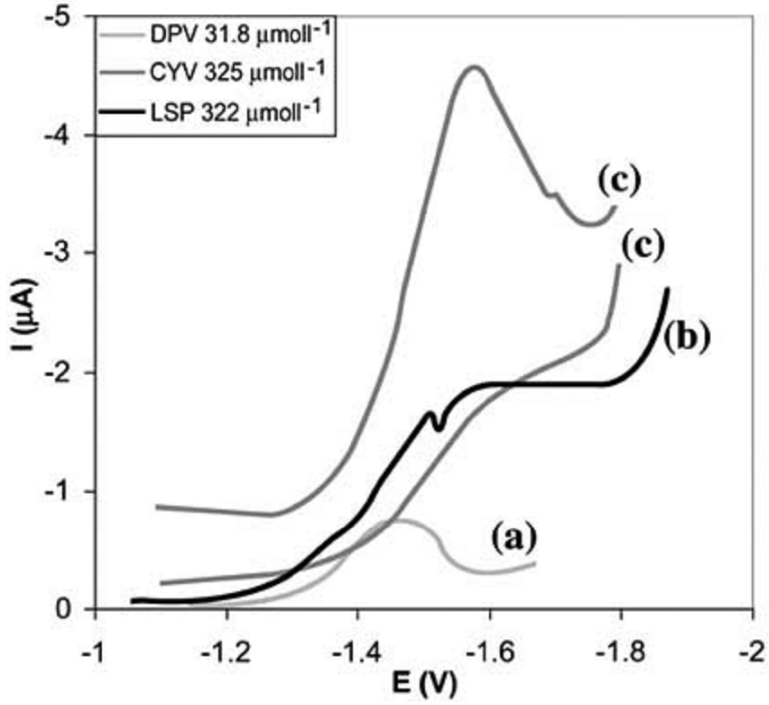

Fig. 13: (a) DPV, (b) LSP and (c) CYV curves of clofibric acid [119].

Fig. 14 shows possible non-covalent interactions between clofibric acid and polypyrrole.

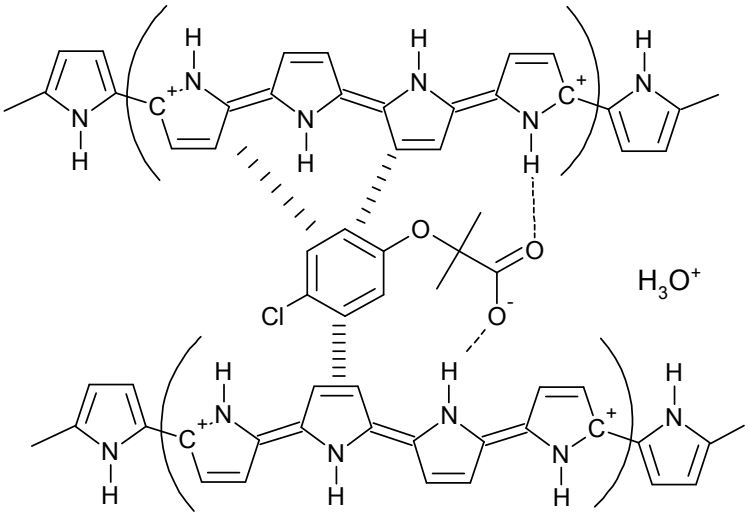

Fig. 14: Non-covalent interactions of clofibric acid with polypyrrole.

3 Aim and concept

Aim of this work is the development of a molecularly imprinted conducting polymer for the electrochemical sensing of clofibric acid. To produce an adhesive film of polypyrrole on the substrate, the electrochemical polymerization conditions should be optimized. This includes the polymerization method, the polymerization time, the monomer and template concentration, and the type of solvent. For first feasibility studies, a common template such as caffeine should be used. The influence of clofibric acid as template on the polymerization should be investigated. The deposited mass can be observed directly by polymerization on quartz crystal microbalance sensors. For sensing purposes, the template should be removed after polymerization from the binding sites by a washing step. If a simple rinsing step with solvent is not sufficient, more elaborate methods such as potential pulses should be investigated. The binding of clofibric acid is investigated with PAD, as this method should open the polymer film structure and make more binding sites accessible. The properties of the polymer structure such as the atomic composition, the roughness, the hydrophilicity, and the zeta potential should be investigated and the alteration of these properties through electrochemical treatments should also be studied. The use of pyrrole derivatives with functional groups might positively influence non-covalent interactions between template and polymer to improve the recognition properties of the sensor and should be studied as well.

4 Materials and methods

4.1 Chemicals

Pyrrole was purchased from Sigma Aldrich and freshly distilled at 128 °C, flushed with nitrogen and stored in the dark at 4 °C to prevent oxidation.

Caffeine, clofibric acid, 2,4-dichlorophenoxy acetic acid (2,4-D), carbamazepine (CBZ), dimethylsulfoxide (DMSO), phenoxyacetic acid (PES), potassium chloride (KCl), potassium dihydrogen phosphate (KH_2PO_4), potassium nitrate (KNO_3), pyrrole propionic acid (PPA), 2-(1H-pyrrole-1-yl)ethanamine, sodium hydroxide, sodium p-toluenesulfonate (Na-pTS), hydrochloric acid (37%) (HCl), hydrogen peroxide (30%), sulfuric acid (95%), acetonitrile, ethanol (EtOH), isopropanol, and methanol (MeOH) were all of analytical grade and used as received. Nitrogen gas (Alphagaz) was obtained from Air Liquide. Ultrapure water from a Millipore Milli-Q purification system was used for preparation of solutions. Stock solutions of clofibric acid (1 mM)

were prepared in KNO_3 or phosphate buffer solution (pH 7) and kept refrigerated. Stock solutions of 2,4-D and CBZ (1 mM) were prepared in phosphate buffer solution (pH 7) and kept refrigerated. CBZ was first dissolved in 2 mL DMSO and filled up to 100 mL with buffer solution. Solutions for polymerization and binding were filtered before use with 0.2 µm polypropylene syringe filters. Solutions for electrochemical measurements were deaerated for 10 min with nitrogen before use.

4.2 Instrumentation

Voltammetric measurements were performed with a potentiostat (Autolab PGSTAT 12, Metrohm / Eco Chemie, The Netherlands) with GPES software (Eco Chemie). Part of the coating experiments were done in a beaker with gold coated glass slides as working electrodes, a platinum wire as counter electrode, and a $Ag/AgNO_3$ electrode as reference electrode.

QCM measurements were performed with a Q-Sense E1 system (Q-Sense, Biolin Scientific AB, Sweden) with an electrochemistry flow module (QEM 401), which was connected to the potentiostat. Sample solutions were introduced into the electrochemistry module with a peristaltic pump (IKA). Quartz crystal gold sensors (4.95 MHz, AT cut) were used as working electrode (exposed area 1.1 cm^2), a platinum plate as counter electrode, and a Dri-REF Ag electrode (WPI, USA) as reference electrode. Quartz crystals and gold coated glass slides were cleaned with a 2:1 (v/v) mixture of sulfuric acid and hydrogen peroxide for 10 min, rinsed with plenty of Milli-Q water, and dried with a stream of nitrogen before use.

The mass of deposited material on the sensor surface was calculated from frequency changes with the Sauerbrey equation (Equation 1). For calculating the thickness of the polypyrrole coating a density of 1.48 g cm^{-3} was assumed [51].

Quartz crystals were provided in boxes, which were labeled alphabetically, containing 5 crystals each, which were labeled with numbers.

4.3 Sensor preparation

4.3.1 Gold coated glass slides for caffeine binding experiments

Polypyrrole was deposited onto the gold coated surface of glass slides (1 cm^2) through potential pulses or cyclic voltammetry of pyrrole (100 mM) in the presence of caffeine (2 mM) in KCl (100 mM). The potential was cycled between -0.2–0.8 V for 5 or 10 cycles. After preparation, the samples were washed with ultrapure water and ethanol. After storing for 1 h in buffer solution, the slides were kept in ultrapure water.

4.3.2 Gold coated glass slides for XPS measurements

Polypyrrole was deposited onto the gold coated surface of glass slides (1 cm^2) through cyclic voltammetry of pyrrole (100 mM) in the presence of caffeine (2 mM) or clofibric acid (2 mM) in KCl (100 mM). The potential was cycled between -0.2–0.9 V for 5 or 10 cycles.

4.3.3 QCM sensors for caffeine binding experiments

Polypyrrole was deposited onto the gold coated surface of piezoelectric quartz crystals through cyclic voltammetry of pyrrole (100 mM) in the presence of caffeine (2 mM) in aqueous KCl solution (100 mM). The potential was cycled between -0.2–0.9 V. After preparation, the samples were washed with ultrapure water and ethanol.

4.3.4 Gold coated glass slides for clofibric acid polymerization tests

Polypyrrole was deposited onto the gold coated surface of glass slides (1 cm^2) through cyclic voltammetry of pyrrole (1–50 mM) in the presence of clofibric acid (2 mM) in KNO_3 solution (100 mM). The potential was cycled between -0.2–0.9 V for 10, 20, or 30 cycles.

4.3.5 QCM sensors for clofibric acid polymerization tests

Polypyrrole was deposited onto the gold coated surface of piezoelectric quartz crystals through cyclic voltammetry of pyrrole (10 mM–50 mM) in the presence of clofibric acid (0.5 mM–4 mM) in aqueous KNO_3 solution (100 mM). The potential was cycled between -0.2–0.8 V for 10, 20, 30, 40, or 50 cycles. NIPs were synthesized in the same way, but without clofibric acid.

Pyrrole (40, 60, and 80 mM) was polymerized in buffer solution (pH 7) with or without 1 mM of clofibric acid on gold coated quartz crystals by cyclic voltammetry with 40, 80, and 120 cycles between -0.2–0.8 V. Phosphate buffer solution (pH 7) was prepared by dissolving 6.81 g KH_2PO_4 in ultrapure water, adding 291 mL of 100 mM NaOH and filling up to 1000 mL.

4.3.6 QCM sensors for binding tests

Pyrrole (10 or 20 mM) was polymerized in KNO_3 solution (100 mM) with or without clofibric acid (0 mM, 0.5 mM, 1 mM) by cyclic voltammetry with 40 or 80 cycles between -0.2–0.8 V. After polymerization the sensors were washed with ethanol for 30 min to remove the template and excess monomer, rinsed with water and dried with a stream of nitrogen.

Pyrrole was polymerized in phosphate buffer solution (pH 7) with or without clofibric acid by cyclic voltammetry between -0.2–0.8 V (for parameters, see Table 7, Table 9). After polymerization the sensors were washed with ethanol for 30 min to remove the template and excess monomer, rinsed with water and dried with a stream of nitrogen.

4.4 Surface characterization

4.4.1 XPS

With X-ray photoelectron spectroscopy (XPS) information about atomic composition and chemical bonds of the surface of a material can be obtained. Electrons from inner-shell orbitals are ejected by x-ray photons. The kinetic energy of the emitted electron, which depends on the binding energy of the electron and the x-ray energy, is characteristic for each element. Due to the low energy of the photoelectrons, which would be absorbed in air, ultra high vacuum is used [120].

For XPS measurements of NIPs and MIPs imprinted with caffeine, samples were prepared with 5 potential cycles on gold coated glass slides (see Table 5 for parameters). The measurements were performed at the Department of Experimental Physics of the Saarland University.

For XPS measurements of NIPs and MIPs imprinted with clofibric acid, samples were prepared on gold coated glass wafers or QCM sensors. Two sets of samples were made in KNO_3 solution with potential cycling between -0.2–0.9 V. Two more sets of samples were made in KNO_3 solution with potential cycling between -0.2–0.8 V. After preparation samples were washed with ethanol (70%) and/or ultrapure water, acetonitrile, or remained unwashed. Another set of samples was subject to PAD washing and binding experiments and prepared in phosphate buffer solution (see Table 13 for polymerization parameters).

The imprinted polypyrrole films were characterized by XPS with a monochromatic Al Kα source. Wide scan spectra and high resolution spectra of C1s (carbon), N1s (nitrogen), O1s (oxygen), and Cl2p (chlorine) were recorded. Binding energies refer to C1s (285 eV).

The measurements of the first set were performed by the SGS Fresenius Institut in Dresden, of the second and third set in the Advanced Analysis Center of the Korea Institute of Science and Technology, Seoul, of the fourth set at the Department of Experimental Physics of the Saarland University, and the last set at the Institute for Applied Materials of the Forschungszentrum Karlsruhe (Table 13).

4.4.2 AFM

With AFM, small surface areas of a material are scanned with a sharp tip on a cantilever for properties such as height profile or elasticity. In contact mode, the cantilever deflection is a measure of the force exercised by the sample. In non-contact mode, a piezoelectric modulator drives the cantilever to vibrate near its resonance frequency. Van der Waals attractive forces between tip and sample change the amplitude and the phase of the cantilever vibration. The distance of the tip from the sample is controlled by a feedback loop.

Surfaces of MIPs and NIPs were analyzed with AFM (Nanosurf mobile S, non-contact mode) after polymerization, after washing, and after binding tests. Measurements were made on 3–5 different areas on a sample (10 μm^2, 1 line s^{-1}).

4.4.3 Contact angle

The wetting characteristics of a material can be determined by contact angle measurements. In air, a drop of liquid is placed on the surface (sessile drop), or a gaseous drop is applied into a liquid beneath the surface (captive bubble). The contact angle, formed by the liquid–solid interface and the liquid–vapor interface, indicates the wettability of the surface. At high wettability, the drop spreads fully over the surface, while at low wettability the drop maintains it spherical form. In case of water, a surface with high wettability would be called hydrophilic and a surface with low wettability hydrophobic [121]. Contact angle measurements were performed in the Department of Technical Chemistry II at the University of Duisburg-Essen with the optical OCA 20 (dataphysics) measurement system in the sessile drop mode. 15-20 drops of Milli-Q water per sample were analyzed (dosing volume 0.5 µl, 0.5 µl s^{-1}).

4.4.4 Ellipsometry

Sample thicknesses of some samples were determined with ellipsometry instead of QCM. When light interacts with a surface material, its polarization is changed. This is described with an amplitude ratio, ψ, and the phase difference, . A model analysis of these values gives information about film thickness, optical constants, the refractive index, and other material properties.

Pyrrole was polymerized with cyclic voltammetry on QCM sensors with 50, 120 and 240 cycles (40 mM pyrrole, 1 mM or no clofibric acid, phosphate buffer solution). The thickness was determined in Duisburg in the Department of Technical Physics at the

University of Duisburg-Essen by ellipsometry measurements (Horiba Jobin Yvon MM-16). The thickness was fitted with the instruments DeltaPsi2 software.

4.4.5 Zeta potential

When a solid surface is in contact with an electrolyte solution, dissociation of surface functional groups and adsorption of ions from the solution lead to electric surface charge and to a potential difference between the surface and the solution (Fig. 15). Counterions from the solution compensate this surface charge by forming the electrical double layer [122]. Near the surface the inner Helmholtz layer consists of partially hydrated counterions. In the outer Helmholtz layer hydrated counterions are strongly adsorbed via Coulomb forces. Inner and outer Helmholtz layer form the Stern layer, in which the potential drops linearly. Ions in the diffuse layer, which are further away from the surface, are attracted to the surface charge, but at the same time repelled by the ions of the Stern layer. In this layer, the potential drops exponentially. The ions in the diffuse layer move relatively faster than the ions in the Stern layer. The potential at this plane of shear is the zeta potential ζ.

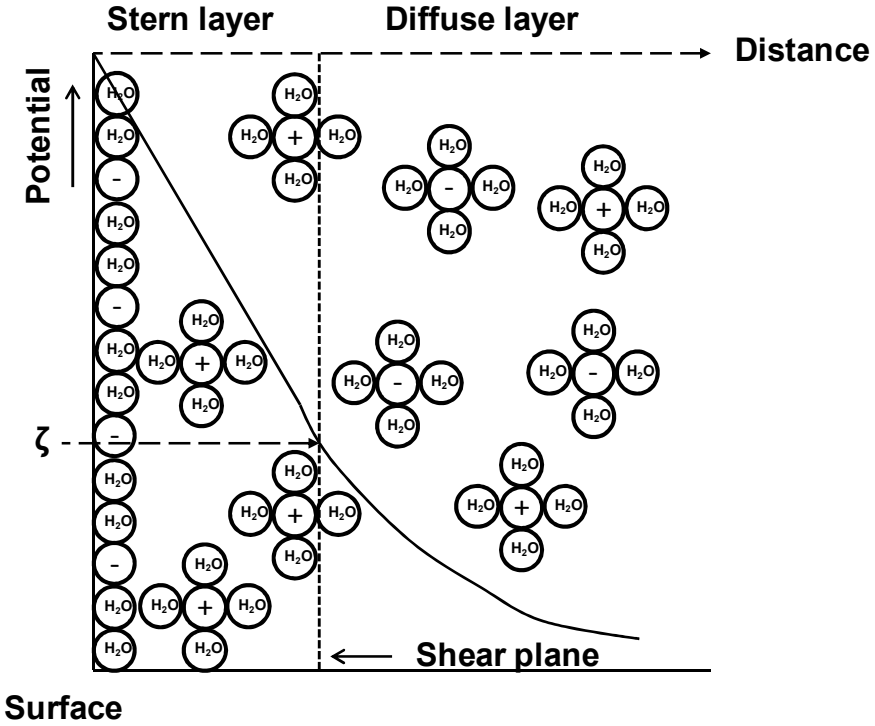

Fig. 15: Scheme of electric double layer (modified from [123]).

The relation of the zeta potential with the streaming potential is given by the Helmholtz–Smoluchowski equation (Equation 2):

$$\zeta = \frac{dU}{dp} \quad \frac{\eta}{\varepsilon \quad \varepsilon_0} \quad \frac{L}{A \quad R} \tag{2}$$

U = Streaming potential
p = Pressure
η = Viscosity
ε = Dielectric constant
L = Length of channel
A = Cross sectional area
R = Electric resistance

The streaming potential is measured by applying a pressure on a stream of liquid inside a channel. Zeta potentials of polymer films were measured with a SurPass electrokinetic analyzer (Anton Paar). In the cell, a 100 mM solution of KCl is passed with a pressure of max. 400 mbar between the surfaces of two samples with a gap of 100 µm. Samples were prepared on rectangular pieces of gold coated glass wafers (2 cm x 1 cm, 40 mM pyrrole, 50 cycles).
Zeta potential measurements were performed after coating, after PAD washing with a mixture of HCl/KCl and ethanol (1:1) (pH 2.5), and after PAD binding measurements with 30 µM clofibric acid in phosphate buffer solution (pH 7).

4.5 Binding tests

4.5.1 Binding with QCM-D

The sensor response to solutions with increasing clofibric acid concentrations was determined with QCM measurements according to Ebarvia *et al.* [124]. First, water was pumped through the cell, until a steady frequency reading was reached. Then, KNO_3 solution was introduced into the cell, until the frequencies were stable. The flow was stopped and the obtained value marked as F_{KNO3}. Clofibric acid solution (containing KNO_3) was then pumped through the cell for some min. After stopping the pump, the stable frequency value was recorded as F_{Cf}. The frequency shift for each concentration was calculated as the sensor response according to Equation 3:

$$F = F_{KNO3} - F_{Cf} \tag{3}$$

4.5.2 Binding with PAD

Binding experiments were also performed with PAD [76,93]. A sequence of 5 potential pulses with a two-step waveform was applied, 1 s at 0 V and 1 s at 0.6 V *vs.* reference electrode (Table 2). This was repeated every minute for overall 10 min.

Table 2: PAD Parameter

Pulse	E (V)	Pulse length (s)
1	0	1
	0.6	1
2	0	1
	0.6	1
3	0	1
	0.6	1
4	0	1
	0.6	1
5	0	1
	0.6	1

The sum of the 5th anodic and cathodic peak current was calculated as I_o. This was repeated every minute for overall 10 min (I_t). The sensor response R_S was calculated from the current change (Equation 4) (Fig. 16).

$$R_S = I_o - I_t \quad (4)$$

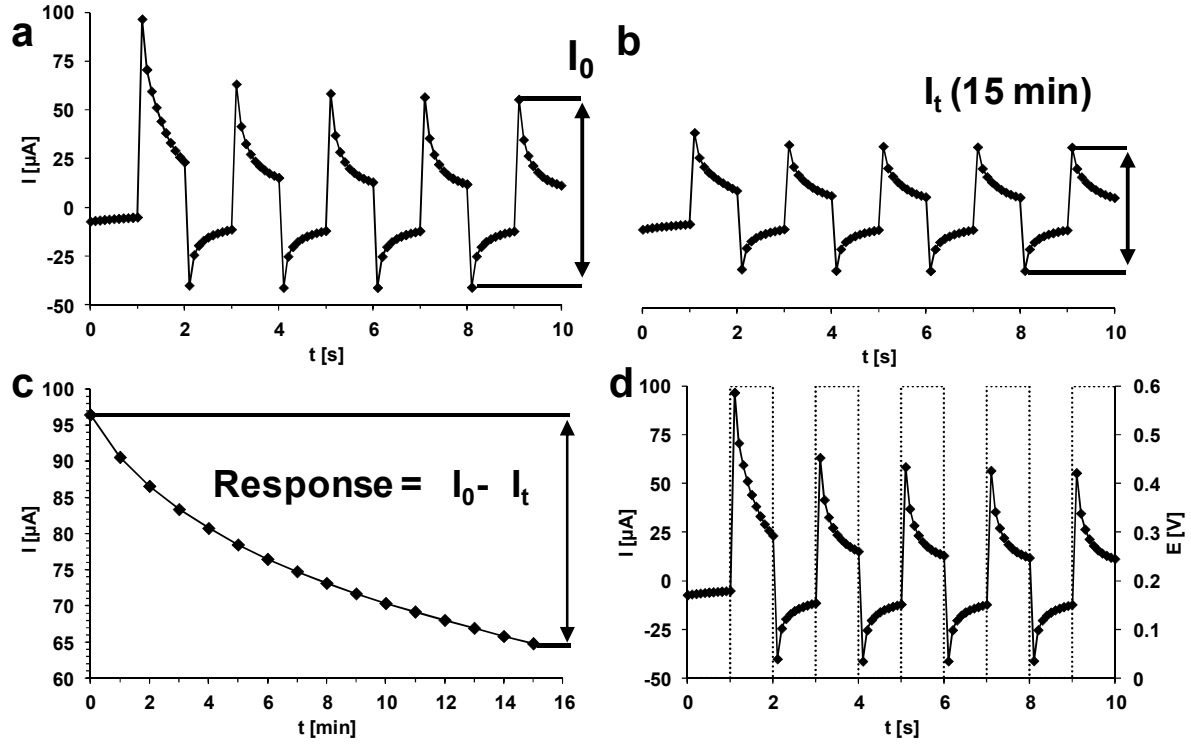

Fig. 16: (a) PAD current response of polypyrrole during first application, last anodic and cathodic peak current gives I_o; (b) PAD current response during 15th application, last anodic and cathodic peak current gives I_{15}; (c) graph of $I_{1\text{-}15}$ against time, I_o- I_t gives sensor response; (d) potential sequence and resulting current.

Applying a voltage to a conducting polymer adds or removes charges from the polymer backbone and induces the insertion or ejection of dopant ions, which

changes the volume of the polymer [125]. During PAD, the polymer is oxidized by a positive potential (0.6 V) and negative counter ions penetrate from the solution into the polymer, which begins to swell. Then, a lower potential (0 V) is applied, which leads to release of anions into the solution. The potential at 0 V might not be sufficient to release all ions that were incorporated during the pulse at 0.6 V, so the polymer might stay a bit more swollen than before. During the next pulses, the swelling of the polymer should increase and should allow the diffusion of more target molecules into the polymer [76].

4.5.3 Preliminary binding tests with caffeine

For preliminary tests of polypyrrole imprinted with caffeine on gold coated glass slides, caffeine detection was performed with phosphate buffer solution (pH 7) containing caffeine with concentrations between 20–50 µM. After caffeine detection, the sensor was soaked in buffer solution for 3 min to remove caffeine from the binding sites. Then, the sensor was soaked in double distilled water to allow ions to diffuse out of the polymer. For binding tests with QCM sensors, caffeine concentrations between 10–100 µM were used. After caffeine detection, buffer and water were pumped into the cell to remove caffeine from the binding sites.

4.5.4 Binding tests with clofibric acid on QCM sensors

Before every experiment, water, isopropanol, and water were pumped subsequently through the cell to remove contaminations and trapped air bubbles. A cyclic voltammogram (CV) of the uncoated or with polymer coated sensor was recorded with stopped flow in phosphate buffer solution with 10 cycles and potential cycling between -0.2–0.6 V. Malfunctioning sensors or bad connections were identified with this method. The first PAD measurement was done in buffer solution. After that, subsequently solutions with increasing clofibric acid solutions were pumped into the cell. PAD measurements for every concentration were done without flow. The last PAD measurement was again made with phosphate buffer followed by cyclic voltammetry (10 cycles, -0.2–0.6 V).

4.6 Washing procedure

QCM sensors coated with polypyrrole were washed with ethanol or a mixture of ethanol and water (70% ethanol) in a PTFE holder with a magnetic stirrer. The solution was changed after 15 min or as indicated in the washing procedure table (Table 10).

In another set of experiments, QCM sensors coated with polypyrrole were washed using a mixture of HCl/KCl and ethanol (1:1) (pH 2.5) under PAD conditions for 5, 10, 15, 30, or 60 min. Before and after the washing step, CVs were recorded in phosphate buffer solution. The mixture of HCl/KCl was prepared by adding 13 mL of 200 mM HCl to 50 mL of 200 mM KCl and filling up with ultrapure water to 200 mL (pH 2).

4.7 Selectivity test

2,4-D (Fig. 59), a common herbicide and structurally related to clofibric acid, CBZ (Fig. 59), an anticonvulsant used for treatment of epilepsy, and phenoxyacetic acid (Fig. 59) were chosen for testing the selectivity of MIP. Like clofibric acid, CBZ is often not completely removed in waste water treatment plants and was found in environmental water bodies [126]. MIP and NIP coated QCM sensors were washed under PAD conditions for 15 min. Binding tests under PAD conditions were done with 30 µM solutions of 2,4-D and CBZ for 10 min and compared with the results of MIP and NIP binding tests with clofibric acid under the same conditions.

4.8 Polymerization with potential pulses

Gold coated glass slides (2 x 1 cm) were used for polymerization experiments. Kapton tape was used to obtain an area of 1 cm^2 for polymerization.

Pyrrole (200 mM) was polymerized in 70% methanol containing Na-pTS (100 mM) or phosphate buffer and KCl as electrolyte by applying a constant current or potential pulses (Table 16) in the presence or absence of 90 or 9 mM clofibric acid.

A second set of samples was prepared with 120 mM or 200 mM pyrrole in ethanolic or methanolic phosphate buffer solution containing KNO_3 or KCl in the absence or presence of 1 mM and 10 mM clofibric acid by potential pulses (Table 17).

Binding was tested with 30 µM clofibric acid in phosphate buffer solution under PAD conditions. After coating and after binding, samples were washed in phosphate buffer by applying a potential of -600 mV for 30 min.

4.9 Polymerization of pyrrole derivatives

Pyrrole propionic acid (PPA) (20 mM) in KNO_3 solution (100 mM) was polymerized on gold coated glass slides with cyclic voltammetry (10 cycles). The potential was cycled between -0.2–1, 1.1, and 1.2 V.

PPA (20 mM) in KNO_3 solution (100 mM) and PPA in KNO_3 solution (100 mM) containing clofibric acid (1 mM) were polymerized on QCM sensors with cyclic voltammetry (40 cycles). The potential was cycled between -0.2–1.2 V.

PPA (20 mM) was copolymerized with pyrrole (20 mM) in KNO_3 (100 mM) on QCM sensors with cyclic voltammetry (40 cycles, -0.2-1 V).

Pyrrole (100 mM) was copolymerized with 2-(1H-pyrrole-1-yl)ethanamine (33 mM) in phosphate buffer solution (pH 7) and in Na-pTS (100 mM) solution in the presence of 1 mM clofibric acid (1 mM) by cyclic voltammetry with 80 cycles (-0.2–0.9 V). After polymerization the sensors were washed with ethanol (70%) for 1 h to remove the template and excess monomer, rinsed with water, and dried with a stream of nitrogen.

5 Results and discussion

5.1 Preliminary tests with caffeine

5.1.1 Imprinting of caffeine

Preliminary tests for testing polymerization and binding were done on gold coated glass slides and with caffeine as template (Table 3), following the protocol of Choong and Milne [76]. Preliminary polymerization tests with potential pulses did not result in adhesive films, so pyrrole was polymerized by cyclic voltammetry.

Table 3: Polymerization parameters for polypyrrole imprinted with caffeine

Glass slide	Pyrrole (mM)	Caffeine (mM)	Cycles	Potential (V)
1	100	0	5	-0.2–0.8
2	100	0	5	-0.2–0.8
3	100	2	5	-0.2–0.8
4	100	2	5	-0.2–0.8
5	100	0	10	-0.2–0.8
6	100	0	10	-0.2–0.8
7	100	2	10	-0.2–0.8
8	100	2	10	-0.2–0.8

5.1.2 Binding of caffeine

The sensor response was investigated with PAD. Polypyrrole is in equilibrium state a closed structure, which can be actuated by potential pulses. Ions penetrate from the electrolyte into the polymer, which begins to swell [125]. This open structure should allow caffeine molecules to penetrate by diffusion into the polymer and to bind to the imprinted sites. The recorded currents should decrease with increasing caffeine concentration because a higher amount of neutral caffeine molecules increases the impedance of electron flow [76].

Fig. 17 shows the sensor response to caffeine solutions with concentrations between 20–50 µM. The current generally decreased with every potential pulse over 10 minutes. For MIPs a higher current was observed than for NIPs. The current also increased for plates prepared with 10 cycles compared to plates prepared with 5 cycles. Fig. 18 shows ΔI values calculated from the current difference of the PAD measurement over 10 min for each plate and each concentration of caffeine as calibration curves. A decrease of the ΔI values starting at ~250 µA with increasing caffeine concentration was observed for plates which were polymerized with 5 cycles. For plates polymerized with 10 cycles, ΔI values <30 µA were obtained with 20 µM

caffeine. With 30 µM caffeine, I values increased to 256 µA (NIP) and 140 µA (MIP) and decreased then with increasing caffeine concentration. The low values with 20 µM caffeine could imply according to Choong and Milne [76] that this concentration is outside of the detection range of the sensor.

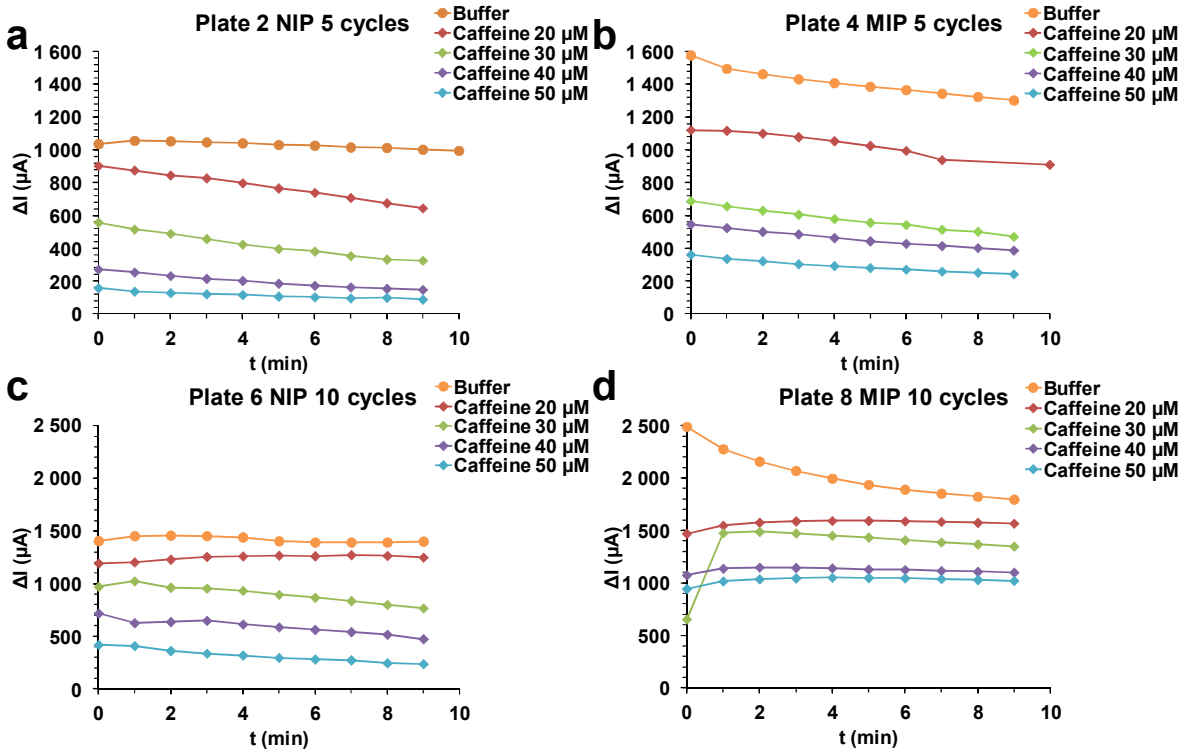

Fig. 17: PAD sensor response to caffeine solutions of (a),(c) NIPs and (b),(d) MIPs prepared with 5 cycles (a),(b) and 10 cycles (c),(d).

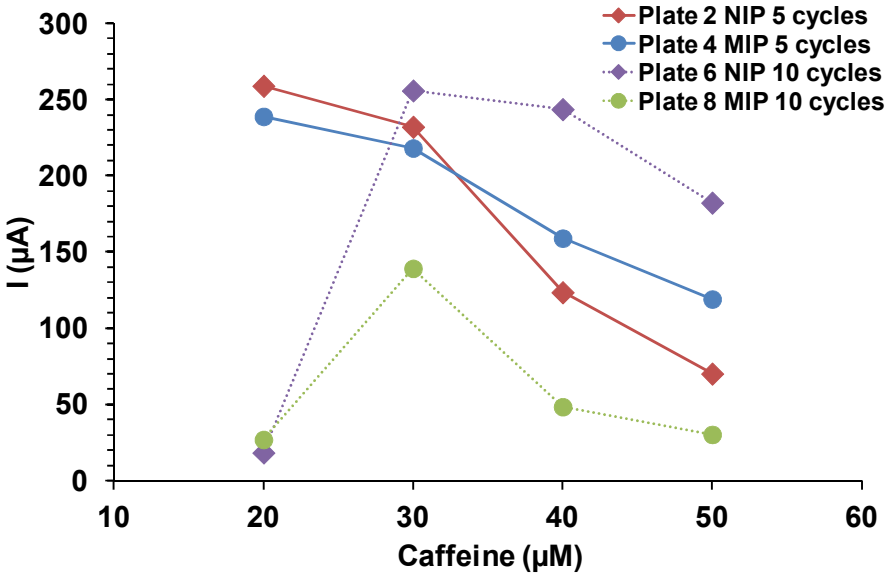

Fig. 18: Calibration curves for MIP and NIP.

Choong and Milne [76] found a varying detection range for imprinted polypyrrole depending on the magnitude of the potential step during PAD binding experiments. It was assumed that increasing penetration depth of the ions from the solution into

the film and the resulting swelling increased the detection range with increasing size of the potential step (Fig. 19).

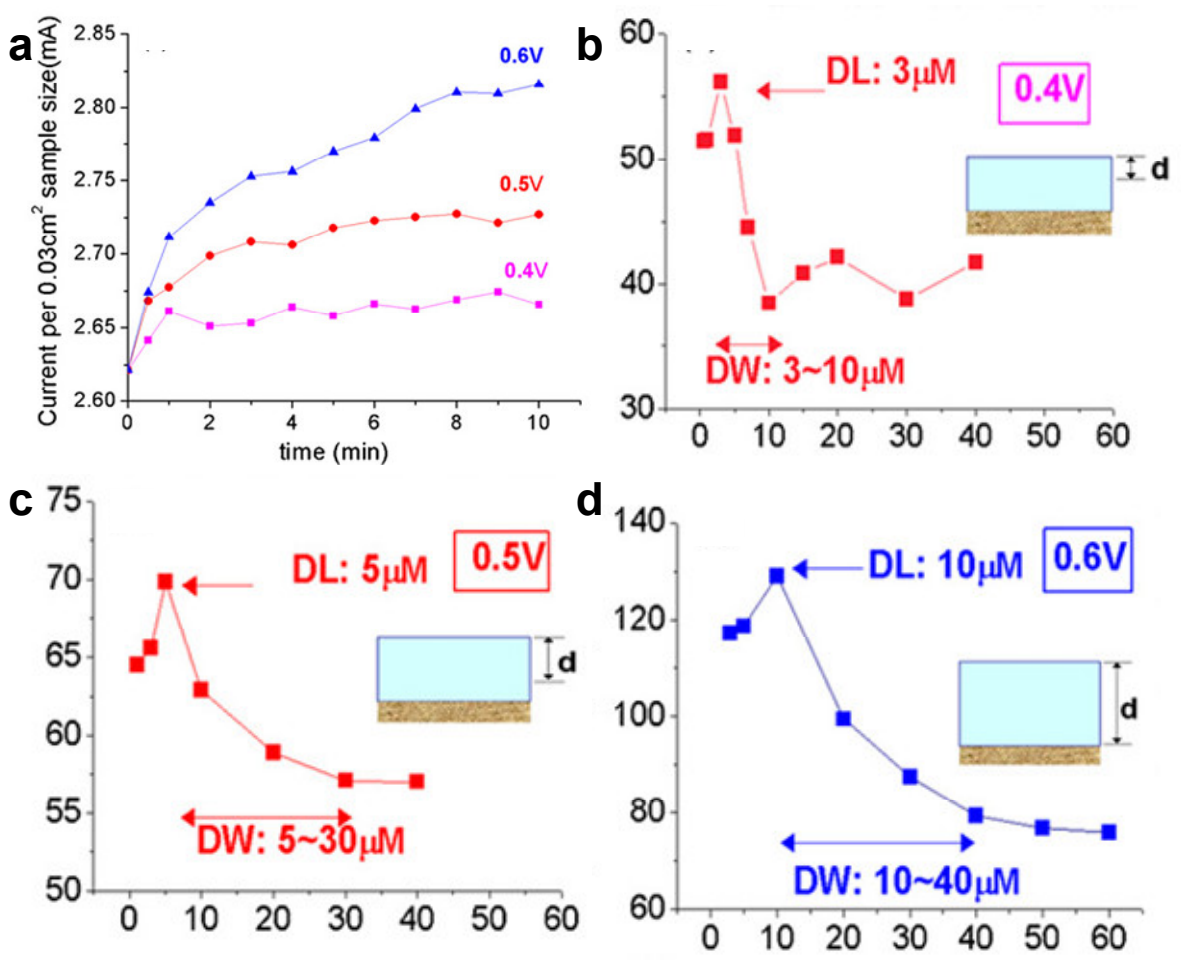

Fig. 19: Results from literature for an analogous system: (a) PAD current response with potential step sizes between 0.4–0.6 V of caffeine imprinted polypyrrole to caffeine solutions; calibration curves showing the detection window (DW) and the penetration depth (d) for (b) 0.4 V, (c) 0.5 V, and (d) 0.6 V [76].

The calibration curves also show a similar behavior of MIP and NIP (plate 2 and 4). The NIP prepared with 10 potential cycles reached higher I values than the MIP (plate 6 and 8). NIPs should have probably nearly the same I values with different caffeine concentrations due to non-specific binding. The height of the I values can be lower or higher than that of the corresponding MIP. Choong and Milne [76] show a NIP calibration curve with I values between 145–150 µA for caffeine concentrations between 10–50 µM (Fig. 20b) and a MIP calibration curve with 130 µA for 10 µM caffeine as the highest I value (Fig. 20a). In a second study [75], the same authors found I values of 58 µA for 40 mM caffeine imprinted MIP on carbon nanotubes (Fig. 20d), while with a NIP (Fig. 20c) I values of 10 µA were

obtained. Ramanaviciene *et al.* [93] do not show any NIP data, but they mention that NIPs were 9–10 times less sensitive than MIPs.

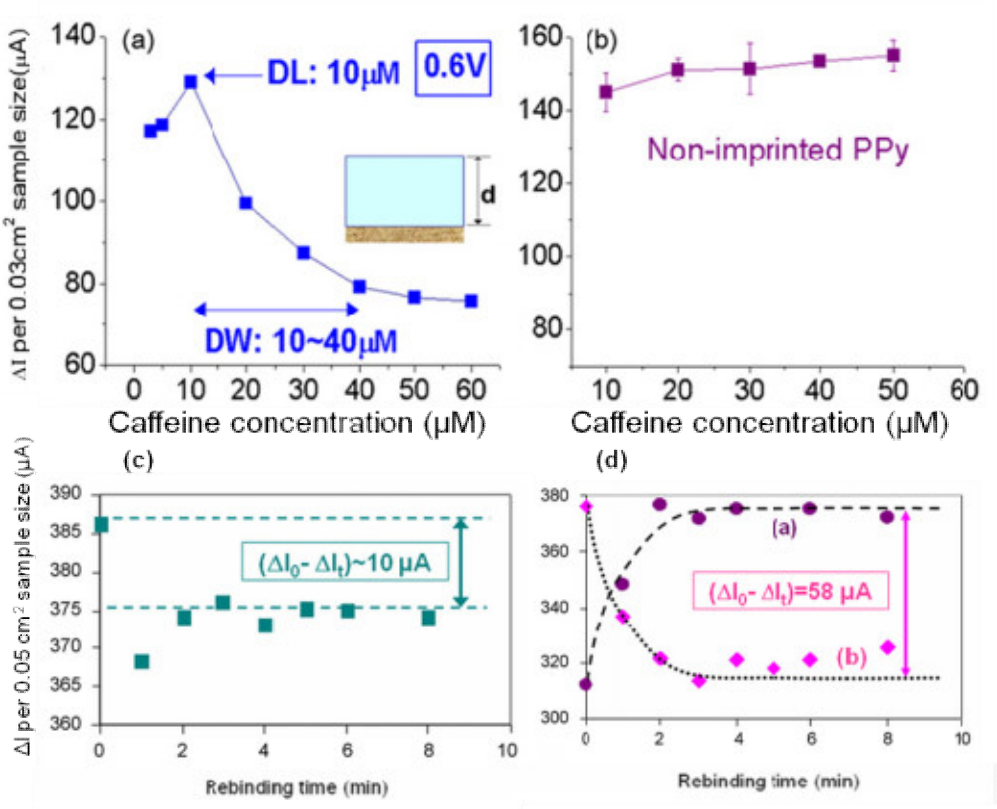

Fig. 20: Results from literature for an analogous system: Calibration curve of (a) MIP film [76] and (b) NIP film [76]; response of sparse carbon nanotubes coated with (c) polypyrrole [75] and (d) caffeine imprinted polypyrrole [75] - a) elution of caffeine - b) binding of 40 mM caffeine.

Further experiments were conducted on gold coated quartz crystals with a QCM-D instrument connected to an electrochemical cell (Table 4). The electrochemical polymerization can be observed directly by the frequency change of the QCM (Fig. 21). The diagrams a and c show the frequency and corresponding mass change of sample 1 and the diagrams b and d show the frequency and corresponding mass change of sample 2.

Table 4: QCM polymerization parameters for polypyrrole imprinted with caffeine

Sample	Pyrrole (mM)	KCl (mM)	Caffeine (mM)	Cycles	Potential (V)	Mass (µg cm^{-2})	Thickness (nm)
1	100	100	2	5	-0.2–0.9	0.4	2.4
2	100	100	2	10	-0.2–0.9	17	117
3	100	100	2	10	-0.2–0.9	65	437
4	100	100	2	10	-0.2–0.9	98	661
5	100	100	2	5	-0.2–0.9	16	105

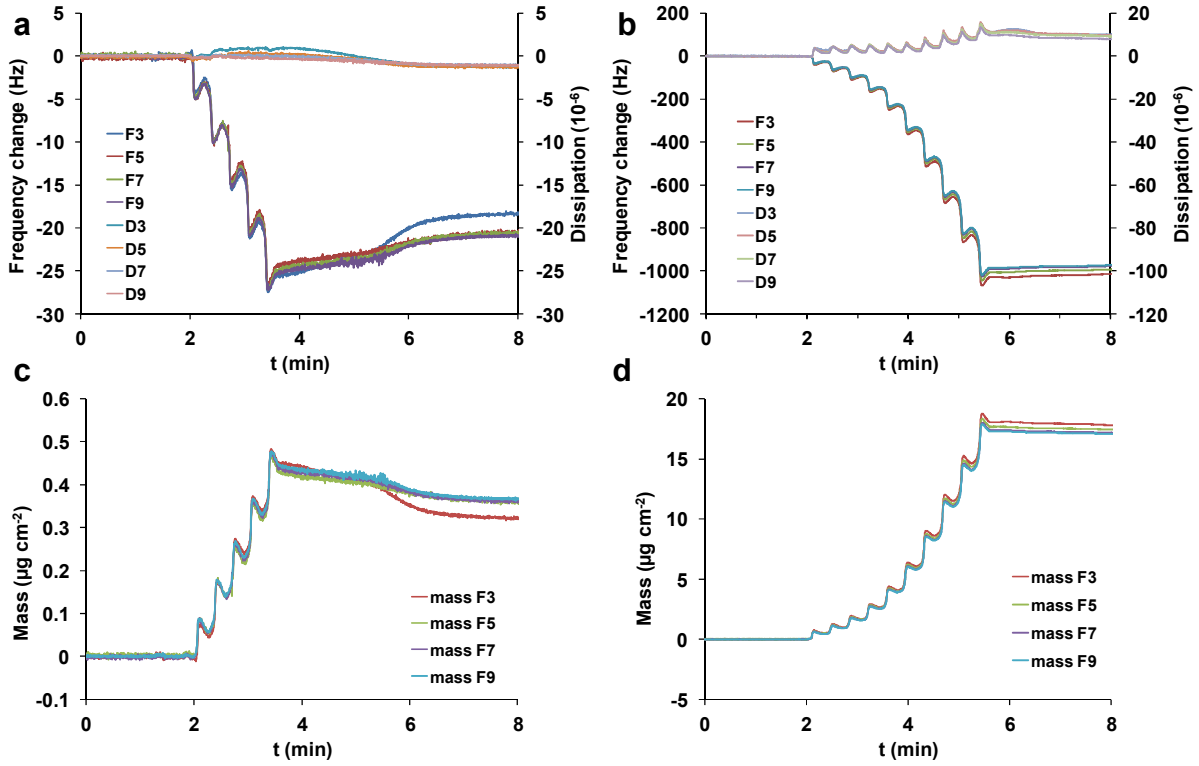

Fig. 21: Frequency change and dissipation during polymerization of pyrrole with (a) 5 cycles and (b) 10 cycles; mass increase during polymerization with (c) 5 cycles and (d) 10 cycles.

The similar behavior of the harmonics and the low change in dissipation (<5% of the frequency change) indicated a rigid film [127]. Therefore the Sauerbrey equation was used to calculate the deposited mass on the sensor surface.

It was found that a concentration of 100 mM pyrrole and 10 potential cycles resulted often in films too thick for frequency measurements (Fig. 22). After the eighth cycle some of the overtone signals of sample 3 were lost. The film deposited after 8 cycles had a thickness of 437 nm (sample 3, Table 4).

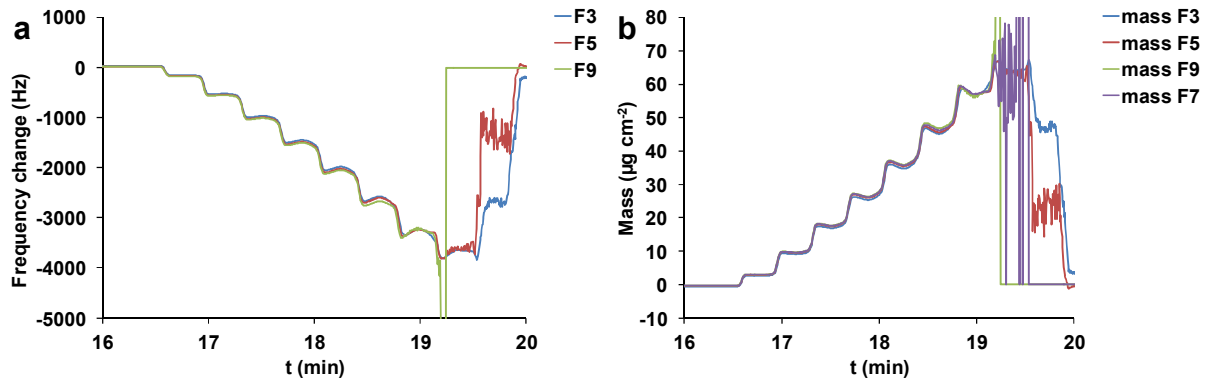

Fig. 22: Frequency change (a) and mass increase (b) during polymerization of pyrrole (100 mM) with 10 cycles (sample 3).

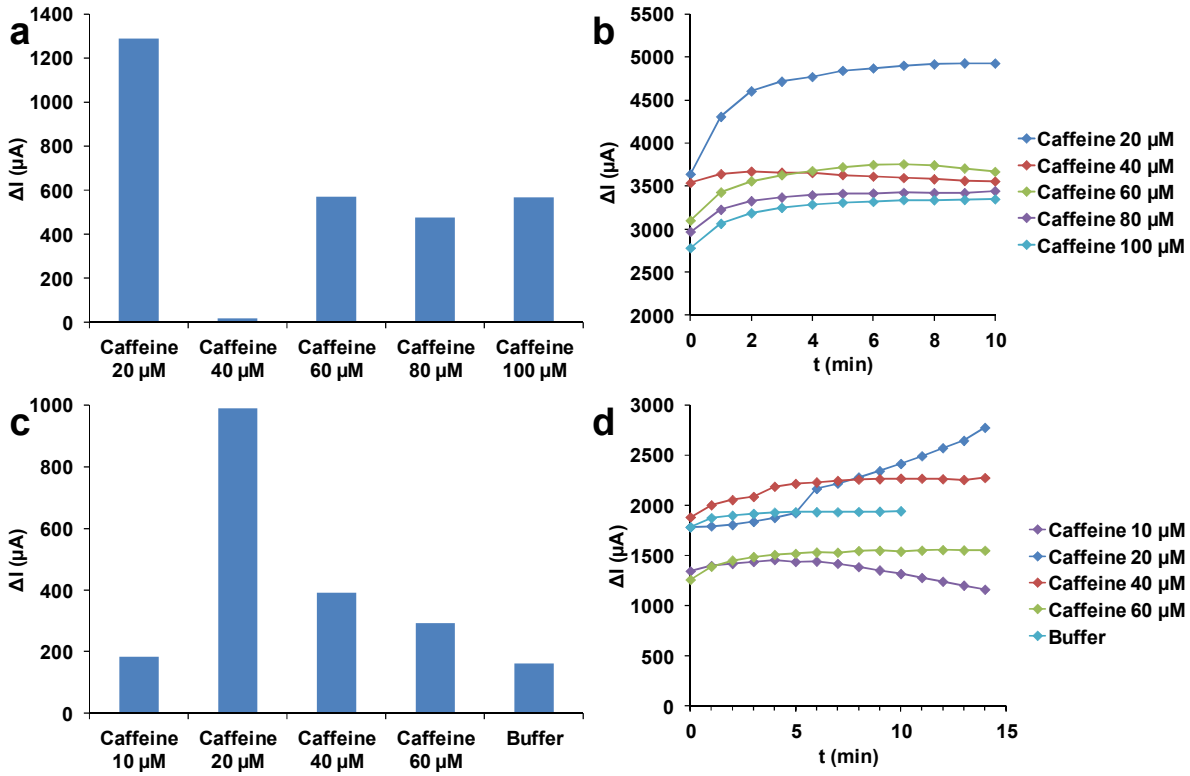

Fig. 23: PAD sensor response and current response of (a) sample 4 and (b) sample 5 to caffeine solutions.

Fig. 23 shows the sensor response to caffeine solutions with concentrations between 10–100 μM. Here in most cases the current increased with every potential pulse over 10 minutes (Fig. 23b, d) contrary to observations made with the gold coated glass slides (Fig. 17). The current was higher for sample 4 prepared with 10 cycles than for sample 5 prepared with 5 cycles. Choong and Milne [76] (Fig. 24) showed for imprinted polypyrrole films on gold surfaces also increasing currents for PAD over 10 min. In a second study from the same group, the response of carbon nanotubes imprinted with caffeine was described as decreasing (Fig. 20d, curve b) [75]. Ramanaviciene *et al.* [93] also found decreasing PAD current responses for polypyrrole films imprinted with caffeine (Fig. 24b).

The response of the sensors, calculated from the current difference of the PAD measurement over 10 min is shown in Fig. 23a, c. I values of sample 4 started at ~2300 μA for the lowest caffeine concentration and decreased to 480–570 μA for 60–100 μM caffeine. For sample 5, I values <200 μA were obtained with 10 μM caffeine. With 20 μM caffeine, I values increased to 990 μA and decreased then with increasing caffeine concentration.

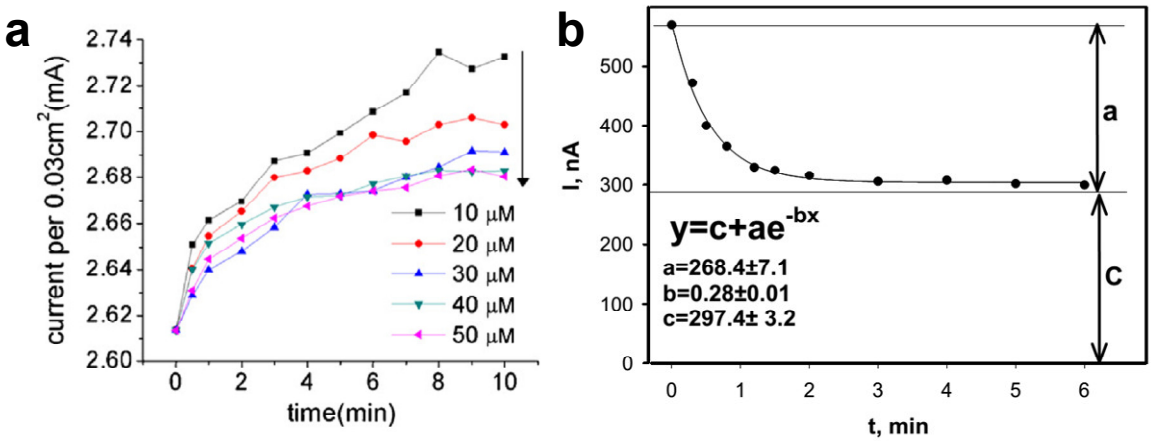

Fig. 24: Results from literature for an analogous system: PAD response of imprinted polypyrrole to caffeine solutions in phosphate buffer; (a) polymer prepared with 100 mM pyrrole, 50 mM KCl, and 2 mM caffeine [76], PAD binding with 10–50 µM caffeine; (b) polymer prepared with 50 mM pyrrole, 100 mM KCl, and 5 mM caffeine, PAD with 100 mM caffeine [93].

5.1.3 XPS measurements

The polymer surfaces of a NIP sample and MIPs imprinted with 2 mM caffeine were analyzed with XPS. The samples were prepared on gold coated glass slides. After preparation, samples 1 and 2 were washed with ethanol and water, while sample 3 remained unwashed (Table 5).

Table 5: Polymerization parameters for XPS measurements of NIP and MIPs

Sample	Pyrrole (mM)	Caffeine (mM)	Cycles	Potential (V)	Wash
1	100	0	5	-0.2–0.9	EtOH, H2O
2	100	2	5	-0.2–0.9	EtOH, H2O
3	100	2	5	-0.2–0.9	%

Curve fitting was not available for this measurement. The main peak of C1s at ~285 eV could be attributed to C-C bonds in the polymer chain (Fig. 25). The small shoulder on the left side of the peak is probably caused by C-N bonds at ~286 eV and by carbonyl groups at ~288 eV [128]. The unwashed sample showed also peaks at ~293 eV and ~296 eV, which could be attributed to $K2p_{3/2}$ and $K2p_{1/2}$ from KCl [129]. The major peak of N1s at 400 eV could be attributed to primary/secondary amine nitrogen (-N-H). The shoulder on the right side of the peak at ~398 eV could be caused by tertiary amine nitrogen (=N-) [130]. The O1s signal at ~532 eV could be attributed to C=O bonds in the polymer [130]. The contribution of caffeine to the XPS spectra could not be distinguished from the contribution of polypyrrole.

Chlorine was found in the unwashed sample with an atomic concentration of 2.5% (Fig. 26), resulting from the use of KCl as conducting salt in the polymerization solution. The C/N ratio of an ideal polypyrrole structure would be 4:1. For polypyrrole polymers prepared with perchlorate as counter ions, the C/N ratio increased to 5.3 for 1V with voltages higher than 0.6 V due to defects of the polymer structure [131]. Sample 1 (NIP) showed a comparable ratio of 5.6. The C/N ratio of the MIP also contains the 2:1 C/N ratio of the caffeine molecule, which might lead to the lower value of 4.9. The C/N ratio of the washed MIP was higher with 5.3 than the ratio of the unwashed MIP, which might indicate that less caffeine is present in the washed polymer than in the unwashed polymer.

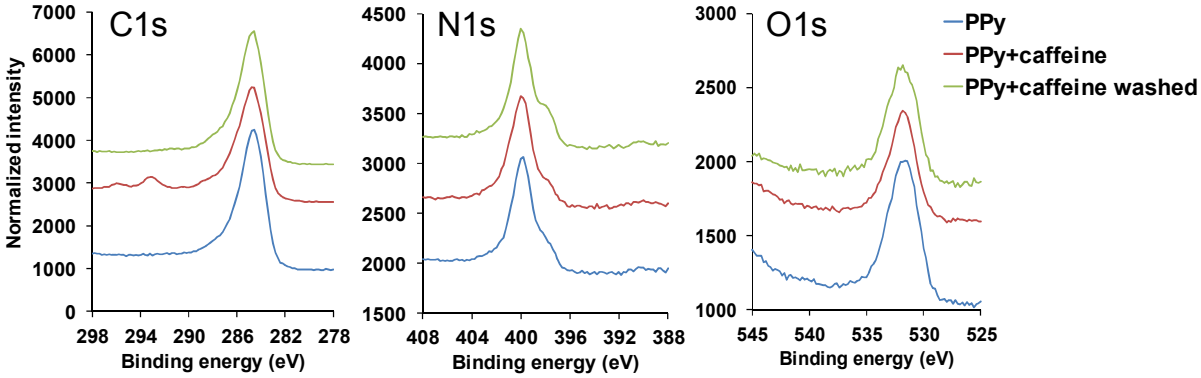

Fig. 25: XPS spectra of polypyrrole, polypyrrole imprinted with caffeine, and polypyrrole imprinted with caffeine after washing.

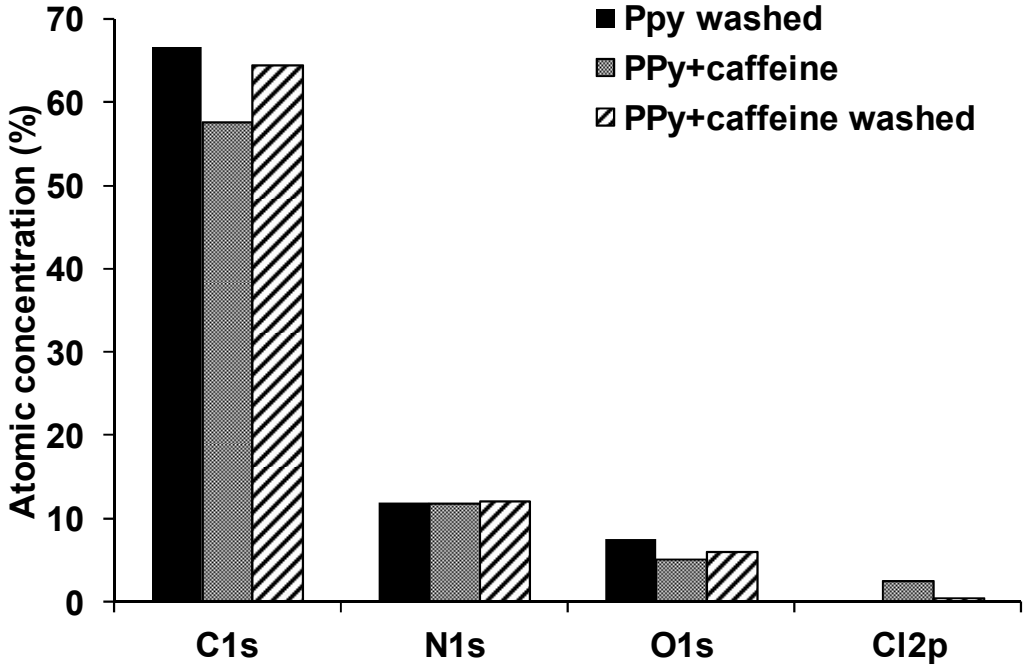

Fig. 26: Atomic concentration of polypyrrole and caffeine imprinted polypyrrole.

5.1.4 Conclusion of caffeine imprinting

XPS measurements showed peaks in accordance with literature data for polypyrrole. Chlorine from KCl was visible in the XPS spectra of an unwashed sample. The preliminary tests with caffeine showed that optimizations of the polymerization conditions were necessary. Cyclic voltammetry was chosen as polymerization method because first tests with potential pulses did not result in adhesive films. The concentration of pyrrole should be lowered because a thick film led to loss of overtone signals in QCM measurements. Although several samples were prepared with the same polymerization parameters, the deposited mass highly varied (Table 4).

A slower polymerization rate might lead to more reproducible results and could be reached by a lower concentration of pyrrole and the replacement of KCl with KNO_3, which has a lower conductivity. PAD binding results showed more resemblance to the results of Choong and Milne [76] than to PAD experiments of Choong and Milne [75] and Ramanaviciene *et al.* [93]. Optimization of the polymerization conditions might produce more coherent PAD results.

5.2 Imprinting of clofibric acid

In the following experiments, the template was changed to clofibric acid. It contains a chlorine atom, which is detectable by XPS measurements and therefore could help to better distinguish MIPs from NIPs. The conducting salt was changed to KNO_3 to avoid interference with the chlorine atom in KCl.

5.2.1 Polymerization experiments

5.2.1.1 Polymerization on glass slides

Pyrrole was polymerized with and without the addition of clofibric acid as template in KNO_3 solution with concentrations of pyrrole between 1–50 mM and 10–30 potential cycles (Table 6).

Table 6: Polymerization parameters for polypyrrole imprinted with clofibric acid

Sample	Pyrrole (mM)	Clofibric acid (mM)	Cycles	Potential (V)
1	1	0	20	-0.2–0.9
2	10	0	10	-0.2–0.9
3	10	0	20	-0.2–0.9
4	10	0	30	-0.2–0.9
5	50	0	20	-0.2–0.9
6	1	2	20	-0.2–0.9
7	10	2	10	-0.2–0.9
8	10	2	20	-0.2–0.9
9	10	2	30	-0.2–0.9
10	10	2	30	-0.2–0.9
11	50	2	10	-0.2–0.9
12	50	2	20	-0.2–0.9

Fig. 27 shows cyclic voltammetry graphs which were recorded after polymerization in KNO_3 solution. With increasing concentration of pyrrole from 1–50 mM during polymerization, the current of the polymer increased from 39 to 1060 µA for NIPs (Fig. 27a,d). The current also increased with increasing cycles numbers from 111 µA with 10 cycles to 287 µA with 30 cycles for NIPs (Fig. 27b,c). The presence of clofibric acid decreased the conductivity of the polymer. For instance, with 1 mM pyrrole and 20 cycles, the current decreased from 39 µA to 17 µA when clofibric acid was present during polymerization (Fig. 27a). With sample 9 and 10, prepared under the same conditions, similar currents were obtained (Fig. 27c).

During oxidation of pyrrole, the formation of protons (Fig. 5) could increase the acidity at the electrode interface [132]. This local acidity could lead to the precipitation of undissociated clofibric acid and the formation of non-conjugated

trimers. For carboxylic acids, a decreasing conductivity and limited growth with increasing pK_a has been observed [65] (*c.f.* section 2.2.2).

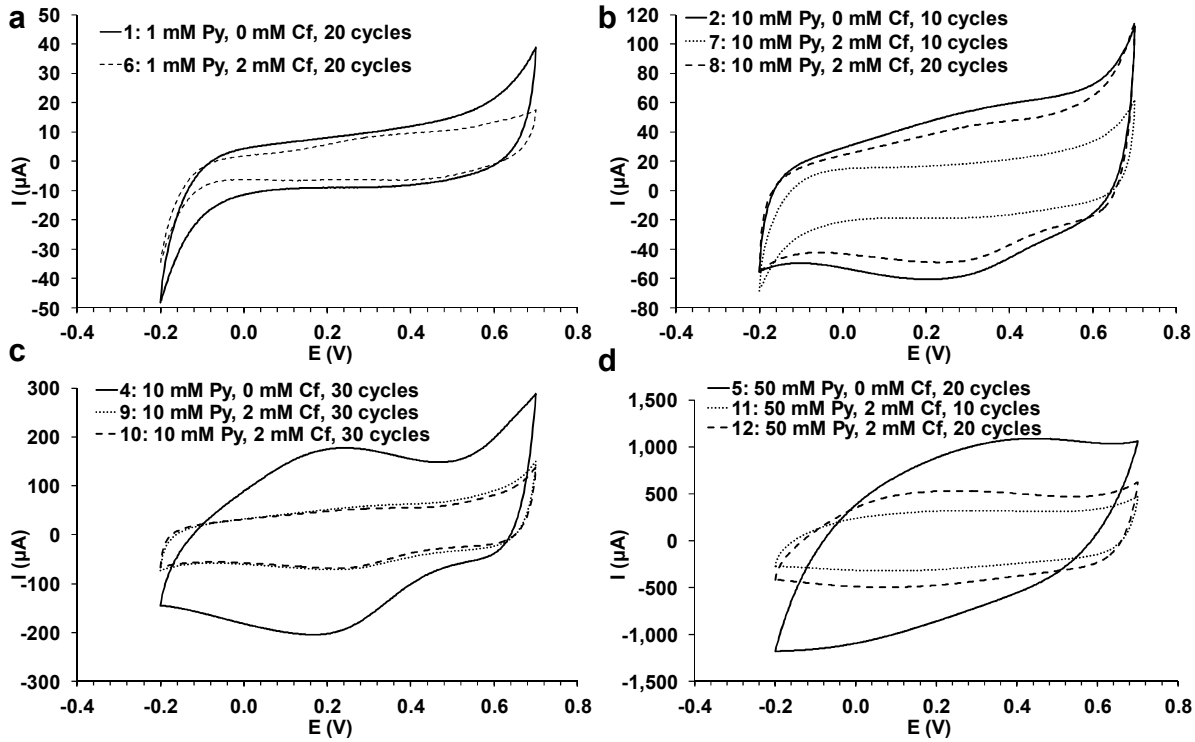

Fig. 27: Cyclic voltammetry of MIP and NIP in KNO_3 solution after polymerization. (a) 1 mM Py; (b),(c) 10 mM Py; (d) 50 mM Py.

5.2.1.2 Electropolymerization on quartz crystals

Pyrrole was polymerized electrochemically on gold coated quartz crystals via cyclic voltammetry (10–50 cycles). The deposition of the polymer can be monitored by QCM, where the quartz crystal connected to a potentiostat is used as working electrode.

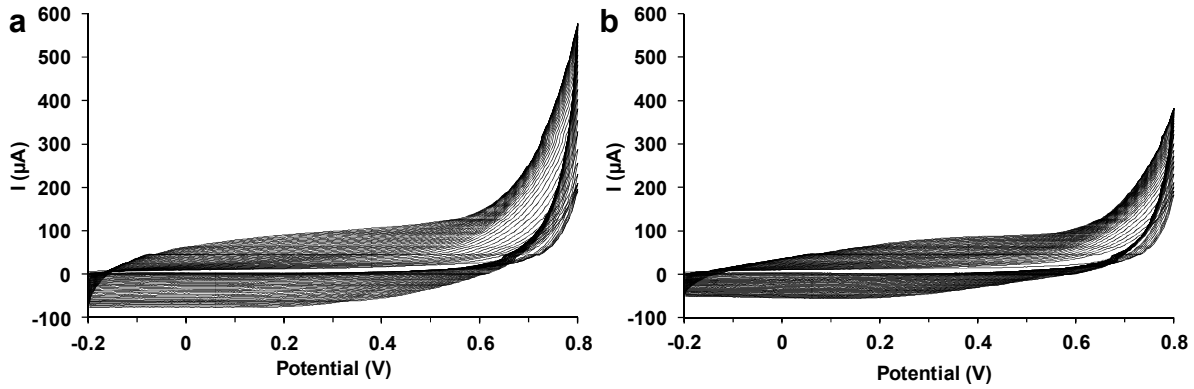

Fig. 28: Polymerization of pyrrole. (a) 10 mM Py in aqueous KNO_3 (100 mM) solution with 40 cycles between -0.2–0.8 V, scan rate 100 mVs^{-1}; (b) 10 mM Py and 0.5 mM clofibric acid in aqueous KNO_3 (100 mM) solution with 40 cycles between -0.2–0.8 V, scan rate 100 mVs^{-1}.

During electropolymerization, an oxidation peak appeared at 0.8 V (Fig. 28). As no reduction peak occurred at the backward scan, the oxidation was irreversible. The first scan showed the highest oxidation peak. The increasing current in the range between 0.2–0.4 V indicated the buildup of polymer. Oxidation peaks were lower when clofibric acid was present in the polymerization solution. The polymerization was also observed by the frequency change of the sensor, which went down with increasing mass on the surface (Fig. 29, Fig. 30). After polymerization, the mass stayed on the sensor and was not washed away by water, KNO_3 or buffer solution. A minor change of frequencies was observed when the solvent was changed, probably due to the viscosity difference.

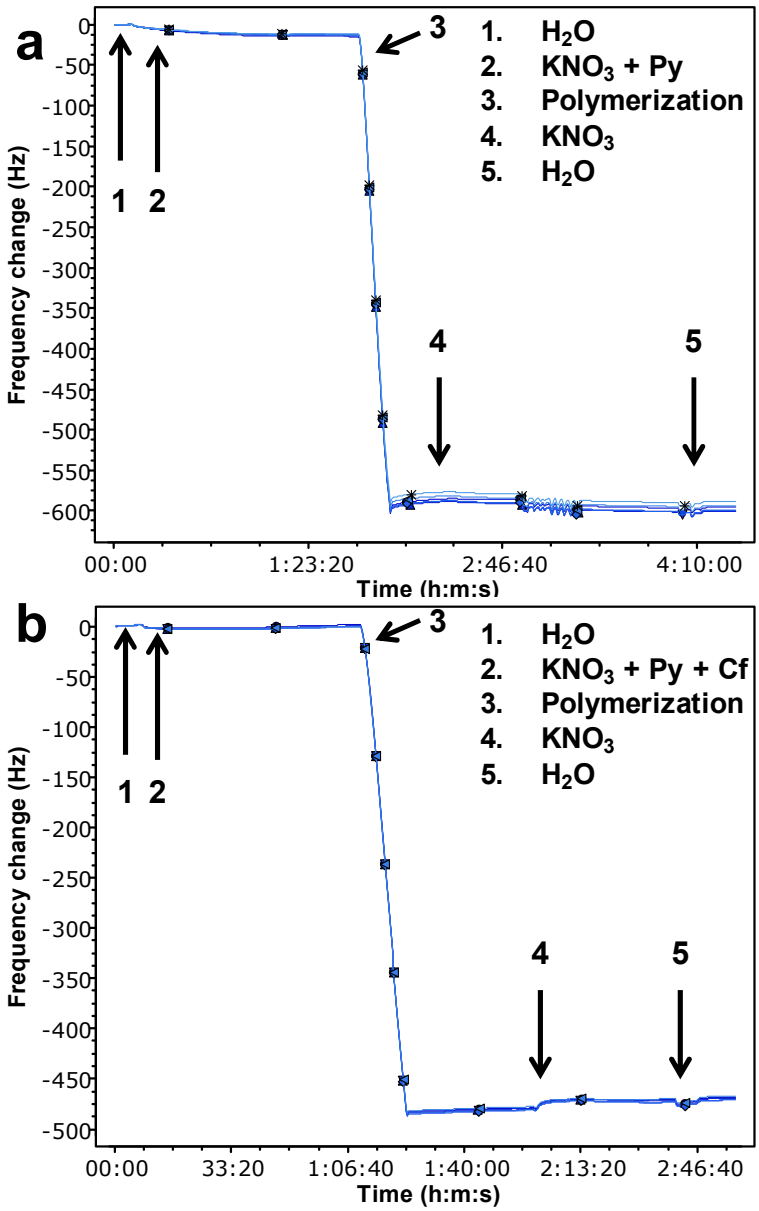

Fig. 29: Frequency change during polymerization of pyrrole with cyclic voltammetry. (a) NIP 20 mM Py, 40 cycles; (b) MIP 20 mM Py, 40 cycles, 1 mM clofibric acid.

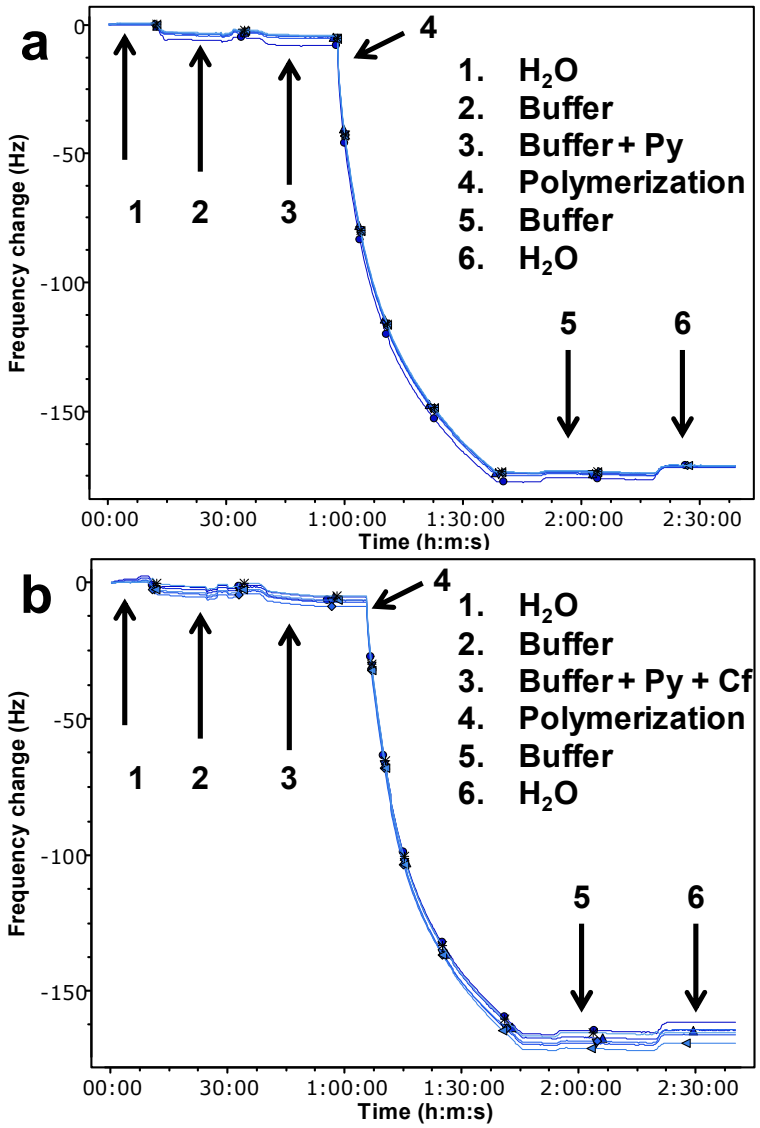

Fig. 30: Frequency change during polymerization of pyrrole with cyclic voltammetry. (a) NIP 40 mM Py, 120 cycles; (b) MIP 40 mM Py, 120 cycles, 1 mM clofibric acid.

Fig. 31 shows cyclic voltammograms recorded after polymerization of 10 mM pyrrole in KNO_3 solution. With increasing cycle numbers between 10–50 cycles during polymerization, the cathodic peak current of the polypyrrole increased from 49 µA to 120 µA for NIPs (Fig. 31a) and from 26 µA to 63 µA for MIPs (Fig. 31b).

For both substrates, the gold coated glass substrates (Fig. 27) and the gold coated quartz crystals (Fig. 31), the electrochemical behavior of MIPs and NIPs was comparable.

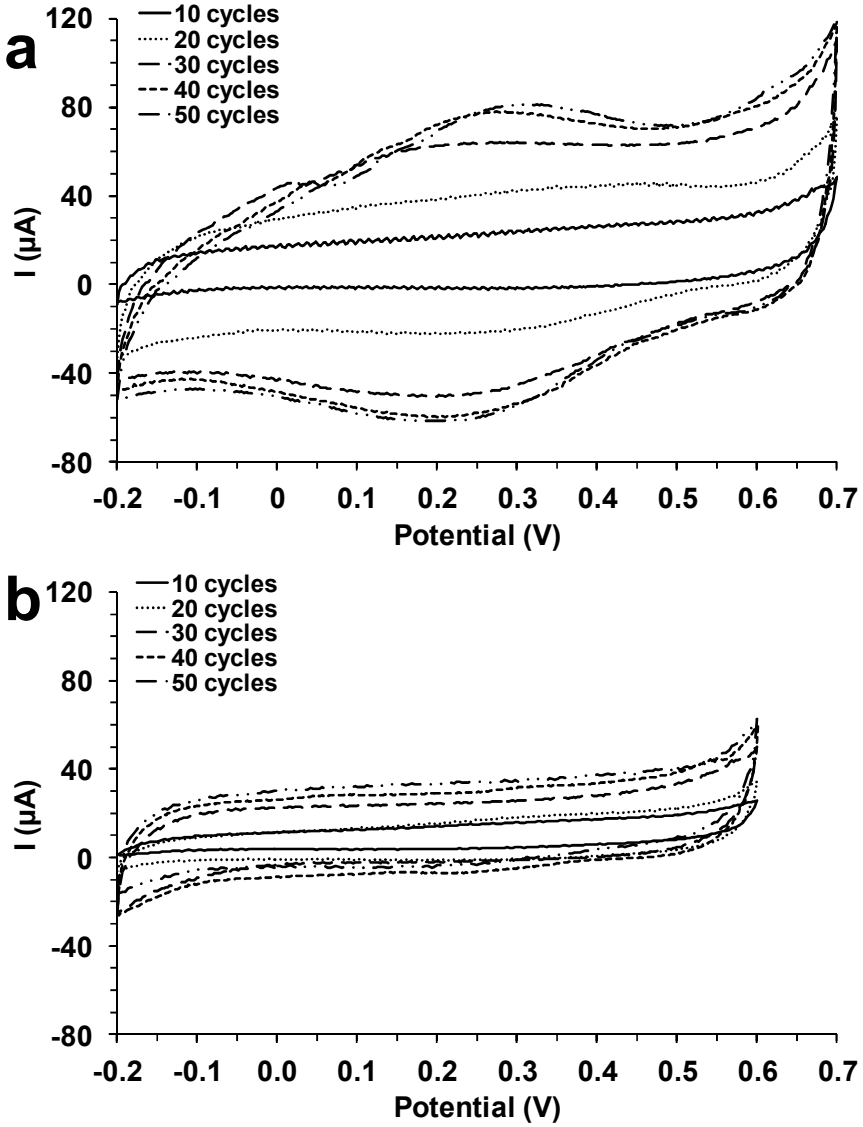

Fig. 31: Cyclic voltammetry of (a) NIP, 10 mM Py; (b) MIP, 10 mM Py, 2 mM clofibric acid.

5.2.1.3 Influence of clofibric acid concentration on polymerization

The influence of clofibric acid on the polymerization of pyrrole was further studied with different amounts of clofibric acid between 0.5–4 mM and compared with NIPs (Fig. 32).

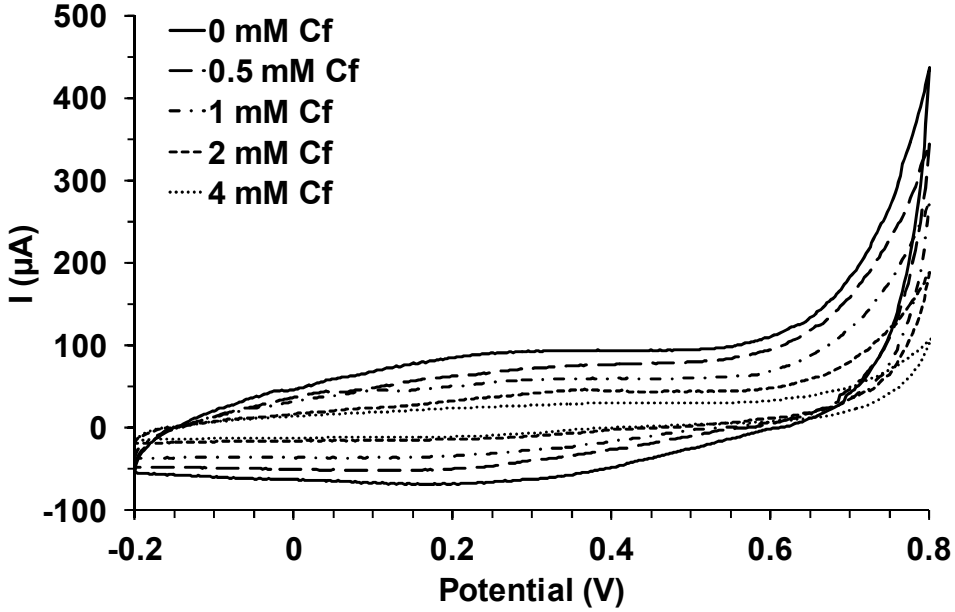

Fig. 32: Cyclic voltammograms recorded during polymerization of pyrrole (10 mM) with clofibric acid (0–4 mM) in KNO_3 (40 cycles).

With increasing amount of clofibric acid present during polymerization, the oxidation peak current decreased. Also the current during the forward and the backward scan decreased with increasing concentration. This indicated inhibited polymerization (*c.f.* section 5.2.1.1) and could also be observed by the QCM data.

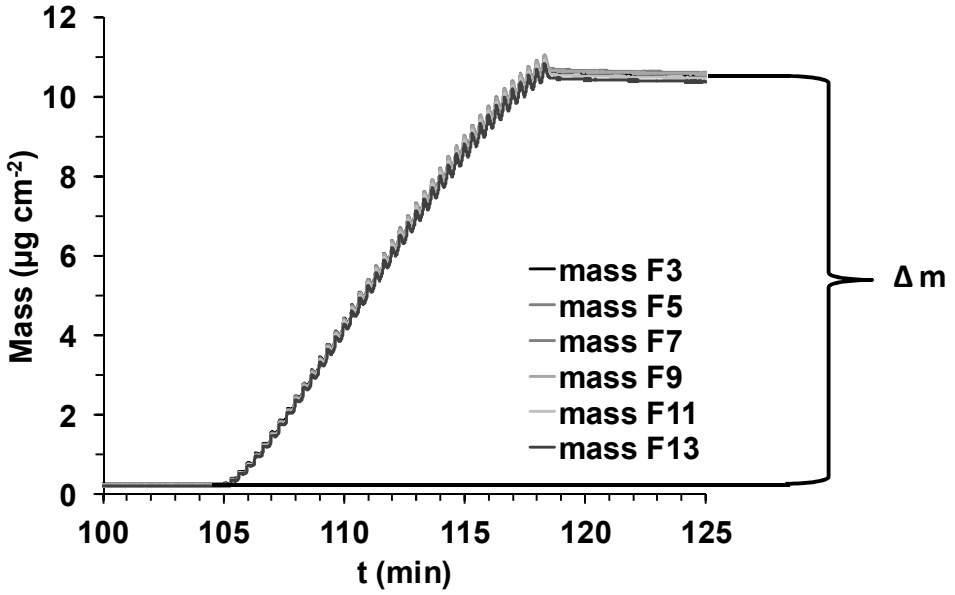

Fig. 33: Calculation of deposited mass.

To obtain the deposited mass, the frequency values were calculated into mass values with the Sauerbrey equation. As the frequencies did not change much when pyrrole-free solvent was pumped into the sensor chamber after polymerization (*c.f.* Fig. 29, Fig. 30, section 5.2.1.2), the mass obtained shortly before polymerization was subtracted from the mass obtained shortly after polymerization (Fig. 33).

Fig. 34 shows the polymer mass on the QCM sensors depending on the number of cycles and the clofibric acid concentration. With increasing cycle number, more and more polymer was deposited on the sensor. At the same time, an increasing concentration of clofibric acid led to less mass deposition.

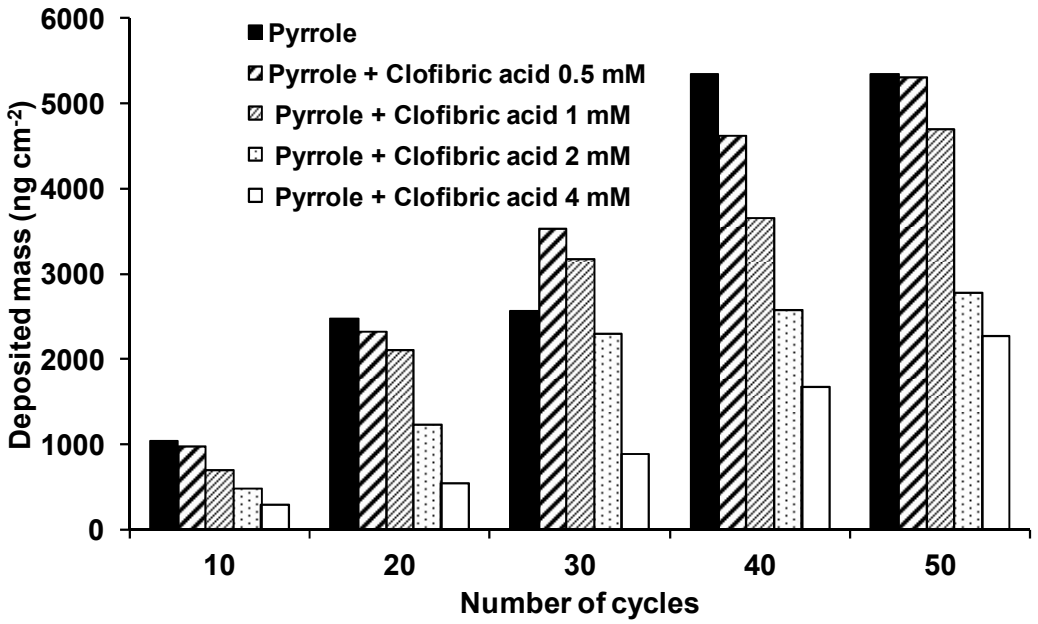

Fig. 34: Deposited mass by polymerization of pyrrole with clofibric acid (0–4 mM) in KNO_3.

For NIPs and MIPs imprinted with 0.5 mM clofibric acid, between 1 µg cm^{-2} (10 cycles)–5.3 µg cm^{-2} (50 cycles) of polymer was deposited on the sensor surface (thickness 7–36 nm). When 1 mM clofibric acid was used, 0.7 µg cm^{-2} (10 cycles)–4.7 µg cm^{-2} (50 cycles) of polymer was deposited (thickness 5–32 nm). With 4 mM clofibric acid, the polymer mass decreased to 0.3 µg cm^{-2} for 10 cycles and to 2.3 µg cm^{-2} for 50 cycles (thickness 2–15 nm). When the pyrrole concentration was increased to 20 mM, masses of 10–13 µg cm^{-2} for NIPs (40 cycles) (69–87 nm) and masses of 9–11 µg cm^{-2} (40 cycles) for MIPs (58–72 nm) were obtained. The highest deposited mass (18 µg cm^{-2}) was reached by using 0.5 mM clofibric acid, 20 mM pyrrole, and 80 cycles (122 nm).

5.2.2 Electroactivity of polypyrrole sensors

The electroactivity was tested by cycling the potential between -0.2–0.6 V in KNO_3 solution with scan rates between 50–500 mV s^{-1}.

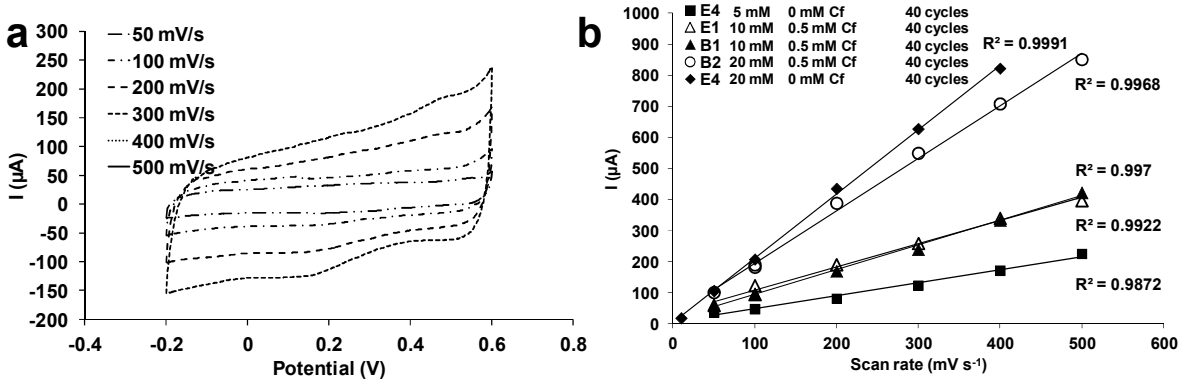

Fig. 35: (a) Cyclic voltammograms with varying scan rates of a sensor prepared with 10 mM pyrrole and 0.5 mM clofibric acid in KNO_3 solution; (b) anodic peak current *vs.* scan rate.

The anodic peak current changed for cyclic voltammograms recorded at different scan rates (Fig. 35). A linear relationship between the anodic peak current and scan rates indicates good electroactivity of the polymer [133]. The polymers showed good electroactivity with R^2 >0.98. MIPs showed lower conductivity than NIPs (B2, E4 in Fig. 35).

5.2.3 Polymerization in buffer solution

As an aqueous solution of pyrrole and clofibric acid has a pH of 3, it was assumed that the reduced polymerization efficiency was caused by the formation of non-conjugated trimers of pyrrole, which inhibit the conductivity through incomplete conjugation [56]. Another possible reason could be the precipitation of undissociated clofibric acid (solubility 583 mg L^{-1} at 25 °C, estimated with EPI Suite v4.11, corresponding to 2.7 mM) at the polymer surface because due to clofibric acid's pK_a of 2.8–3.2, at pH 3 only about 50% of the molecules are dissociated [134,135].

Anionic drugs with low solubility such as diclofenac (4.5 mg L^{-1}) and valproic acid (895 mg L^{-1} at 25 °C) were also found to inhibit the polymerization of polypyrrole [136]. Therefore, the pH of the solution was increased to pH 7 by the use of phosphate buffer solution instead of KNO_3.

Because of the lower conductivity of phosphate buffer due to the lower mobility of the phosphate ions compared to nitrate ions, the mass deposition in buffer solution was much lower than in KNO_3 solution (6–8 µg cm^{-2} in KNO_3 solution, 0.7–1.5 µg cm^{-2} in buffer solution for MIPs). NIPs still had more mass than imprinted polymers

(1.8-2.1 μg cm^{-2}). In electrospray ionization-ion mobility spectrometry experiments, nitrate ions in methanol-water solutions had mobility values of 2.49 $cm^2 V^{-1} s^{-1}$, while for phosphate, hydrogen phosphate, and dihydrogen phosphate values of 1.71, 1.91, and 2.16 $cm^2 V^{-1} s^{-1}$ were found [137]. With a 10 mM pyrrole solution in KNO_3 solution, 4.7 μg cm^{-2} of polypyrrole were deposited on the sensor surface, while with a 40 mM pyrrole solution in phosphate buffer only 2.2 μg cm^{-2} of polypyrrole were formed at the same number of cycles (40). Furthermore, in the presence of clofibric acid, again mass deposition was decreased in most cases compared with NIPs (Fig. 36). For nine MIPs made with 40 mM pyrrole and 120 cycles, 2.7 ± 0.2 μg cm^{-2} (18 ± 1.3 nm) polymer were deposited on the sensor surface according to calculation with the Sauerbrey equation (*c.f.* Table 8). For comparison, with ellipsometry measurements of samples made under the same conditions, thicknesses of 22 ± 1.5 nm were found for MIPs and 23 ± 1.9 nm for NIPs (*c.f.* Fig. 65).

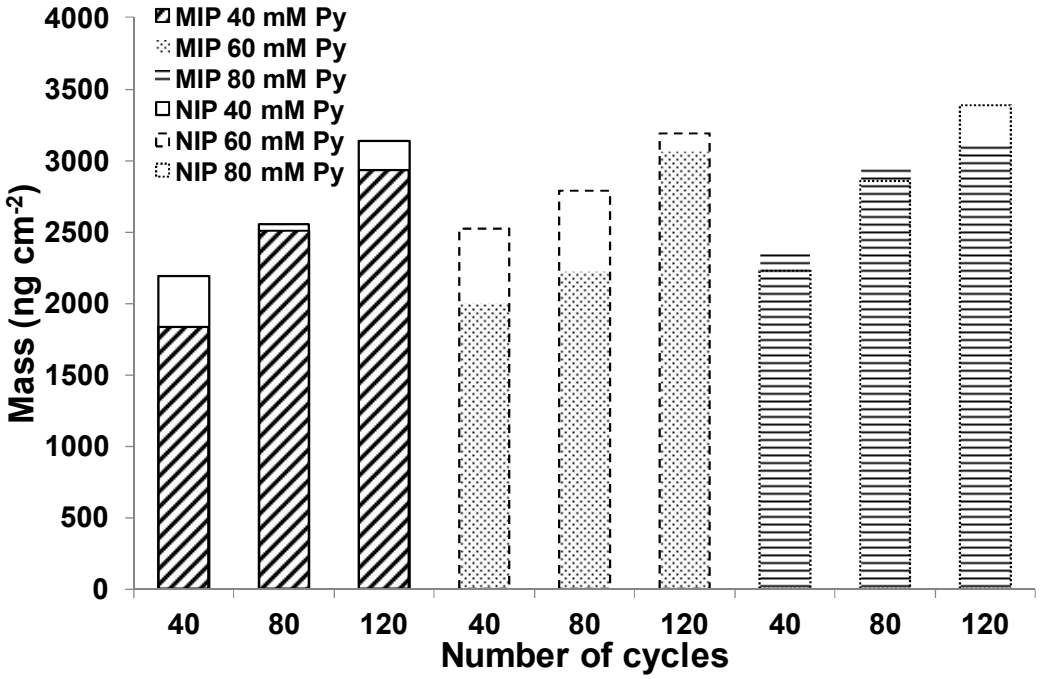

Fig. 36: Deposited mass by polymerization of pyrrole in phosphate buffer (blank columns NIP, filled columns MIP, 1 mM clofibric acid).

It is possible to overoxidize the polymer, which leads to the loss of conductivity through dedoping and the introduction of oxygen containing groups such as carbonyl and carboxyl [77]. On the other hand, overoxidation is viewed as a way to increase the quantity of functional groups that can interact with the template and to stabilize the cavities [73]. Overoxidation was not further studied in this case because delamination of the film from the gold electrode occurred.

5.2.4 Binding experiments

5.2.4.1 Polymerization in KNO_3 and phosphate buffer solution

For binding experiments, pyrrole was polymerized electrochemically on gold coated quartz crystals via cyclic voltammetry in KNO_3 solution and phosphate buffer solution (PBS) (Table 7).

Table 7: Polymerization parameters in KNO_3 and phosphate buffer solution

Sensor	Pyrrole (mM)	Clofibric acid (mM)	Cycles	Solution	Mass (μg cm^{-2})
QCM E4	10	0	40	KNO_3	6.0
QCM B1	10	0.5	40	KNO_3	4.7
QCM B2	20	0.5	40	KNO_3	10.6
QCM E3	20	0	40	KNO_3	12.9
QCM B5	20	0.5	80	KNO_3	18.0
QCM D1	20	0	80	KNO_3	5.8
QCM B1	20	1	40	KNO_3	8.6
QCM E4	20	0	40	KNO_3	10.2
QCM C4*	40	0	80	PBS	2.7
QCM D1*,**	40	1	80	PBS	1.9
QCM C1*	20	0	80	KNO_3	7.4
QCM D2*	20	1	80	KNO_3	12.6
QCM C1**	40	1	80	PBS	2.5
QCM C4**	40	1	40	PBS	1.8
QCM D3**	40	1	80	PBS	2.3
QCM E4**	20	1	40	PBS	1.4
QCM E4**	20	1	40	PBS	1.1

The binding of analytes to molecularly imprinted polypyrrole has been observed before with QCM by several groups [74,78,79]. For an imprinted overoxidized polypyrrole film polymerized with constant current and a film thickness of about 80 nm, a mass change of about 1 μg cm^{-2} was observed for the binding of L-aspartic acid [79] (uptake at constant potential of -0.4 V). For another imprinted overoxidized polypyrrole film polymerized with constant potential and a film thickness of about 120 nm, a frequency decrease of ~220 Hz (1.2 μg cm^{-2}) was observed in the presence of 3 μM dehydrocholate [78] (uptake at constant potential of +0.3 V). Overoxidized polypyrrole films polymerized with constant current and a film thickness of 300 nm for L-glutamic acid imprinted films and 650 nm for D-glutamic acid imprinted films showed mass increases of 9 μg cm^{-2} (L-glutamic acid) and 2 μg cm^{-2} (D-glutamic acid) in the presence of D- and L-glutamic acid when they were polarized between +0.6 V and 0 V [77]. A caffeine imprinted polypyrrole sensor polymerized with constant current with a film thickness of ~2.5 μm showed a linear relationship between the

frequency shift and the logarithm of caffeine concentrations between 0.5 mM and 50 mM (no potential) [74]. Recently, mass increases between 0.2–0.4 µg cm^{-2} in the presence of 1—4 mM caffeine were obtained with a caffeine imprinted polypyrrole sensor polymerized with potential pulses (no potential during binding) [138].

When the sensor surface of polypyrrole polymerized in KNO_3 came in contact with clofibric acid solution, a decrease of the frequencies could be observed (Fig. 37). This could be explained by the uptake of clofibric acid by the polymer. In case of successful imprinting, the response of MIPs should be higher than the response of the corresponding NIP, but in this case the NIP (13 µg cm^{-2}) showed a higher response than the respective MIP (8.6 µg cm^{-2}). A nearly linearly response with a high frequency shift of up to 45 Hz (0.8 µg cm^{-2}) was obtained with the MIP with the highest mass (18 µg cm^{-2}), corresponding to a film thickness of 122 nm.

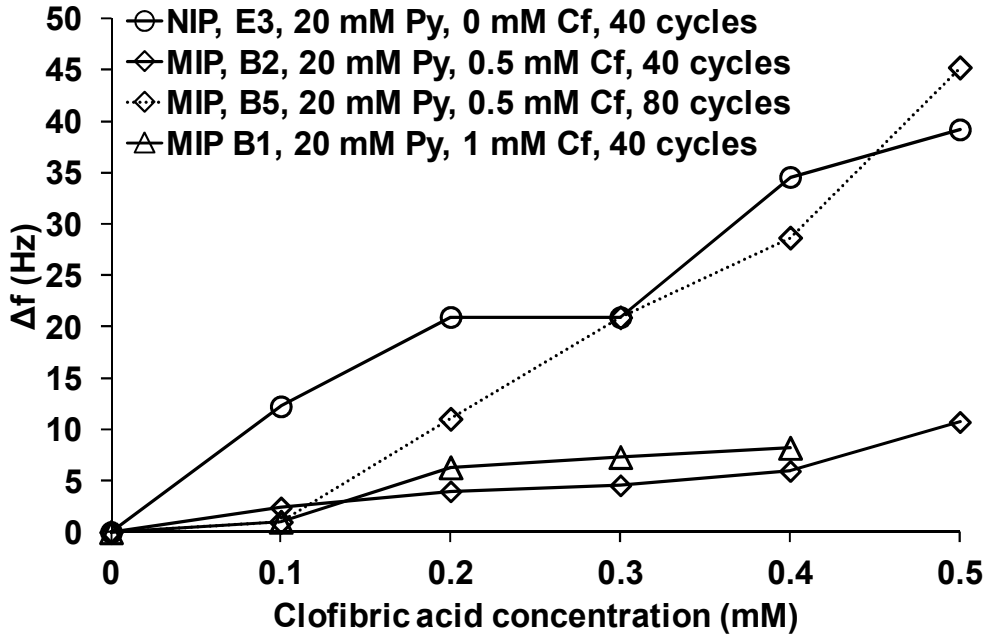

Fig. 37: Frequency shift during binding experiments with MIP and NIP in the presence of clofibric acid.

The sensor response was also tested with polypyrrole polymerized in phosphate buffer solution. A mass increase was observed for MIPs, while for NIPs a mass decrease could be observed (Fig. 38). Fig. 39 shows the sensor response of 6 sensors polymerized with 20 or 40 mM pyrrole and 40 or 80 potential cycles in the presence of clofibric acid. The frequency change was calculated into mass change. For MIPs, the sensor response was lower for polymers made from 20 mM pyrrole with a film thickness of 8–10 nm than for sensors made from 40 mM pyrrole with a film thickness of 13–17 nm. Overall the sensor response obtained with QCM must be considered invalid.

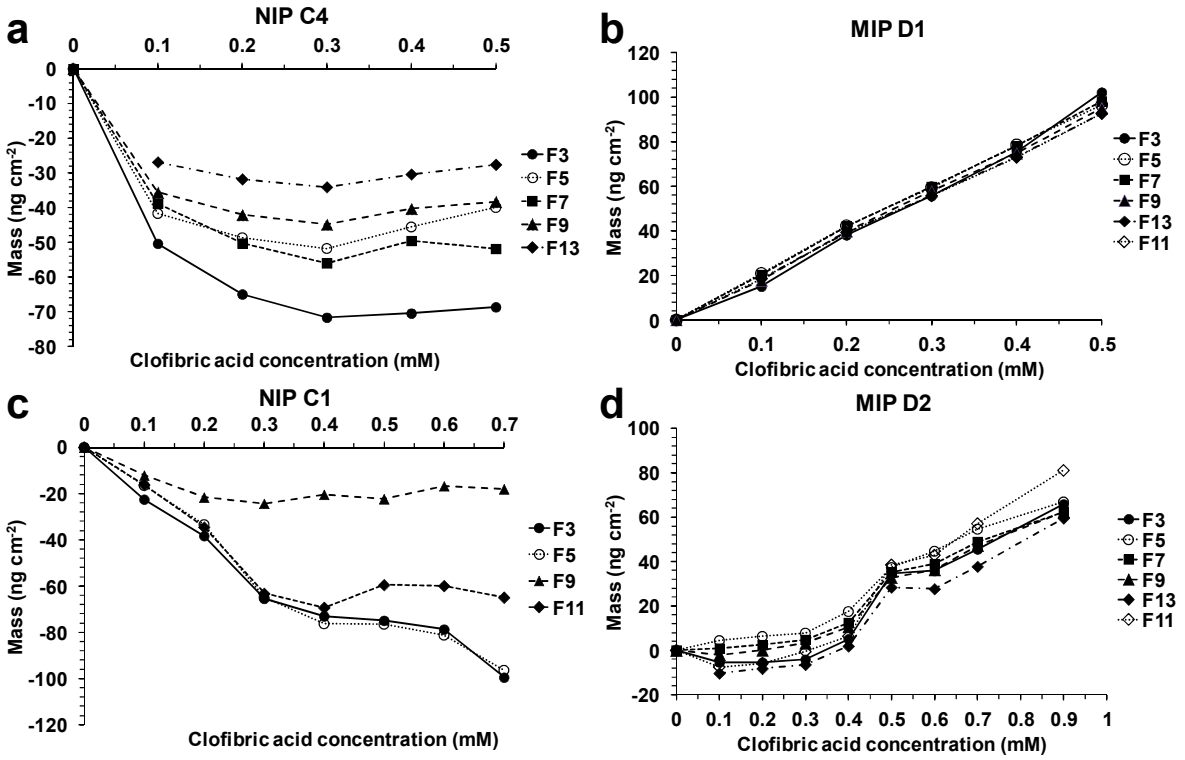

Fig. 38: Mass change during binding experiments with MIP (b),(d) and NIP (c),(d) in PBS with clofibric acid. NIP C4, MIP D1: 40 mM Py, 80 cycles; NIP C1, MIP D2: 20 mM Py, 80 cycles (indicated with * in Table 7).

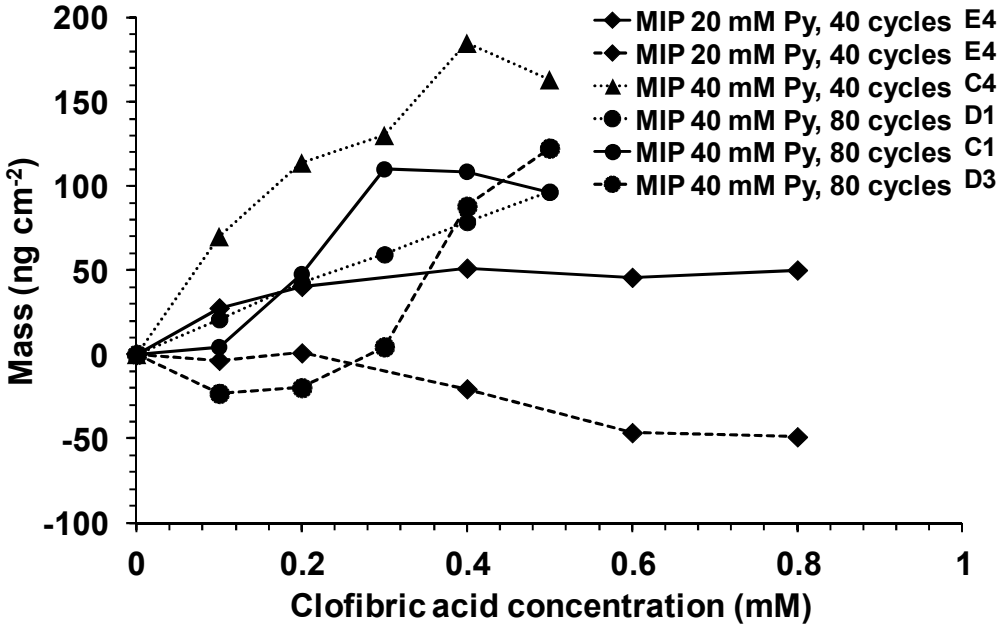

Fig. 39: Mass change of MIPs during binding experiments (samples indicated with ** in Table 7).

A difference to the aforementioned studies is the film thickness, which is in most cases much lower in this study, but even for thicker films no clear difference between MIP and NIP could be obtained. Also overoxidation for increasing the number of functional groups that could interact with the template was not used here due to

delamination (*c.f.* section 5.1.2). Also the polymer film might be too rigid to bind clofibric acid. The use of potential pulses could open up the polymer structure and make more binding sites available. Therefore, PAD was employed again for polypyrrole made in phosphate buffer solution and with clofibric acid as template.

5.2.4.2 Pulsed amperometric detection

The sensor response of polypyrrole films imprinted with clofibric acid was investigated with PAD. Three pyrrole concentrations and three different cycle numbers were chosen for polymerization of MIPs and NIPs (Table 8).

Table 8: Deposited masses of polypyrrole

Pyrrole (mM)	Cycles	Mass (ng cm^{-2})		Thickness (nm)	
		MIP	NIP	MIP	NIP
40	40	1832	2192	12.4	14.8
	80	2508	2552	16.9	17.2
	120	2934	3136	19.8	21.2
60	40	2002	2526	13.5	17.1
	80	2217	2789	15.0	18.8
	120	3059	3187	20.7	21.5
80	40	2369	2226	16.0	15.0
	80	2959	2854	20.0	19.3
	120	3118	3384	21.1	22.9

Table 8 shows the masses which were deposited onto the QCM sensor surfaces for the different polymerization conditions. For calculating the thickness of the polypyrrole coating, a density of 1.48 g cm^{-3} was assumed [51]. With increasing cycle number, more polymer was deposited on the sensors. Doubling the pyrrole concentration from 40 mM to 80 mM increased the thickness slightly for the same number of cycles, ~2 nm for 80 and 120 cycles (Fig. 40). As with polymerization in KNO_3, the mass obtained in phosphate buffer solution was lower in the presence of clofibric acid (MIPs) than without (NIPs). The overall mass obtained in phosphate buffer solution was lower than in KNO_3 solution due to the lower conductivity of phosphate buffer (*c.f.* section 5.2.3).

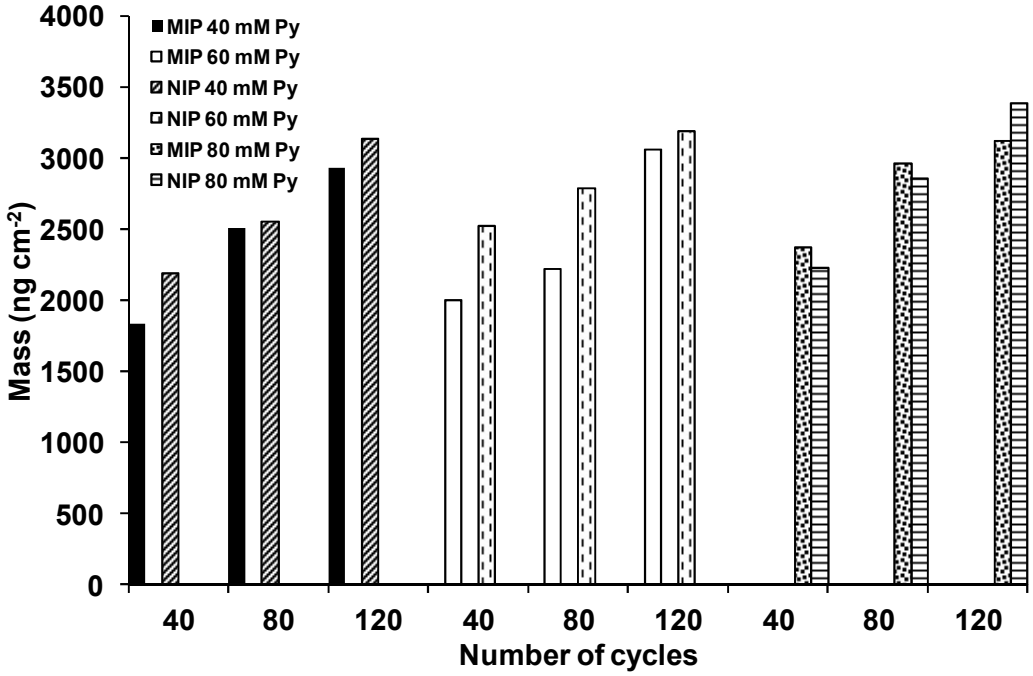

Fig. 40: Mass deposition of polypyrrole for 40, 60, and 80 mM pyrrole.

5.2.4.3 Conditioning of sensors

PAD measurements were performed on gold coated QCM sensors and polypyrrole sensors (40 mM pyrrole) in buffer solution. On gold, the current amplitude of the applied pulses was lower than 100 µA and did not change any more when it reached 50 µA after 15 min (Fig. 41a). On polypyrrole, the current amplitude was at the beginning at 180 µA for a NIP (120 cycles) and at 260 µA for a MIP (240 cycles). A steady state at 100 µA (NIP) and 140 µA (MIP) was reached after 15 min. (Fig. 41b).

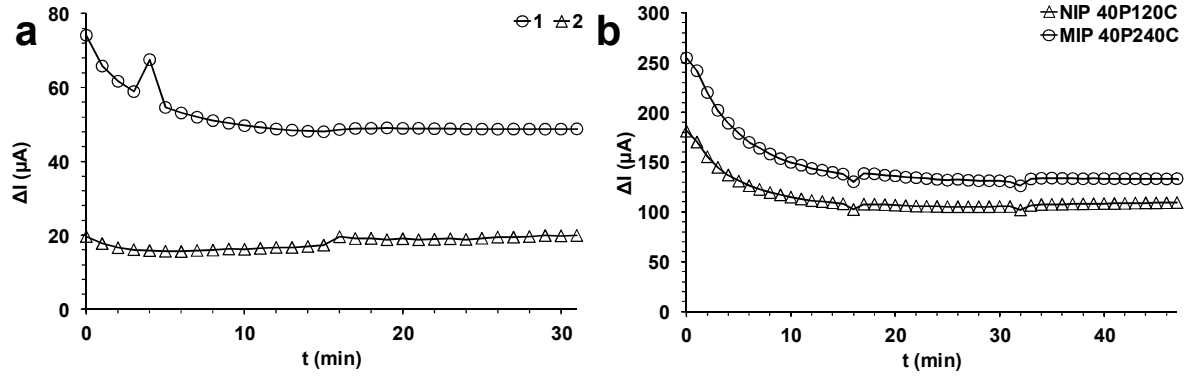

Fig. 41: PAD in buffer solution on (a) gold and (b) polypyrrole.

PAD measurements with clofibric acid solution on the gold surface of a QCM sensor (Fig. 42) showed low I values around 25 µA compared to sensors coated with polypyrrole.

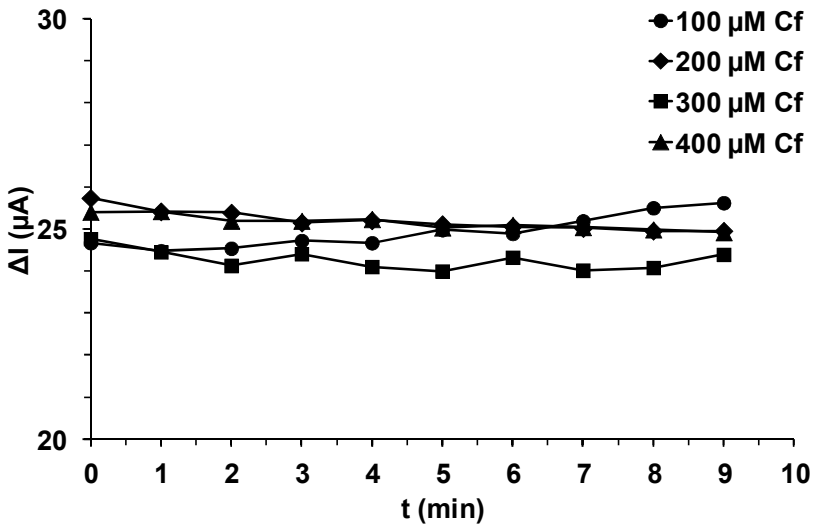

Fig. 42: PAD in clofibric acid solution on uncoated gold sensor.

Part a and c of Fig. 43 show I values and the sensor response of a MIP made from 40 mM pyrrole (40P) and with 80 cycles of cyclic voltammetry (80C); part b and d show the results of the corresponding NIP. The MIP current generally decreased with every potential pulse over 10 minutes. This could be explained with the incorporation of clofibric acid into the polymer. With increasing concentration of clofibric acid, the I values started from lower values. For 100 µM clofibric acid, I values reached 351 µA at the beginning, while with 500 µM I values of 62 µA were obtained. The NIP showed nearly no response to clofibric acid (Fig. 43d).

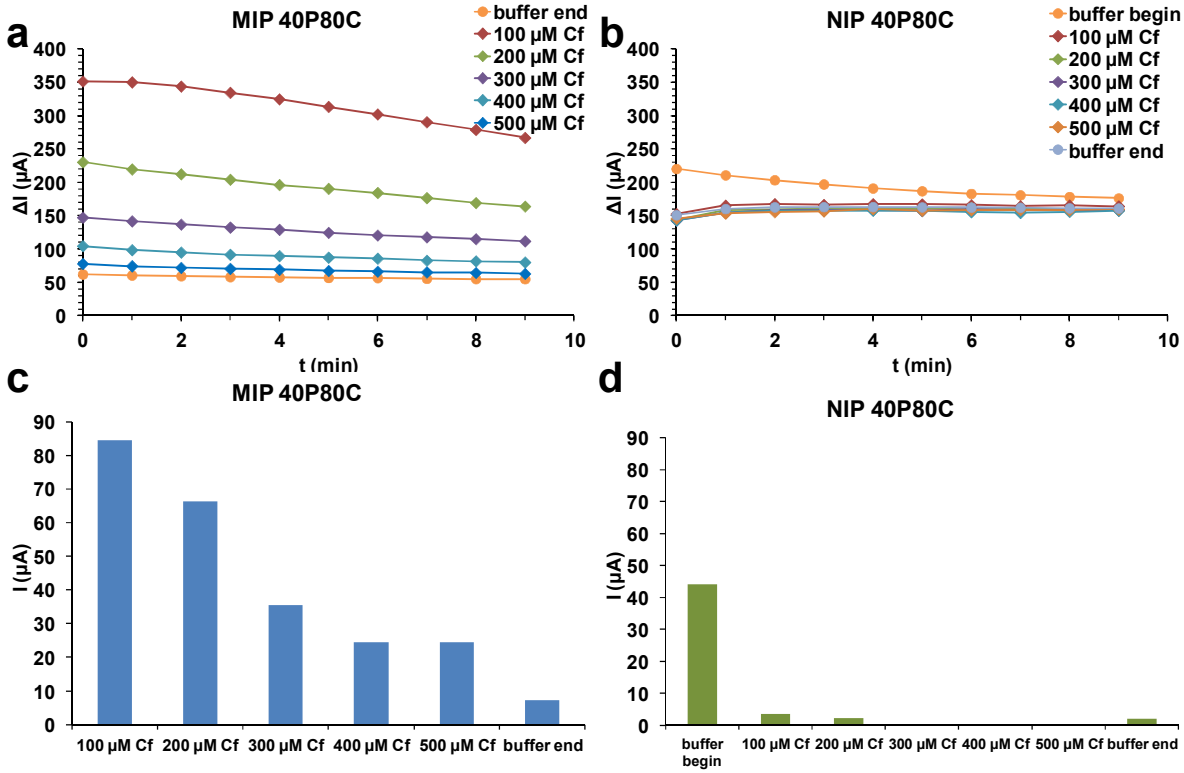

Fig. 43: PAD sensor response to clofibric acid solutions (100–500 µM).

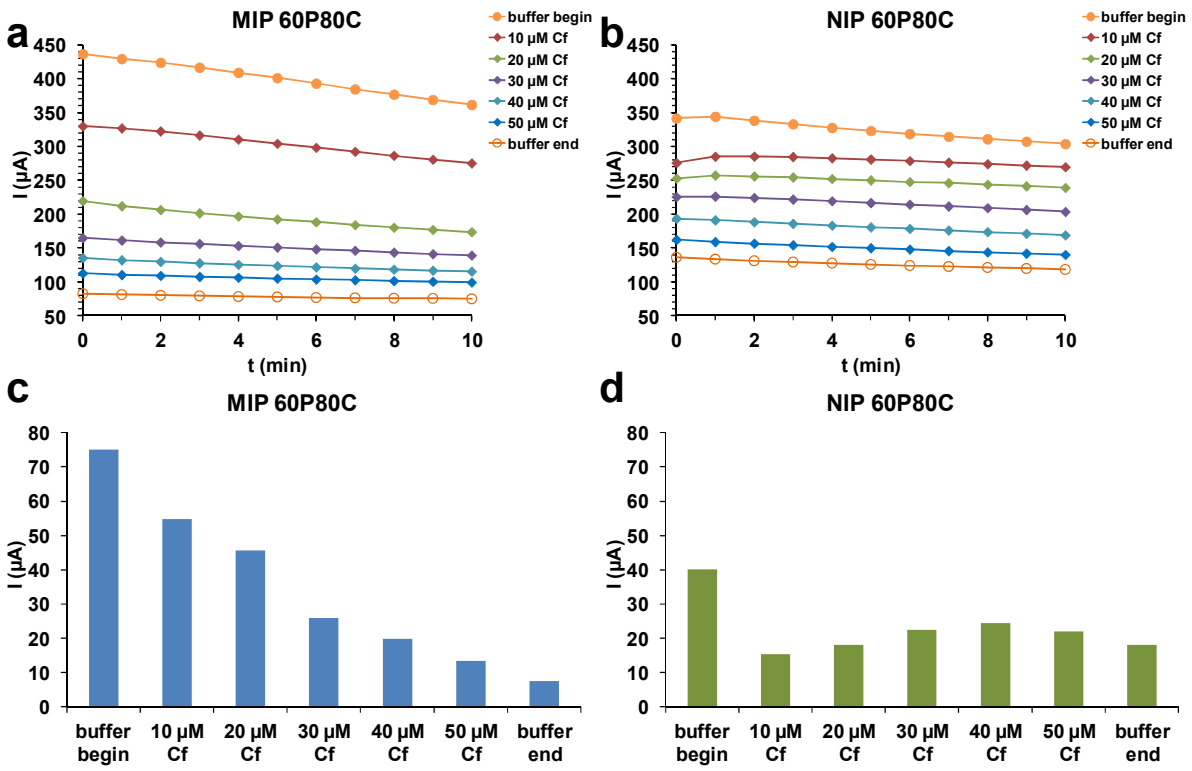

Fig. 44: PAD sensor response to clofibric acid solutions (10–50 µM).

Fig. 44 shows the sensor response of polymers which were made with 60 mM pyrrole and 80 cycles. The MIP showed the same behavior with its decreasing sensor response from 55–8 µA to increasing clofibric acid concentrations as in Fig. 43, while the NIP, contrary to Fig. 43, now also showed a decrease of I values with a sensor response between 15–25 µA on exposure to clofibric acid. A systematic behavior of NIPs was not observed.

For some sensors, a linear decrease could be observed as PAD response in the presence of clofibric acid (10–50 µM), for example, MIP 40P 120C (Fig. 45a) (31-3 µA) and MIP 60P 80C (Fig. 45b) (55–13 µA). But also some NIPs, e.g., NIP 40P 40C with 17–3 µA and NIP 60P 40C with 51—18 µA, showed this behavior (Fig. 45a,b).

Some sensors were also tested with clofibric acid concentrations between 100–500 µM (Fig. 46). A decrease in sensor response to increasing clofibric acid concentrations was observed for MIP 40P 80C from 85–25 µA and MIP 60P 40C from 47–5 µA, while the same sensors showed a low decrease in the response to clofibric acid concentrations between 10–50 µM. MIP 40P 120C showed the reverse behavior with a higher response decrease to clofibric acid concentrations between 10–50 µM than to concentrations between 100–500 µM. The graphs of PAD sensor responses of samples not shown here can be found in the supplementary data section (Fig. S 1–Fig. S 5).

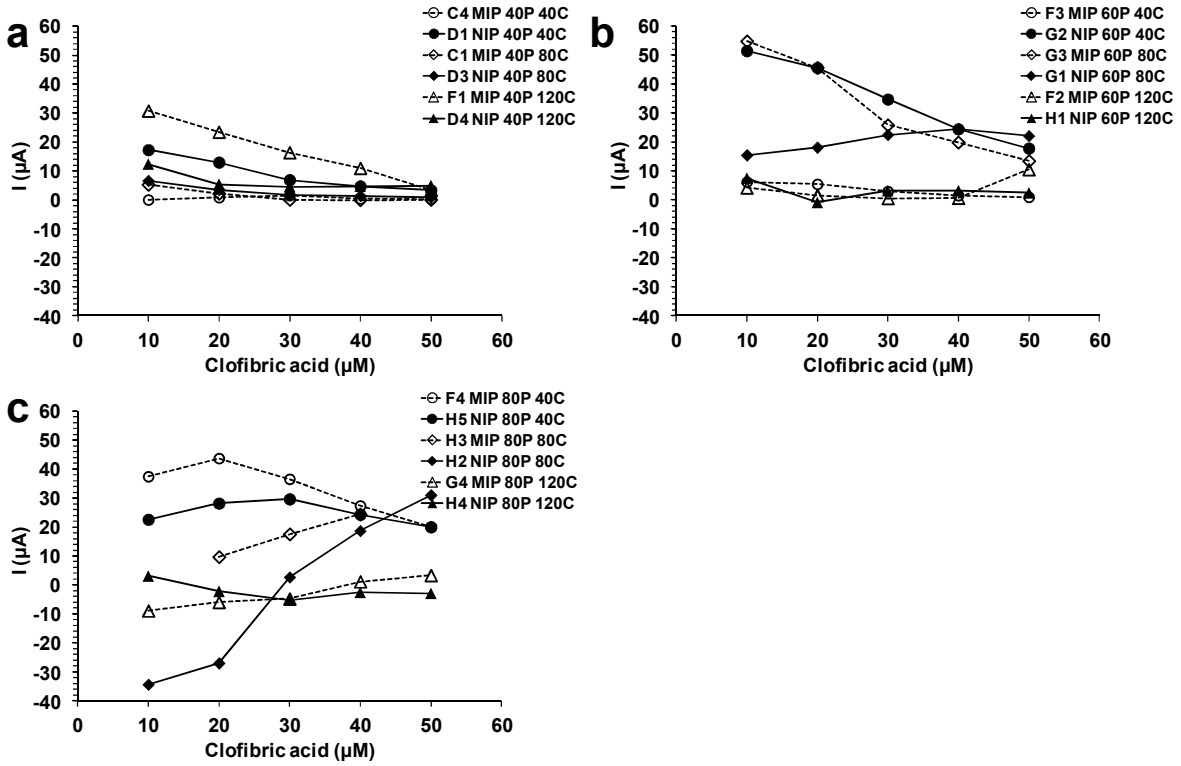

Fig. 45: PAD sensor response of MIP and NIP (40, 60, and 80 mM pyrrole) to 10–50 µM clofibric acid. (a) 40 mM pyrrole; (b) 60 mM pyrrole; (c) 80 mM pyrrole.

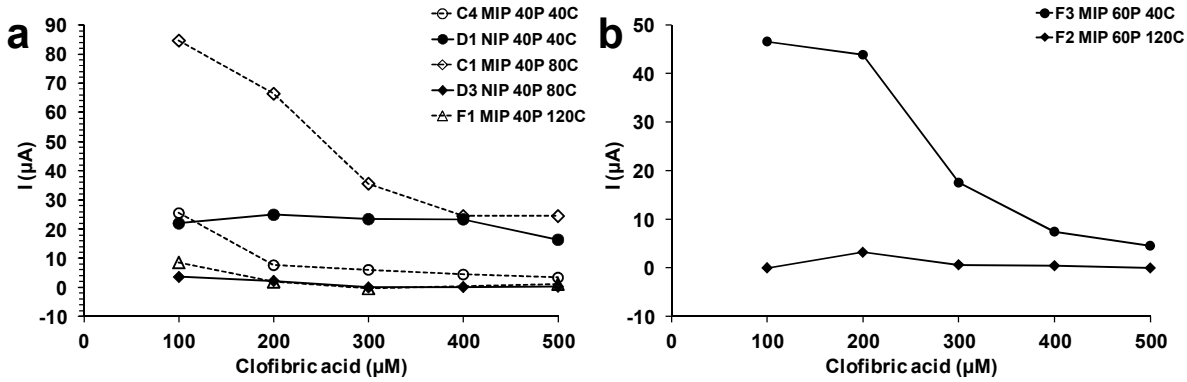

Fig. 46: PAD sensor response of MIP and NIP to 100–500 µM clofibric acid. (a) 40 mM pyrrole; (b) 60 mM pyrrole.

Cyclic voltammetry was performed in buffer solution before and after three series of PAD measurements (Fig. 47a,c,e). There was a noticeable decrease in the current after the polymer had been in contact with clofibric acid. Fig. 47b,d,f shows the respective PAD current responses. In between the experiments, the sensors were washed for 30 min in ethanol under stirring. The current did not increase between the second and the third experiment, which could indicate that clofibric acid was washed out of the polymer only partly. After the third set of PAD measurements, the current had changed in a lesser extent than after the second experiment. Also the

I values were much lower for the third experiment than for the second. It could also be possible that repeated PAD caused degradation of the polymer, which would decrease the conductivity.

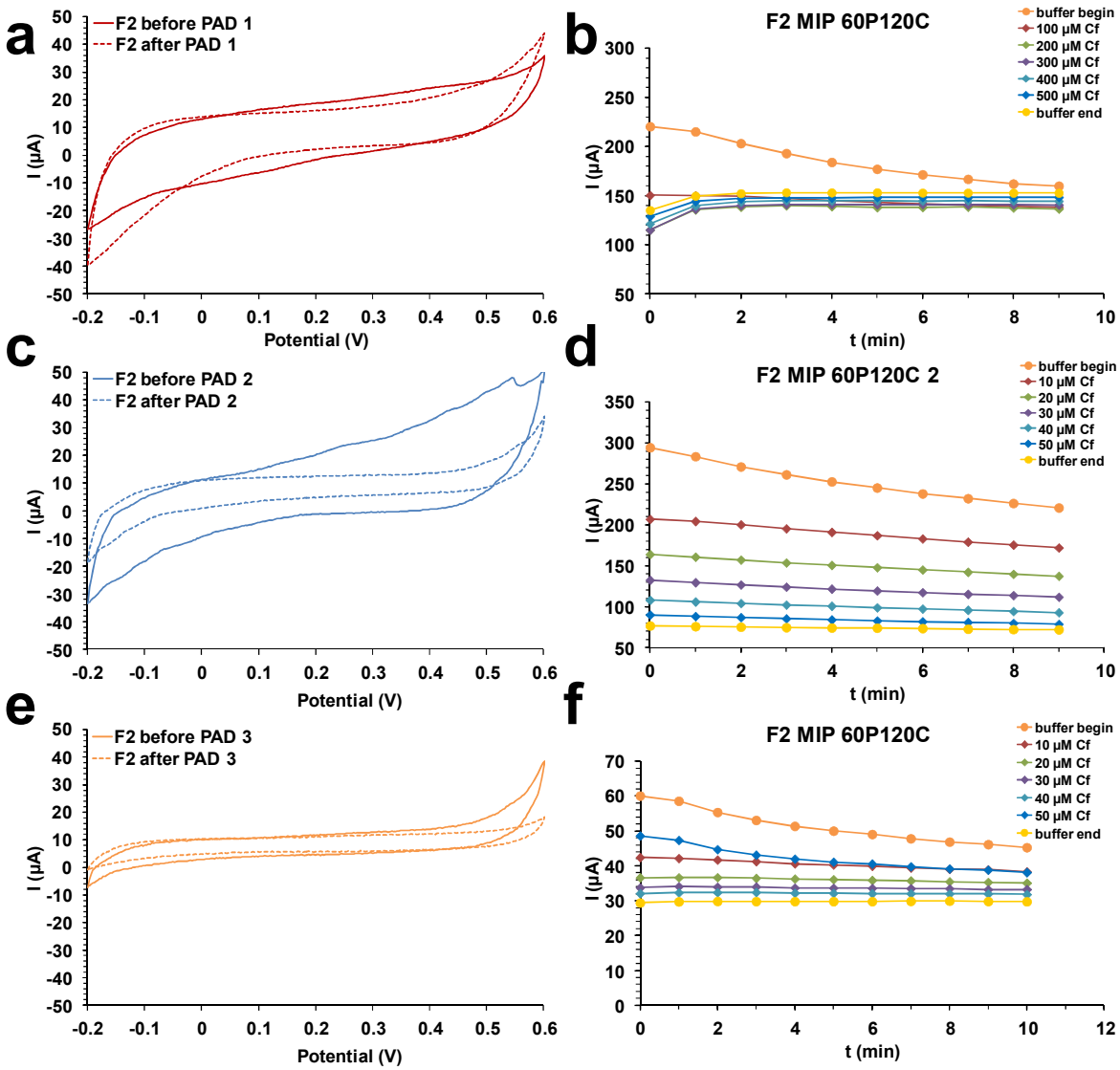

Fig. 47: (a),(c),(e) Cyclic voltammograms before and after PAD measurements; (b),(d),(f) current responses.

5.2.5 Washing procedure

Washing experiments were performed to find a procedure which could remove clofibric acid from the polymer, so that a sensor could be used repeatedly without loss of sensitivity. MIPs were prepared on 11 gold coated quartz crystals in the presence of 1 mM clofibric acid and by cycling the potential between -0.2–0.8 V (Table 9).

Table 9: Polymerization parameters

Sensor	Pyrrole (mM)	Cycles	Mass (ng cm^{-2})	Thickness (nm)
G5	80	80	2832	19.1
H3	80	80	2570	17.4
H1	40	120	2400	16.2
H2	40	120	2740	18.5
H4	40	120	3081	20.8
H5	40	120	2852	19.3
H1	40	120	2721	18.4
H2	40	120	2648	17.9
H1	40	120	2782	18.8
H4	40	120	2611	17.6
H5	40	120	2672	18.0
Standard deviation of mass deposition for 40 mM Py, 120 cycles (9 samples): 6%, 174 ng cm^{-2}				

Table 10: Washing procedures under stirring

	G5	**H3**	**Time**
wash 1	Ethanol /H_2O 70 /30	Ethanol /H_2O 70 /30	2*15 min
PAD 1	10, 30, 50 µM Cf	10, 30, 50 µM Cf	
Wash 2	Methanol /H_2O 70/30	Methanol /H_2O 70/30	2*15 min
PAD 2	10, 30, 50 µM Cf	10, 30, 50 µM Cf	
Wash 3	Ethanol /H_2O 70 /30	Ethanol /H_2O 70 /30	2*15 min
PAD 3	10, 30, 50 µM Cf	10, 30, 50 µM Cf	
Wash 4	Methanol /H_2O 70/30	Methanol /H_2O 70/30	2*15 min
PAD 4	10, 30, 50 µM Cf	Overload	

	H1	**H2**	
Wash 1	Ethanol /H_2O 70 /30	Methanol /H_2O 70/30	2*15 min
PAD 1	10 µM Cf	10 µM Cf	
Wash 2	Ethanol /H_2O 70 /30	Methanol /H_2O 70/30	2*15 min
PAD 2	30 µM Cf	30 µM Cf	
Wash 3	Ethanol /H_2O 70 /30	Methanol /H_2O 70/30	2*15 min
PAD 3	50 µM Cf	50 µM Cf	
Wash 4	Methanol /H_2O 70/30		2*15 min
PAD 4	10 µM Cf		
Wash 5	Methanol /H_2O 70/30		2*15 min
PAD 5	30 µM Cf		
Wash 6	Methanol /H_2O 70/30		2*15 min
PAD 6	50 µM Cf		

	H4	
Wash 1	Ethanol /H_2O 70 /30	2*2.5 min
PAD 1	10 µM Cf	
Wash 2	Ethanol /H_2O 70 /30	2*2.5 min
PAD 2	30 µM Cf	
Wash 3	Ethanol /H_2O 70 /30	2*2.5 min
PAD 3	50 µM Cf	

	H5	
Wash 1	Ethanol /H_2O 70 /30	2*5 min
PAD 1	10 µM Cf	
Wash 2	Ethanol /H_2O 70 /30	2*5 min
PAD 2	30 µM Cf	
Wash 3	Ethanol /H_2O 70 /30	2*5 min
PAD 3	50 µM Cf	
Wash 4	Ethanol /H_2O 70 /30	2*5 min
PAD 4	10 µM Cf	
Wash 5	Ethanol /H_2O 70 /30	2*5 min
PAD 5	30 µM Cf	
Wash 6	Ethanol /H_2O 70 /30	2*5 min
PAD 6	50 µM Cf	

	H1	
Wash 1	Ethanol /H_2O 70 /30	2*15 min
PAD 1	10 µM Cf	
Wash 2	Ethanol /H_2O 70 /30	4*15 min
PAD 2	30 µM Cf	
Wash 3	Ethanol /H_2O 70 /30	4*15 min
PAD 3	50 µM Cf	
Wash 4	Ethanol /H_2O 70 /30	4*15 min
PAD 4	10 µM Cf	
Wash 5	Ethanol /H_2O 70 /30	4*15 min
PAD 5	30 µM Cf	
Wash 6	Ethanol /H_2O 70 /30	4*15 min
PAD 6	50 µM Cf	

	H1	H4	H5	
Wash 1	Ethanol /H_2O 70 /30	Ethanol /H_2O 70 /30	Ethanol /H_2O 70 /30	4*15 min
PAD 1	10 µM Cf	30 µM Cf	50 µM Cf	
Wash 2	Ethanol /H_2O 70 /30	Ethanol /H_2O 70 /30	Ethanol /H_2O 70 /30	4*15 min
PAD 2	10 µM Cf	30 µM Cf	50 µM Cf	
Wash 3	Ethanol /H_2O 70 /30	Ethanol /H_2O 70 /30	Ethanol /H_2O 70 /30	4*15 min
PAD 3	10 µM Cf	30 µM Cf	50 µM Cf	

After PAD measurements with 3 concentrations of clofibric acid, the sensors G5 and H3 were washed alternately with ethanol and methanol for 30 min under stirring. Washing of the sensors H1 and H2 was done after PAD with a single concentration of clofibric acid. The concentration of clofibric acid was increased in the next measurement. Sensor H4 was washed for 5 min between measurements. Sensor H5 was washed for 10 min between measurements. The washing time was extended to

1 h for H1 and H2. For PAD measurements with H1, H4, and H5 always the same concentration of clofibric acid for one sensor was used (Table 10).

During washing of G5 with ethanol and methanol, the I values during PAD measurements decreased after every wash (Fig. 48b). During cyclic voltammetry, there was a noticeable decrease in the current after PAD with clofibric acid (Fig. 49b). The current increased after the second washing (wash 1 MeOH), but after the third and fourth washing no significant current increase could be observed (Fig. 49a). The response of H3 resembled the response of G5 (Fig. S 6a). When sensors were washed in between PAD with increasing concentration of clofibric acid (H1, H2) with ethanol or methanol, the response to 10 µM clofibric acid was lower than to 30 µM clofibric acid, but higher than to 50 µM clofibric acid after the third wash (Fig. S 6b,c). It was assumed that clofibric acid was not washed out of the polymer properly. Another possibility could be a degradation or oxidation of the polymer structure with repeated PAD measurements, which would decrease the conductivity. The washing procedure could not be improved by the use of methanol.

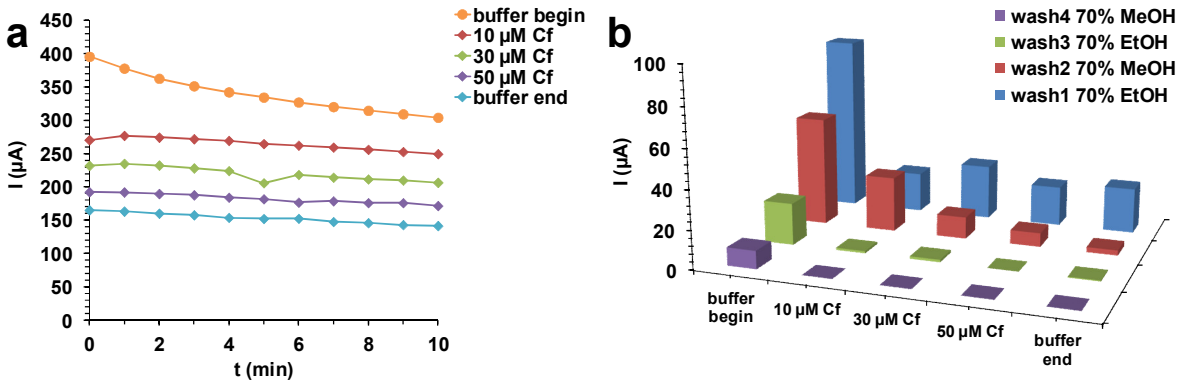

Fig. 48: (a) I values and (b) PAD sensor response of sensor G5 (MIP 80P 80C) after washing with 70% ethanol and 70% methanol.

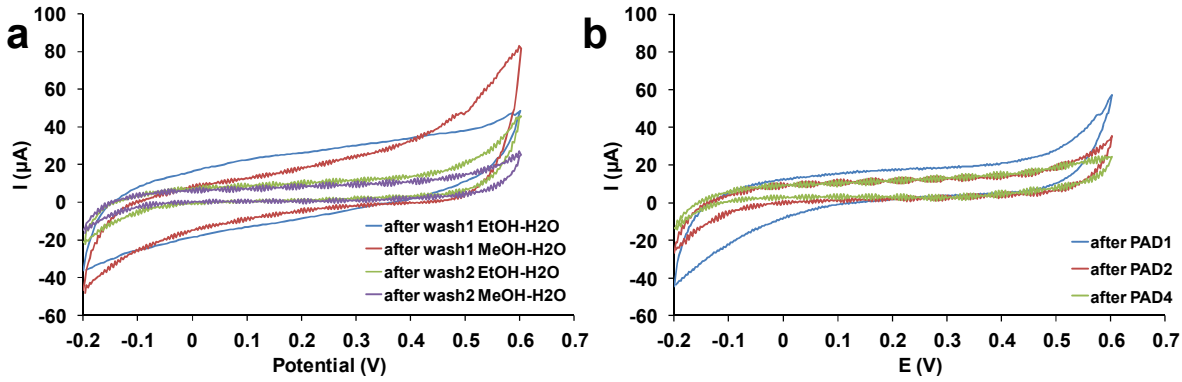

Fig. 49: Cyclic voltammograms of sensor G5 in phosphate buffer solution after (a) washing with 70% ethanol and 70% methanol and (b) after PAD.

To see if the washing conditions were too harsh for the polypyrrole coating, the washing time was reduced to 5 min (Fig. 50). With 5 min washing the sensor response to clofibric acid (Fig. 50b) increased from the first (15 µA) to the second wash (25 µA) and decreased after the third wash (4 µA) similar to H1 and H2 with 30 min washing. It was assumed that a 5 min wash was too short.

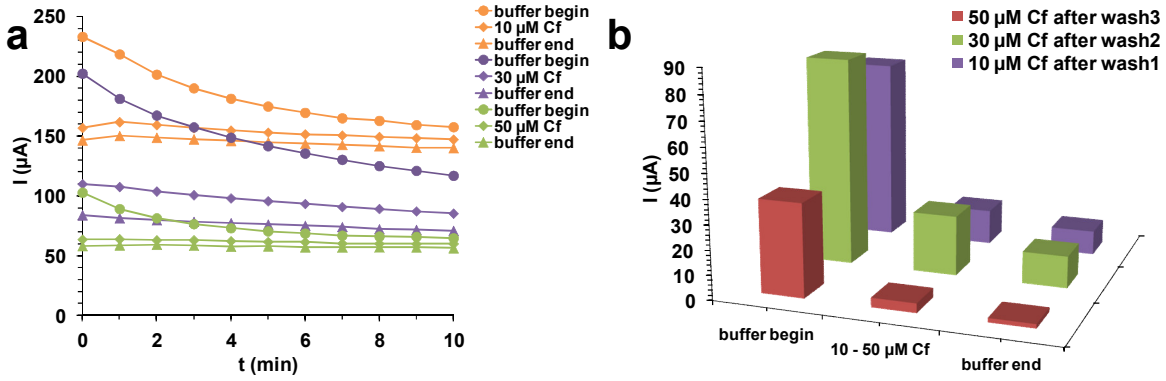

Fig. 50: PAD measurements of sensor H4 after washing for 5 min.

H5 was washed for 10 min between measurements. Here the same behavior as with H4 could be observed. The sensor response to clofibric acid increased from 3 µA after the first wash to 19 µA I after the fourth wash and decreased again after the fifth and sixth wash to 2 µA (Fig. S 6d).

The washing time was extended to 1 h. For H1 the sensor response was very low in buffer solution with 7 µA after the first wash (Fig. 51). This value increased after the second wash and remained between 30–35 µA until after the fourth wash. The response to clofibric acid solutions also increased from 1 µA after the first wash to 9 µA after the third wash and the decreased again to 2 µA (sixth wash).

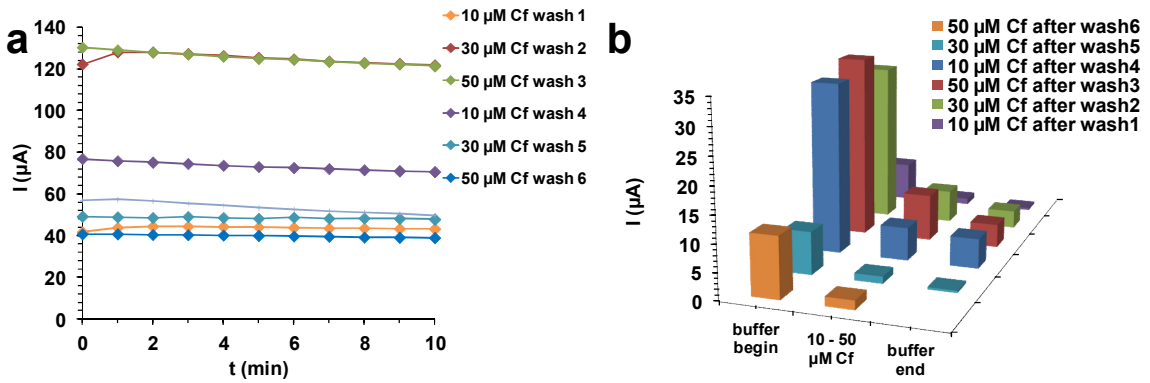

Fig. 51: I values (a) and PAD sensor response (b) of sensor H1 (MIP 40 mM Py, 120 cycles) after washing with 70% EtOH for 1 h.

The next experiments were also performed with 1 h washing, but this time the sensors were always in contact with the same concentration of clofibric acid between

washing (Fig. 52). Sensor responses in buffer solution were high after first and second wash (120–80 µA for H1, 70–80 µA for H4, 90–100 µA for H5) and decreased afterwards (50 µA, 40 µA, and 60 µA for H1, H4, and H5). The sensor response of the three sensors to clofibric acid was always the highest after the second wash (Table 11, Fig. 52a,c,e). Also with 1 h washing, the sensors could not be used repeatedly and also did not distinguish between different concentrations of clofibric acid.

Table 11: Sensor response to clofibric acid after 1 h wash

	Clofibric acid (µM)	Wash1 ΔI (µA)	Wash2 ΔI (µA)	Wash3 ΔI (µA)
H1	10	24	41	9
H4	30	15	25	4
H5	50	17	46	18

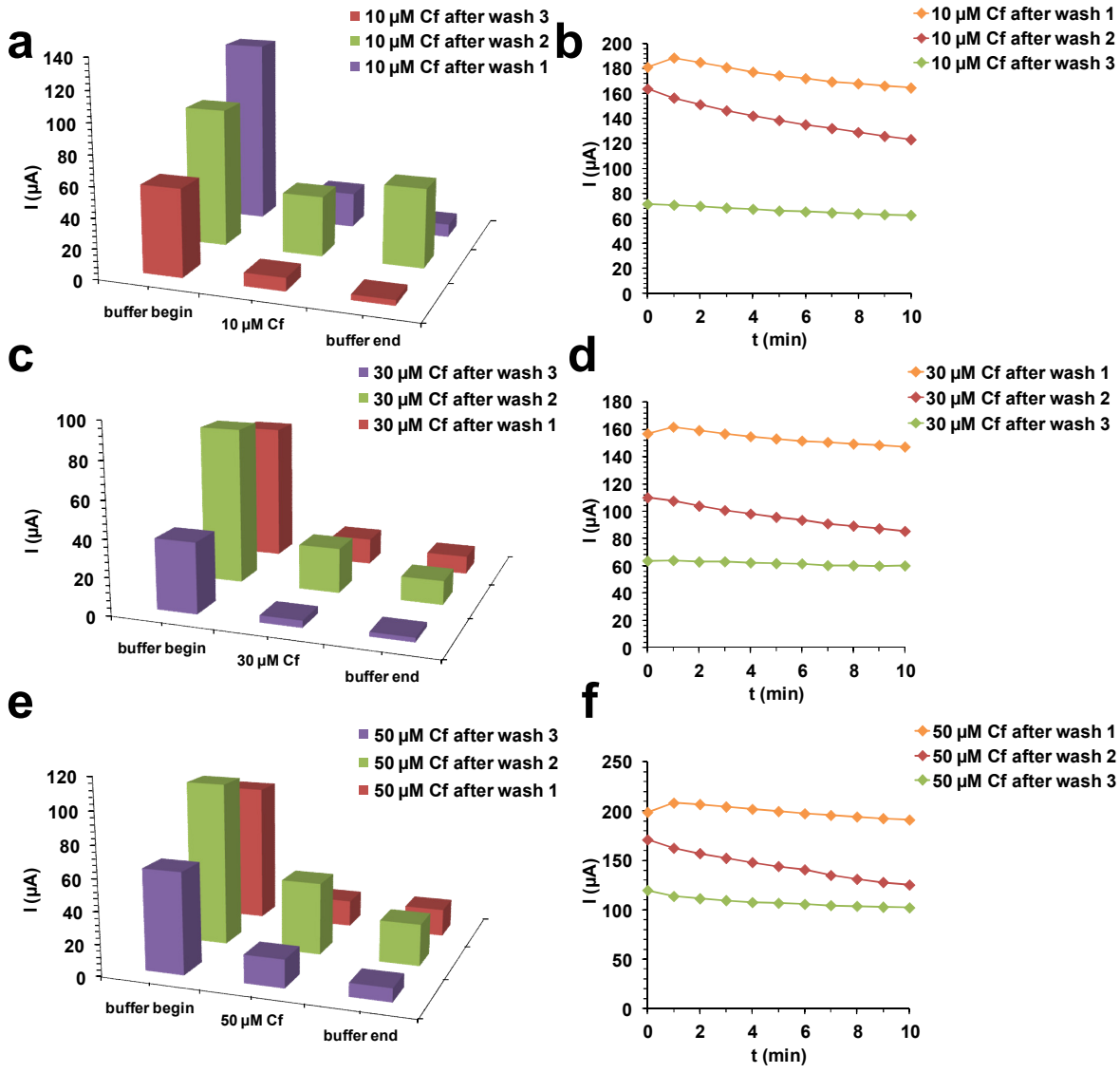

Fig. 52: PAD measurements of sensor H1, H4, and H5 after washing for 1 h (MIP 40 mM Py, 120 cycles).

5.2.6 Application of PAD during washing

It was tested if the application of PAD during washing could increase the sensor response. PAD washing for 15 min was compared with washing under stirring with a 1:1 mixture of ethanol and HCl/KCl (pH 2) (Table 12). To prevent precipitation in the narrow channels of the electrochemical flow cell, the ethanol content was reduced to 50%. After washing, binding tests were done with 30 µM clofibric acid.

Table 12: Washing procedures

PAD wash	Stirring
PAD Wash1	Wash1
PAD 30 µM Cf 1	PAD 30 µM Cf 1
PAD Wash2	Wash2
PAD 30 µM Cf 2	PAD 30 µM Cf 2
PAD Wash3	Wash3
PAD 30 µM Cf 2	PAD 30 µM Cf 3

	Sensor	Polymer	Wash method	Mass (ng cm^{-2})	Thickness (nm)
1	G1	MIP	PAD	2948	19.9
2	G2	MIP	stirring	2864	19.3
3	I3	NIP	stirring	2562	17.3
4	I4	NIP	PAD	2863	19.3
5	I5	NIP	PAD 0.5 s	2911	19.7
6	J2	MIP	PAD 0.5 s	2676	18.1
7	H1	NIP	PAD	2972	20.1
8	H2	MIP	PAD	2835	19.2

The I values of MIP (G1) and NIP (I4) decreased the most for a pulse time of 1 s during the first PAD washing (Fig. 53). The decrease was lower during the second and third wash. MIP G1 showed a gradual decreasing sensor response, while the NIP showed nearly no response during the second and third wash. A shorter pulse length of 0.5 s at 0.6 V gave much lower current values (Fig. 54a,c) and sensor responses (Fig. 54b,d) of MIP and NIP compared to a pulse length of 1 s.

The highest response to 30 µM clofibric acid with 53 µA was obtained with PAD washing and a pulse length of 1 s. Additionally, this high response occurred already after the first washing (Fig. 55), while for NIP (16 µA), for MIP (51 µA) and NIP (22 µA) under stirring (Fig. 57), and for MIP (6 µA) and NIP (9 µA) with a shorter pulse length (Fig. 56) the highest sensor response occurred after the second wash. With additional samples (H1, H2), the highest current response to clofibric acid also

occurred after the first PAD wash (Fig. S 7). Therefore, PAD wash was used for the following experiments.

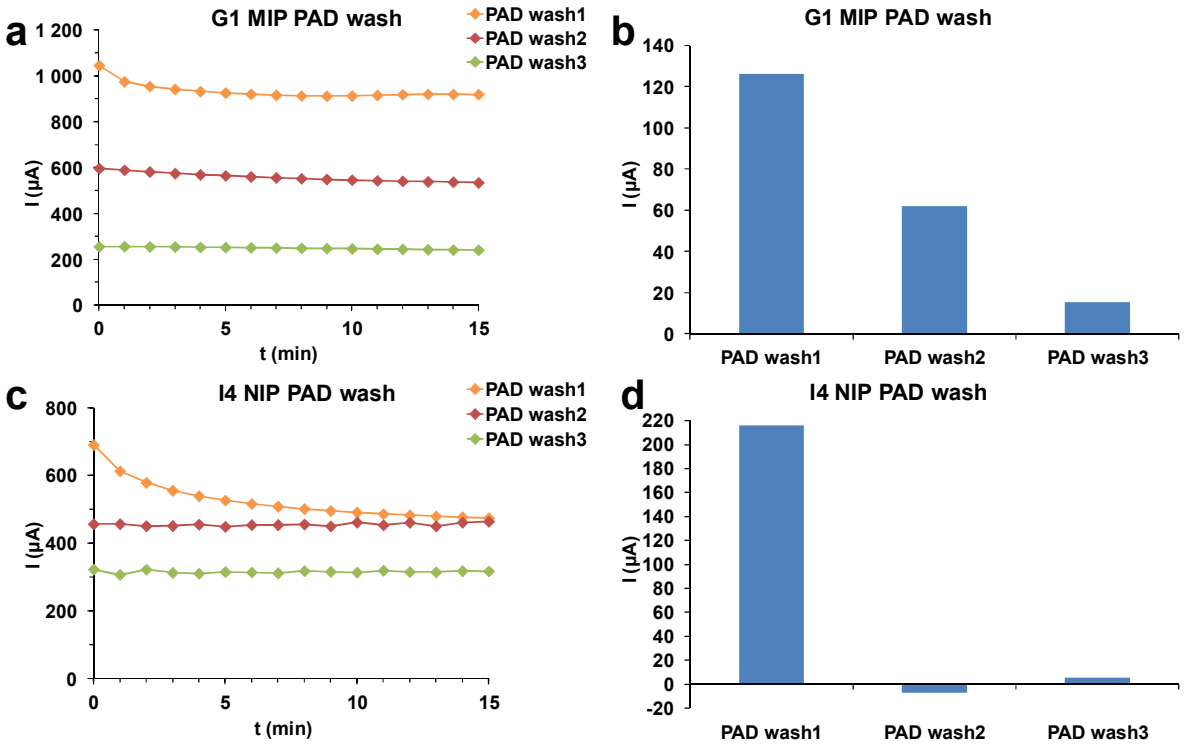

Fig. 53: PAD washing of MIP G1 and NIP I4 (pulse time 1 s).

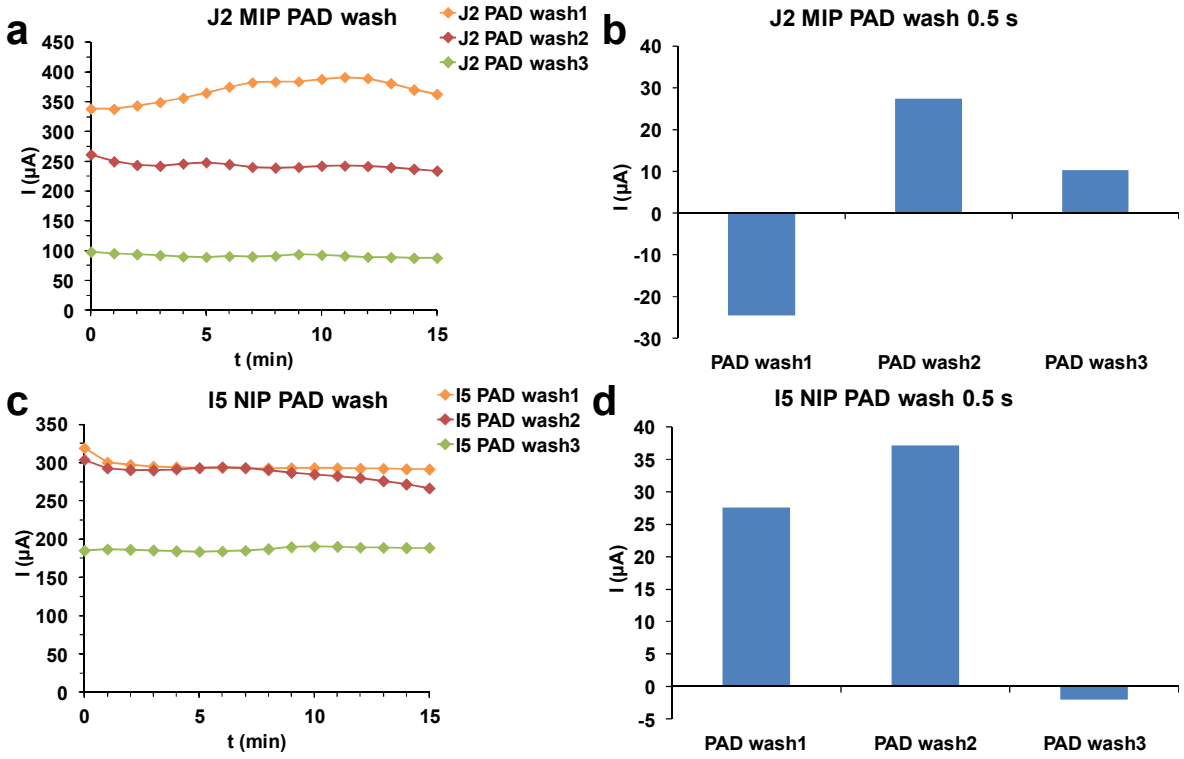

Fig. 54: PAD washing of MIP J2 and NIP I5 (pulse time 0.5 s).

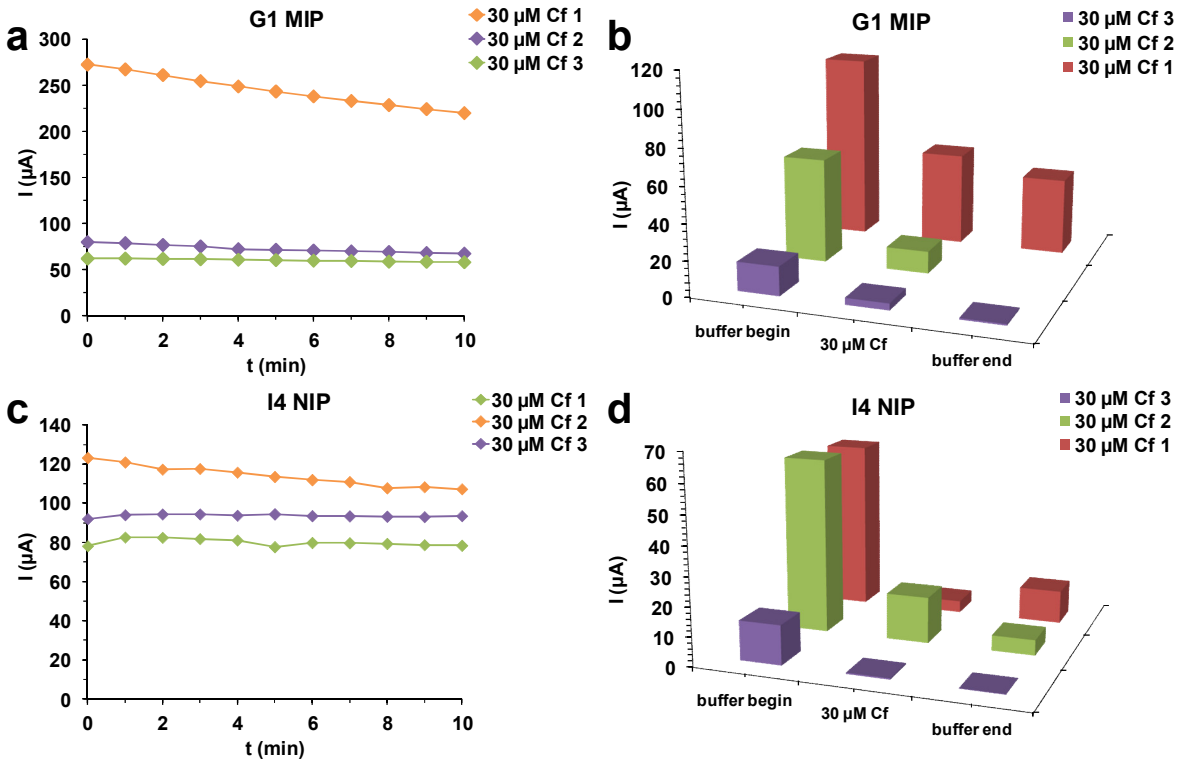

Fig. 55: I values (a),(c) and PAD sensor response (b),(d) after PAD wash of MIP G1 and NIP I4.

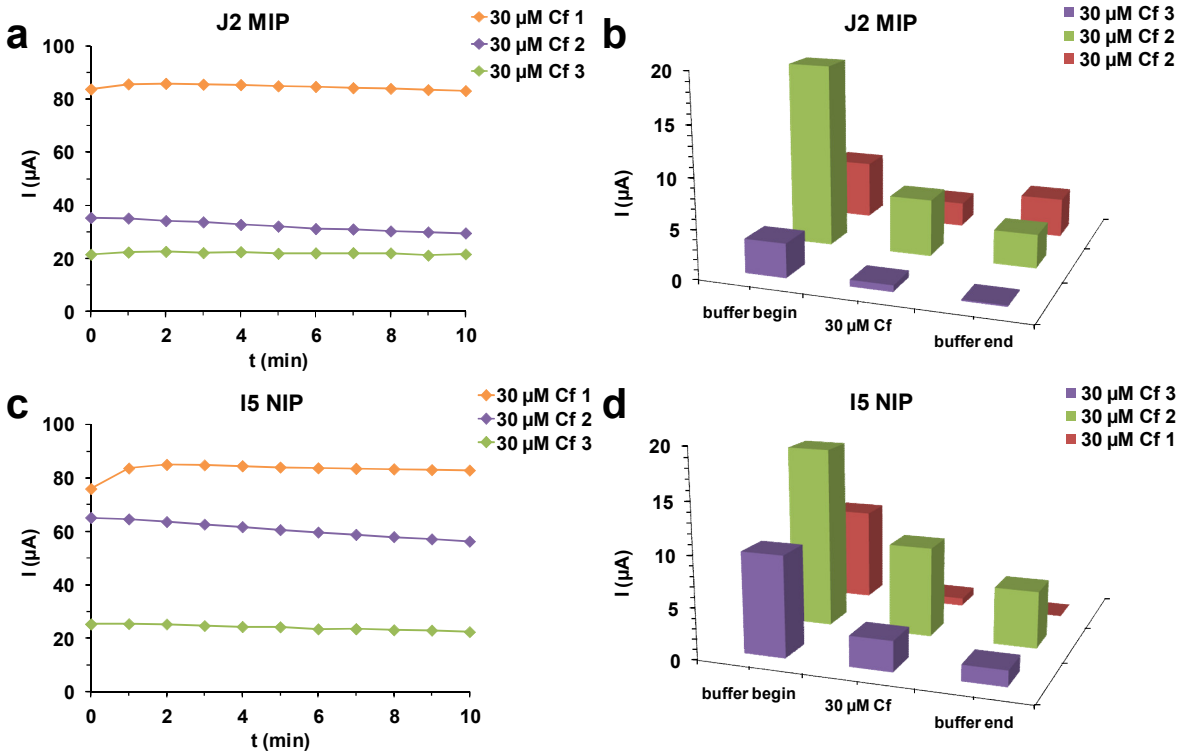

Fig. 56: I values (a),(c) and PAD sensor response (b),(d) after PAD wash of MIP J2 and NIP I5 with a pulse length of 0.5 s.

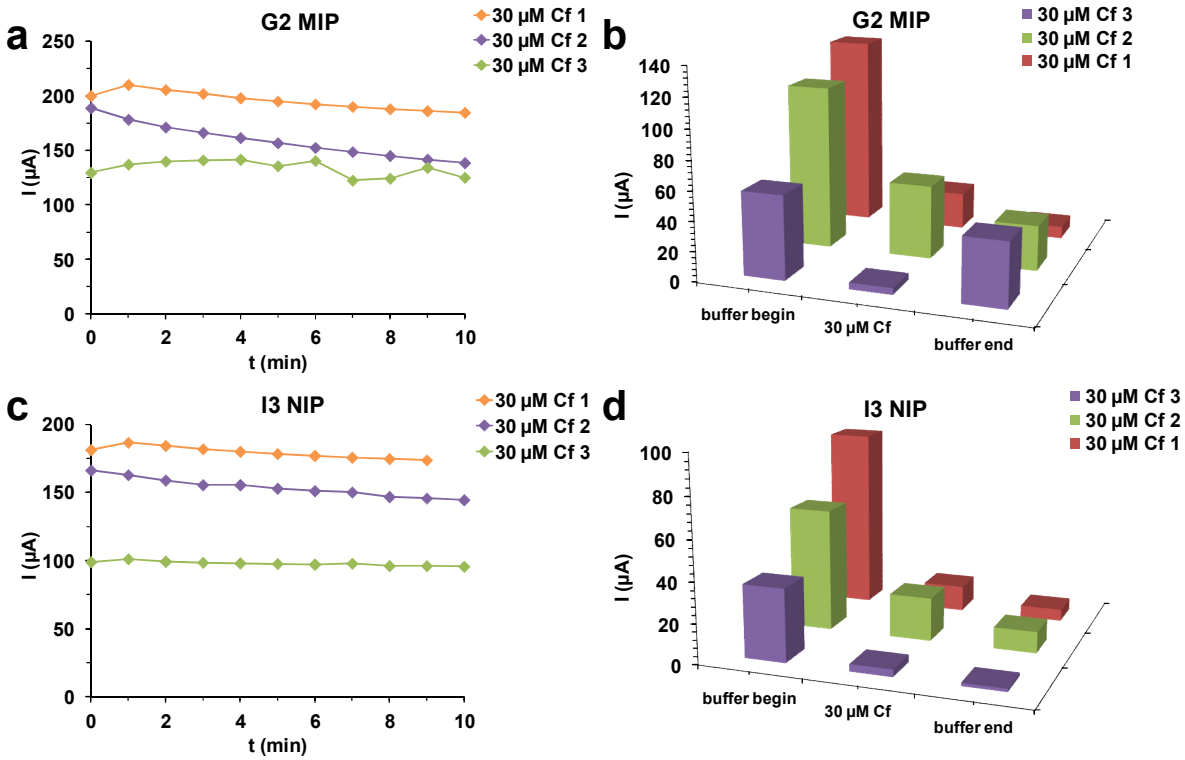

Fig. 57: I values (a),(c) and PAD sensor response (b),(d) after wash under stirring of MIP G2 and NIP I3.

MIPs and NIPs were polymerized with 50, 120, and 240 cycles. Binding was tested with 30 µM clofibric acid (Fig. 58a).

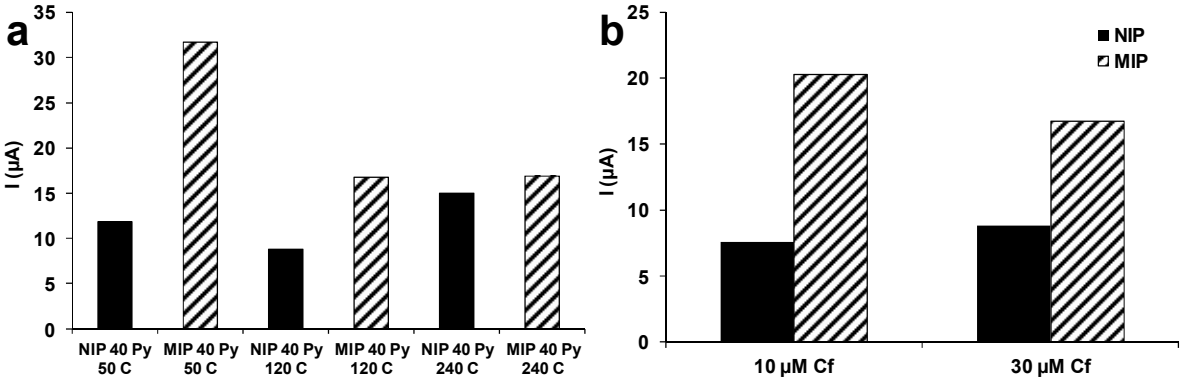

Fig. 58: PAD sensor response of MIP and NIP to clofibric acid solutions. (a) PAD response to 30 µM clofibric acid solution of NIP and MIP prepared with 50, 120, and 240 cycles (40 mM pyrrole); (b) PAD response to 10 and 30 µM clofibric acid solution of NIP and MIP prepared with 120 cycles (40 mM pyrrole).

The results showed for MIPs higher responses to clofibric acid solution than for NIPs, but the extent of non-specific binding was high. With increasing number of cycles, the response decreased for the MIPs. This could be explained by the thickness of the polypyrrole film, which increased from ~16 nm for 50 cycles to ~23 nm for 120 cycles

and to ~29 nm for 240 cycles. A decreasing sensitivity and a decreasing specificity with increasing number of cycles was also observed with other polypyrrole coated electrodes and was explained by slower diffusion of analyte molecules to the recognition sites [85,139]. Also with 10 µM clofibric acid, the difference between NIP and MIP was observable (Fig. 58b). The response to PAD washing was for NIPs 153 ± 47 µA (4 samples, 40 mM Py, 120 cycles) and for MIPs 170 ± 23 µA (4 samples, 40 mM Py, 1 mM Cf, 120 cycles).

The electrochemical behavior of MIPs and NIPs prepared on two kinds of substrates were comparable. The presence of clofibric acid decreased the polymerization rate of pyrrole in KNO_3 and phosphate buffer (pH 7). Phosphate buffer was used to avoid the precipitation of undissociated clofibric acid and the formation of non-conjugated trimers, but the polymerization rate was still decreased, probably due to the affinity of dissociated carboxylic acids to positive charged polypyrrole [65]. PAD binding tests with MIPs and NIPs did not show a systematic behavior of the polymers. Cyclic voltammetry before and after repeated PAD measurements showed a decrease in the current with increasing use, which could indicate incomplete removal of clofibric acid during washing or that PAD caused degradation of the polymers. The application of PAD during washing produced the highest current response to clofibric acid and a differentiation between NIP and MIP, but repeated use was not possible without decreasing current response.

Consequently, the feasibility of sensor fabrication via molecular imprinting with electrochemical deposition of polypyrrole could be demonstrated, but the specificity (response for MIP *vs.* NIP) was strongly dependent on preparation and washing conditions and only modest success had been achieved. The possible reasons were investigated in more detail by film and surface analyses (*c.f.* section 5.2.8).

5.2.7 Selectivity test

Selectivity of the imprinted polymer and imprinting specificity were tested with 2,4-D, PES, and CBZ (Fig. 59).

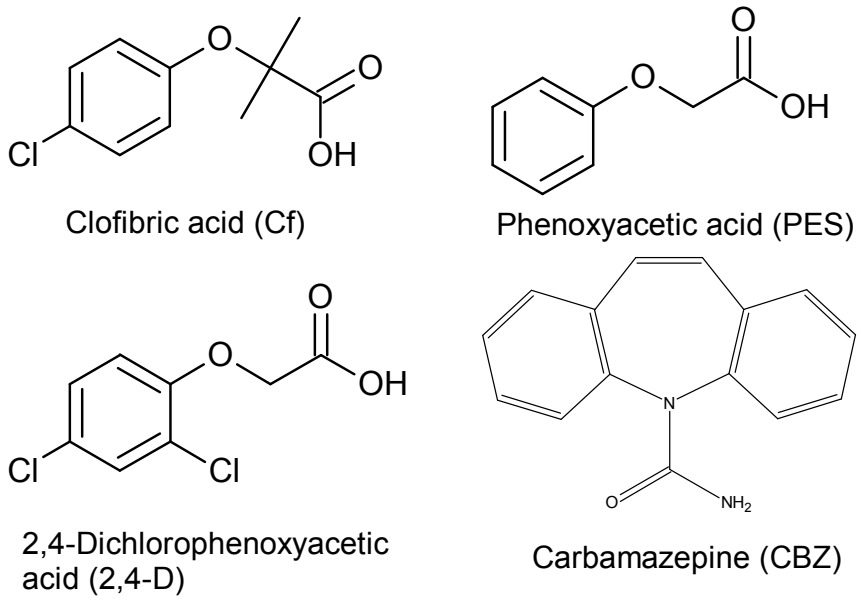

Fig. 59: Chemical structures of molecules used for selectivity tests.

The MIP showed a higher response to clofibric acid than the NIP (Fig. 60, *cf.* Fig. 58). The structurally closely related 2,4-D showed higher responses for both NIP and MIP. This higher sensitivity might result from the structure of 2,4-D, which consists of an acetic acid group instead of an isobutyric acid group. The hydrogen atoms in the acetic acid group might allow more hydrogen bonds between 2,4-D and polypyrrole than between clofibric acid and polypyrrole (Fig. 61). The high response of MIP and NIP to PES could also be explained by the acetic acid group. The responses of MIP and NIP to CBZ were lower than to clofibric acid. The dibenzazepine structure of CBZ might form π–π-interactions with polypyrrole, but the carboxamide group might form less hydrogen bonds due to its resonance structures. However, when comparing the response to clofibric acid *vs.* that to CBZ, a significantly higher selectivity of the MIP (3.8) compared to the NIP (1.4) is obtained. The low response of the MIP to CBZ suggests imprinted cavities selective for clofibric acid and closely structurally related molecules; *i.e.*, this and the comparison with the NIP reveals some specificity of the imprinting process.

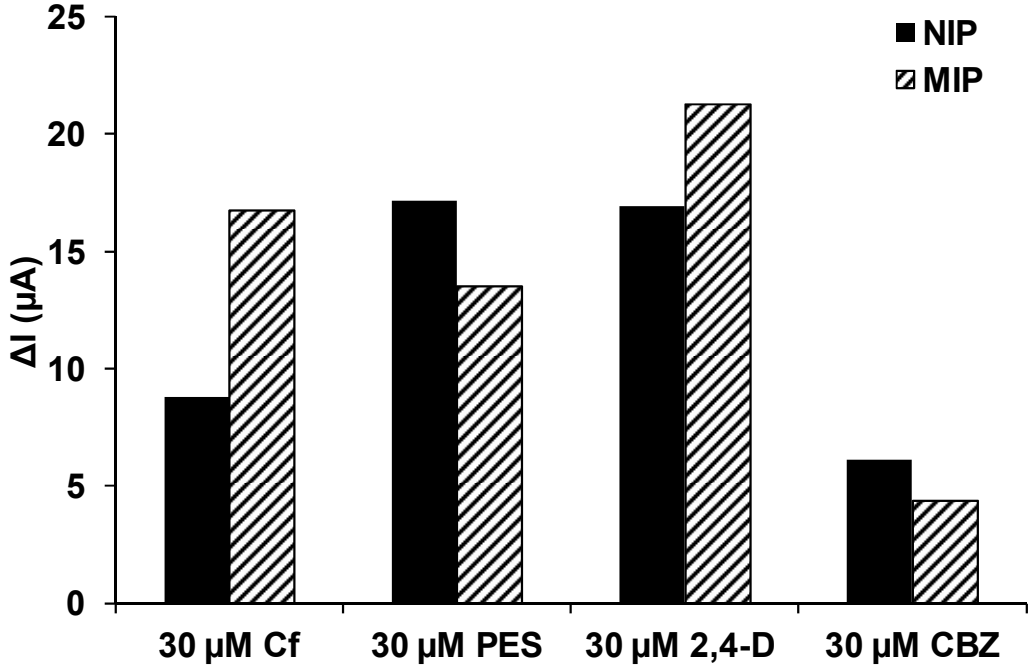

Fig. 60: Selectivity test. PAD response of MIP and NIP prepared with 120 cycles (40 mM pyrrole) to 30 μM clofibric acid, 30 μM PES, 30 μM 2,4-D, and 30 μM CBZ.

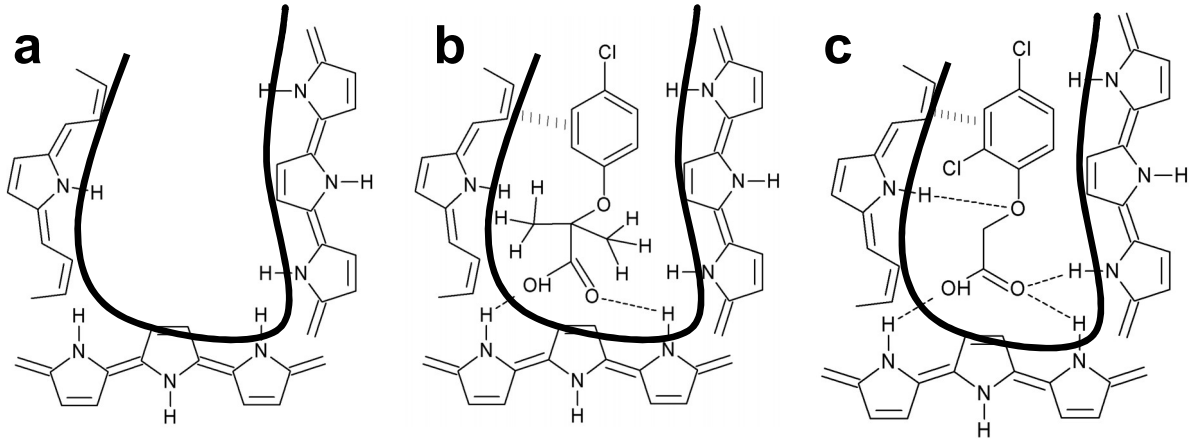

Fig. 61: (a) Schematic visualization of imprinted polypyrrole cavity and possible orientation and non-covalent interactions of (b) clofibric acid and (c) 2,4-D in the cavity.

5.2.8 Surface studies

5.2.8.1 AFM measurements

AFM images were obtained in the non-contact mode from QCM sensors with clean gold surface and from MIP and NIP films polymerized in phosphate buffer solution. The images show the line fit, where the best fit line is subtracted from the raw data, and the derived data, which is calculated from the differences of successive data points.

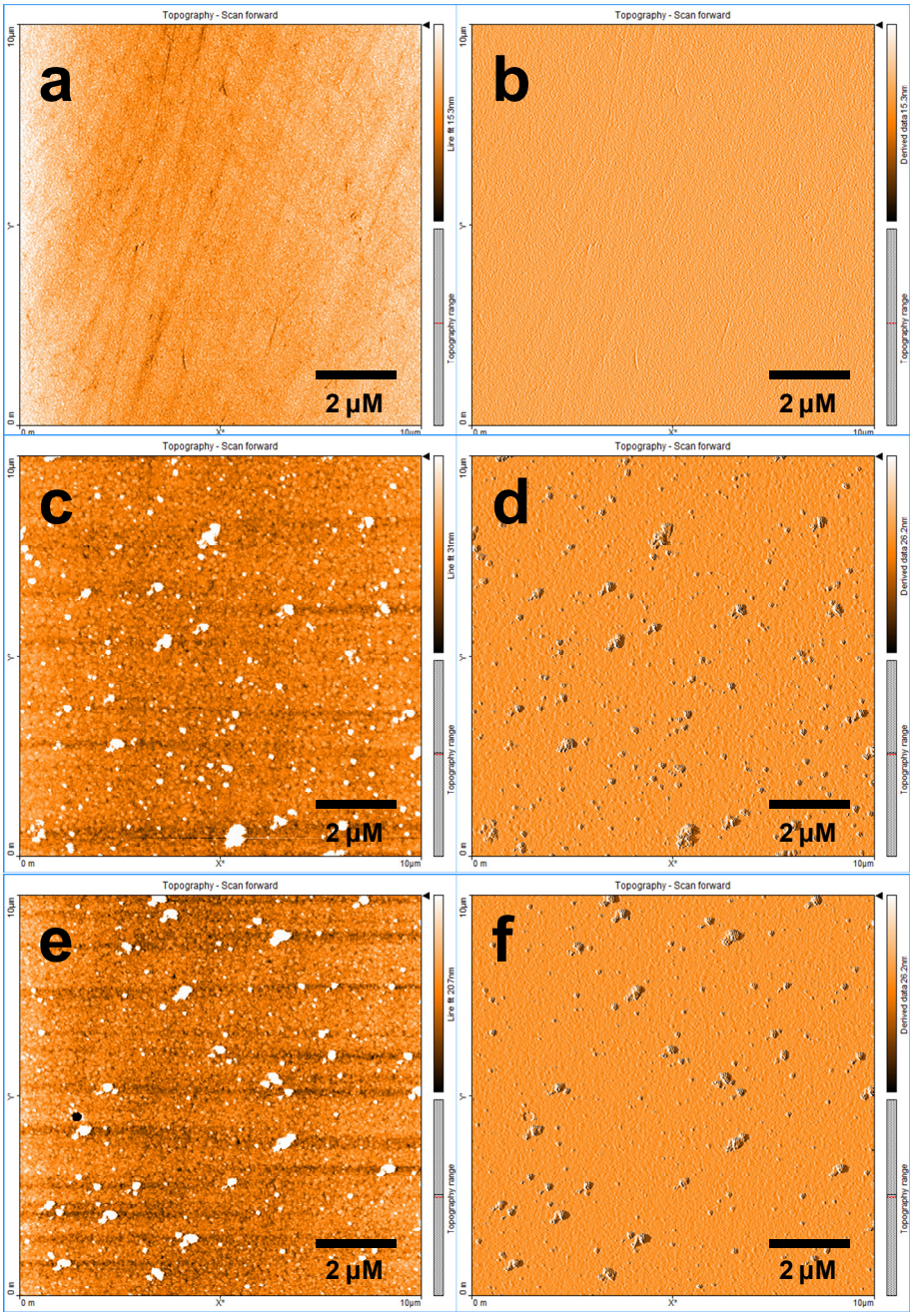

Fig. 62: AFM images of QCM sensors. (a) line fit; (b) derived data of gold surface; (c) line fit, (d) derived data of NIP; (e) line fit, (f) derived data of MIP.

The surface of a new, unused gold sensor showed a smooth surface (Fig. 62a,b). AFM images of MIP and NIP films polymerized in phosphate buffer solution revealed circular structures <1 µm on the surface (Fig. 62c–f). Fig. 63 shows root mean square (rms) roughness values for MIP and NIP after coating, washing and binding, and for an uncoated sensor. The rms values were in the range between 6–8 nm and were slightly higher for MIPs than for NIPs after the washing steps. Due to the circular structures on the surface, which disturbed the tip of the AFM, not enough data could be evaluated. The surface is relatively smooth compared to other polypyrrole films synthesized with different dopants. A polypyrrole film doped with p-toluenesulfonic acid owned cauliflower-like structures with diameters of 10–20 µm [70]. A comparable roughness of 6 nm was found for polypyrrole films doped with poly(2-methoxyaniline-5-sulfonic acid) [140]. For theophylline imprinted polyterthiophenes the roughness increased after removal of the template [141].
For imprinting, a rougher surface would be favorable because more binding sites would be available on the surface, leading to higher binding capacity.

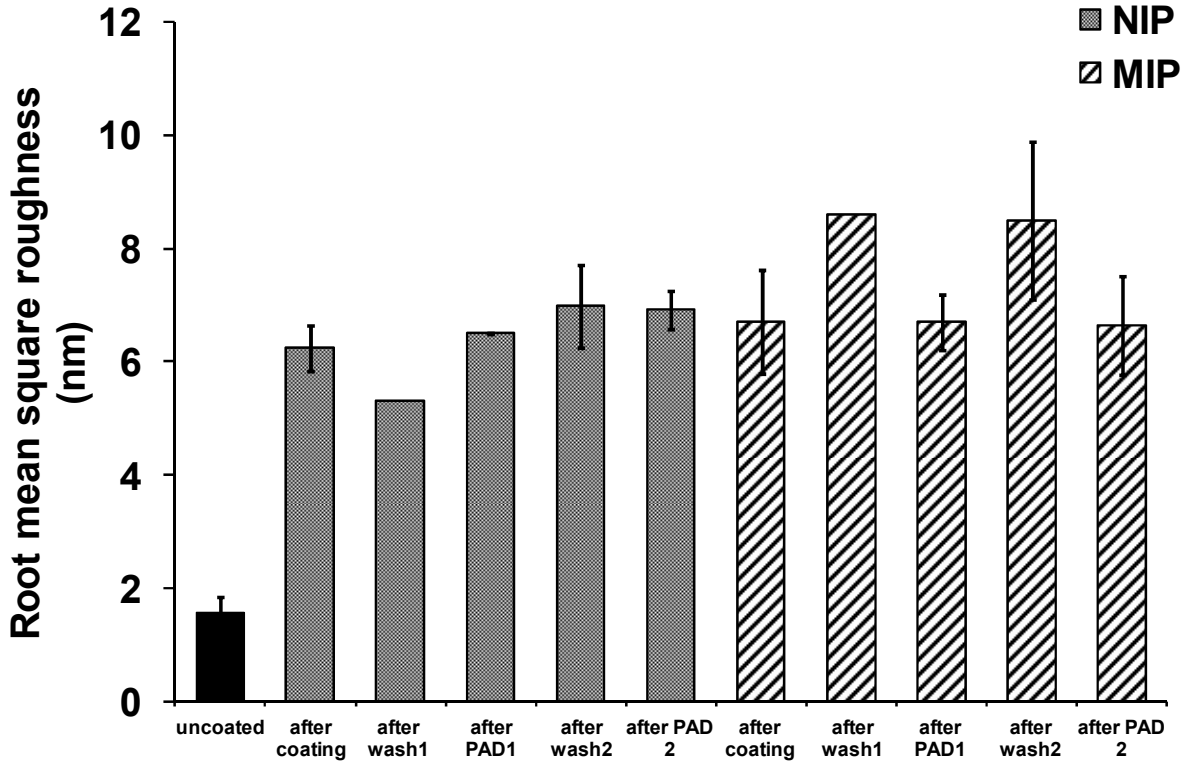

Fig. 63: Roughness (rms) values for MIP and NIP before and after washing.

5.2.8.2 Contact angle measurements

Contact angle measurements were done with NIP and MIP of three different thicknesses after coating, after PAD wash, and after binding (Fig. 64a). For two gold samples, the contact angles were 82 ± 2° and 81 ± 3° (Fig. 64b). It was found that MIPs have higher contact angles (51 ± 3°–59 ± 5°) than NIPs (45 ± 5°–47 ± 3°). The incorporation of lipophilic clofibric acid (log P_{OW} 2.72) might make the polymer more hydrophobic. For both MIPs and NIPs, the contact angles decreased after washing, but the difference between MIPs and NIPs could still be observed (MIPs: 45 ± 3°–49 ± 3°, NIPs: 37 ± 4°–40 ± 3°). This is in accordance with the results from Apodaca *et al.* [142], who found higher contact angles for copolymers imprinted with bisphenol A than for non-imprinted copolymers. Polypyrrole films grown with various dopants had contact angles between 50°–65° [70].

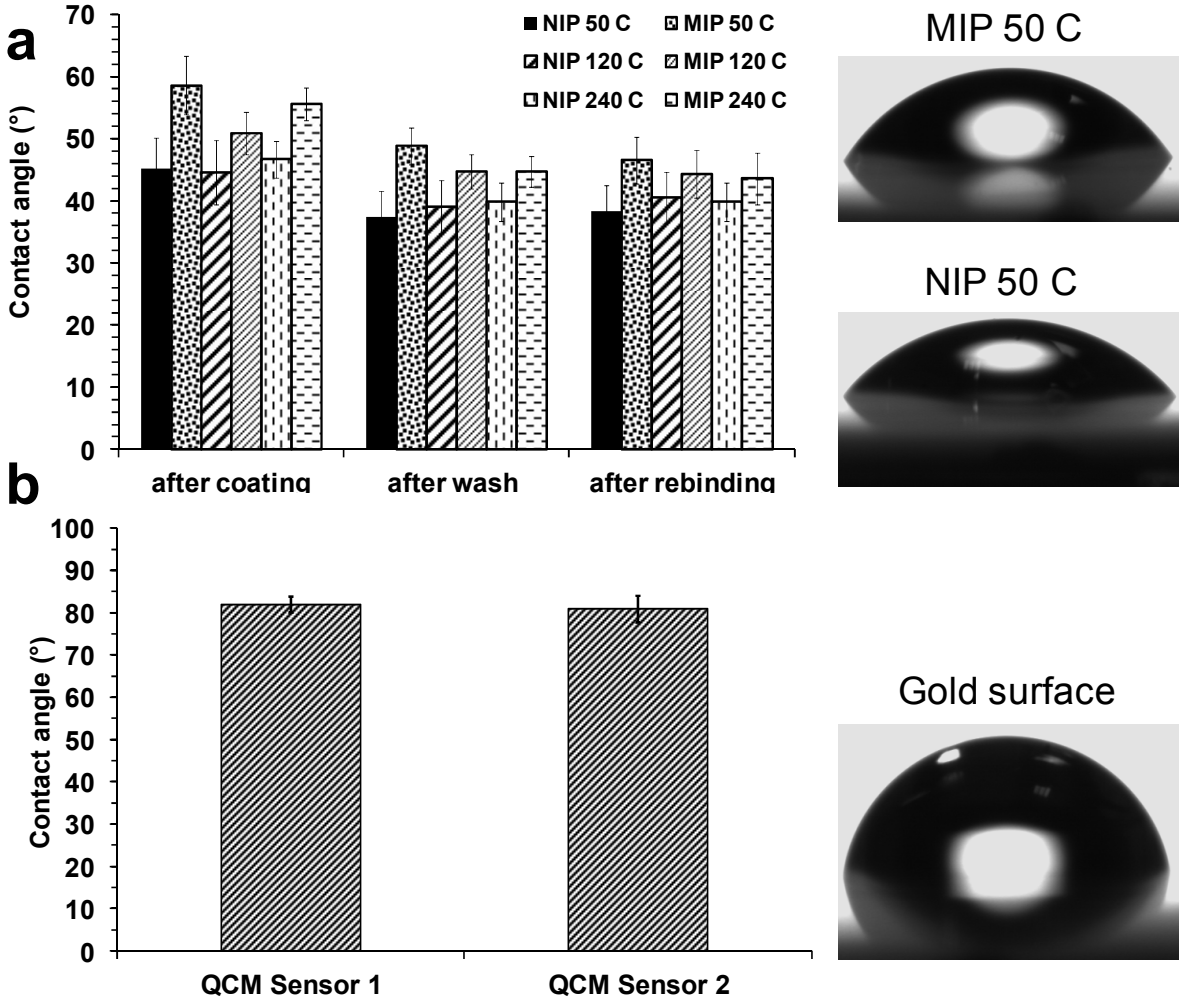

Fig. 64: Contact angles of (a) MIP and NIP after coating, after wash, and after rebinding, and of (b) gold surfaces.

5.2.8.3 Ellipsometry

The thickness of a range of MIP and NIP samples polymerized with cyclic voltammetry on QCM sensors with 50, 120 and 240 cycles (40 mM Py) was measured with ellipsometry (Fig. 65). These samples were made in the electrochemical cell of the QCM instrument, but without frequency measurements because the QCM instrument itself was not available at that time. With 50 cycles, the film thickness was ~15–16 nm. For 120 cycles, the film thickness was between 20–26 nm, with 22±1.5 nm for MIPs and 23±1.9 nm for NIPs. For 240 cycles, the film thickness increased to 27–30 nm. For comparison, QCM measurements of MIPs made with 40 mM pyrrole and 120 cycles gave thicknesses of 18±1.3 nm (*c.f.* Table 8, section 5.2.5).

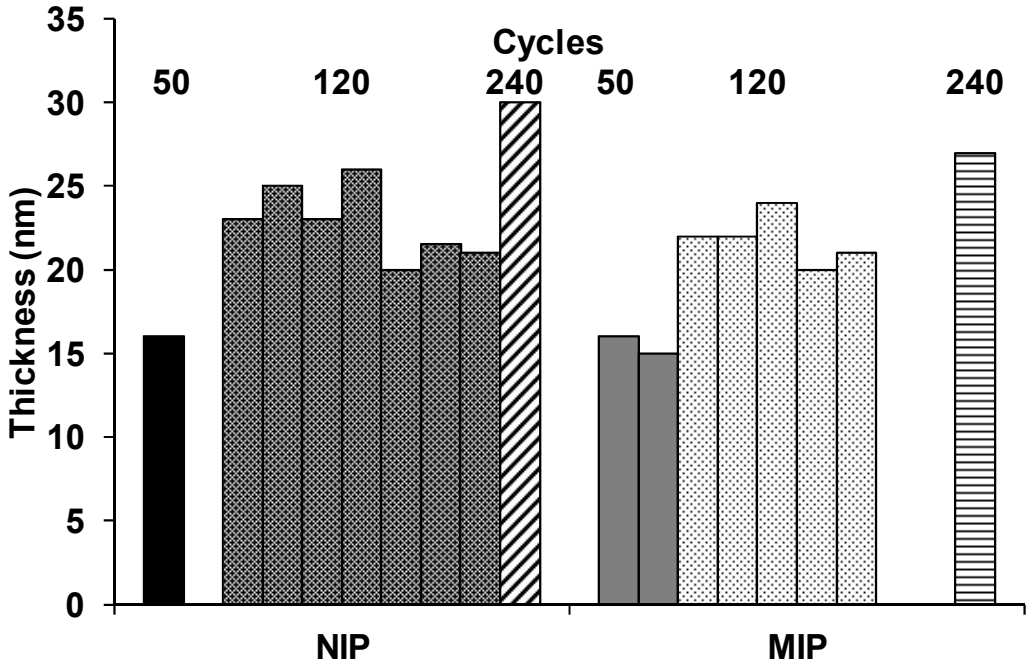

Fig. 65: Thicknesses of NIP and MIP films obtained with ellipsometry.

5.2.8.4 Zeta potential measurements

Zeta potential measurements (Fig. 66a,b) showed that the isoelectric point of the NIP after coating was at pH 5.3, while for the MIP the isoelectric point was at pH 4.8. The isoelectric point might be lower in the MIP due to the imprinting of clofibric acid, which itself is dissociated to 98–99% at pH 4.8. After washing, the zeta potential of the NIP was positive for pH values between 4.2–6.5. This kind of plateau could also be observed with the MIP, where the zeta potential is positive for pH 4.2–4.7 and changed only slightly to -1 mV until pH 5.6. During washing, the amine group of pyrrole might be protonated by the hydrochloric acid in the washing solution. Also the release of clofibric acid might reveal the positive charge of the polymer. After

binding, the isoelectric point of the NIP changed back to the same value as after coating and changed significantly to pH 4.5 for the MIP. The negative charge of clofibric acid could interact with the positive charge of the polymer (Fig. 14). The low positive zeta potential values agree with the results of the XPS measurements, where no signal could be found for positive charged nitrogen atoms. After binding, the zeta potential curve of the NIP was nearly similar to the curve after coating, while the MIP showed more negative values. At pH 7, for the NIP the difference between the zeta potentials after coating and after binding was 3 mV (-32 mV *vs.* -35 mV), while for the MIP it was 10 mV (-40 mV *vs.* -50 mV). For polypyrrole particles with chlorine counter ions, positive zeta potentials in the range between pH 2–10 have been found [143].

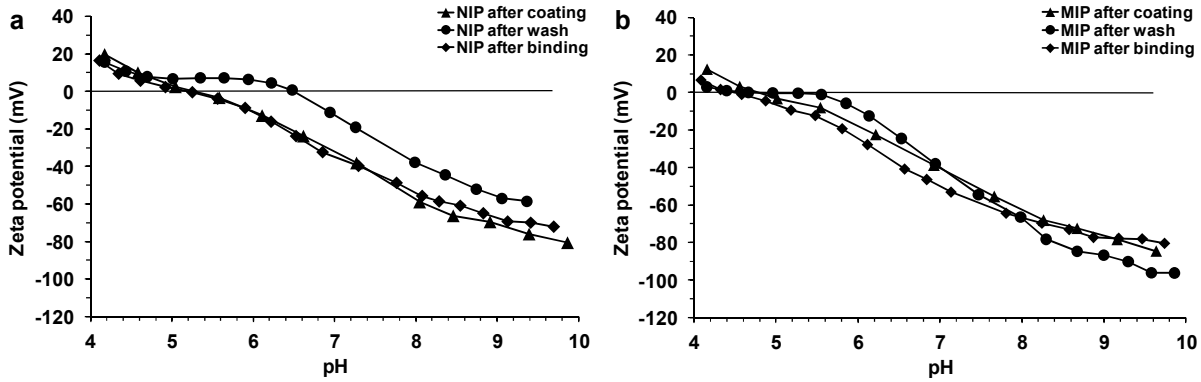

Fig. 66: Zeta potentials of NIP (a) and MIP (b) films after coating, after wash, and after rebinding.

5.2.8.5 XPS measurements

For XPS measurements of NIPs and MIPs imprinted with clofibric acid, samples XPSD1–5 and samples 3, 4, 8, 10, and 13 were prepared on gold coated glass slides. QCM samples were prepared on gold coated quartz crystals (Table 13).

Table 13: Polymerization parameters for XPS measurements

Sample	Pyrrole (mM)	Clofibric acid (mM)	Cycles	Solution	Potential (V)	Washing
XPSD1	100	0	5	KNO_3	-0.2–0.9 V	EtOH, H_2O
XPSD2	100	2	5	KNO_3	-0.2–0.9 V	%
XPSD3	100	2	5	KNO_3	-0.2–0.9 V	EtOH, H_2O
XPSD4	100	2	5	KNO_3	-0.2–0.9 V	ACN, 0.6 V
XPSD5	100	2	5	KNO_3	-0.2–0.9 V	ACN
3	10	0	20	KNO_3	-0.2–0.9 V	EtOH, H_2O
4	10	0	30	KNO_3	-0.2–0.9 V	EtOH, H_2O
8	10	2	20	KNO_3	-0.2–0.9 V	EtOH, H_2O
10	10	2	30	KNO_3	-0.2–0.9 V	EtOH, H_2O
13	10	2	30	KNO_3	-0.2–0.9 V	%
QCM D4	10	0	30	KNO_3	-0.2–0.9 V	H_2O
QCM D5	10	0	30	KNO_3	-0.2–0.8 V	H_2O
QCM C1	10	0.5	10	KNO_3	-0.2–0.8 V	H_2O
QCM C4	10	0.5	50	KNO_3	-0.2–0.8 V	H_2O
QCM D1	10	1	50	KNO_3	-0.2–0.8 V	H_2O
QCM D2	10	1	10	KNO_3	-0.2–0.8 V	H_2O
QCM D3	10	0	50	KNO_3	-0.2–0.8 V	H_2O
QCM B2	20	0	40	KNO_3	-0.2–0.8 V	H_2O
QCM E3	20	1	40	KNO_3	-0.2–0.8 V	H_2O
QCM G1	40	0	120	PBS	-0.2–0.8 V	H_2O
QCM G2	40	1	120	PBS	-0.2–0.8 V	H_2O
QCM I3	40	1	120	PBS	-0.2–0.8 V	PAD wash
QCM I4	40	1	120	PBS	-0.2–0.8 V	PAD wash

Survey spectra of the samples showed mainly O1s, N1s, C1s and Cl2p peaks. O KLL peaks represent the energy of auger electrons. When a photoelectron leaves from a low energy level (inner shell), an electron from a higher energy level can move to the low energy level to maintain a stable state and loses the transition energy, which can be transferred to another electron, which is then emitted as auger electron.

Peak assignment of samples XPSD1–5 (Fig. 68)

The C1s peaks were interpreted to consist of four components at ~285 eV, ~286 eV and ~288 eV. The two peaks near 285 eV were assigned to C-C bonds, the peak at ~286 eV to C-O bonds, and the peak at ~288 eV to C=O bonds. The two components of the NIP N1s peak (XPSD1) were assigned to N-H bonds at ~400 eV and to C-N bonds at ~398 eV. A comparison of the nitrogen peaks of all samples showed no shift of signals from the different treatment methods (Fig. 67a). The Cl2p peaks of XPSD2 and 3 consist of two signals at ~200 eV and 202 eV, which could be assigned to $Cl2p_{1/2}$ and $Cl2p_{3/2}$ in organic chlorine. A third peak at ~197.5 eV of XPSD2 could be attributed to chloride, although chlorine containing components besides clofibric acid were not used during polymerization. A shift in binding energy of the Cl2p peak to ~197 eV and ~198.5 eV was observed for samples washed with acetonitrile (Fig. 67b). No chlorine was found in sample 1 which was polymerized without template molecules (Fig. 72). Samples 2–5 contained chlorine. Chlorine was found in the MIP samples XPSD2–4 (Cl2p ~200 eV), where the highest amount of chlorine was found for the unwashed sample XPSD2. The lowest amount of chlorine was found for XPSD3 which was washed with ethanol (70%) and water. Washing with acetonitrile (XPSD4,5) was less effective, so that washing with ethanol (70%) was chosen for template removal in successive binding experiments.

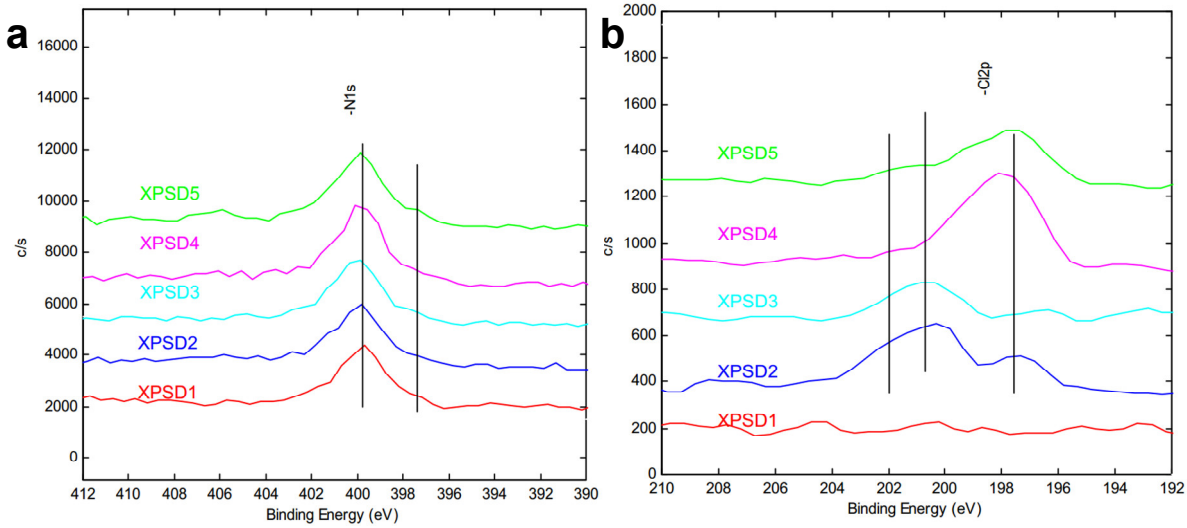

Fig. 67: Comparison of (a) N1s spectra and (b) Cl2p spectra of XPSD1–5.

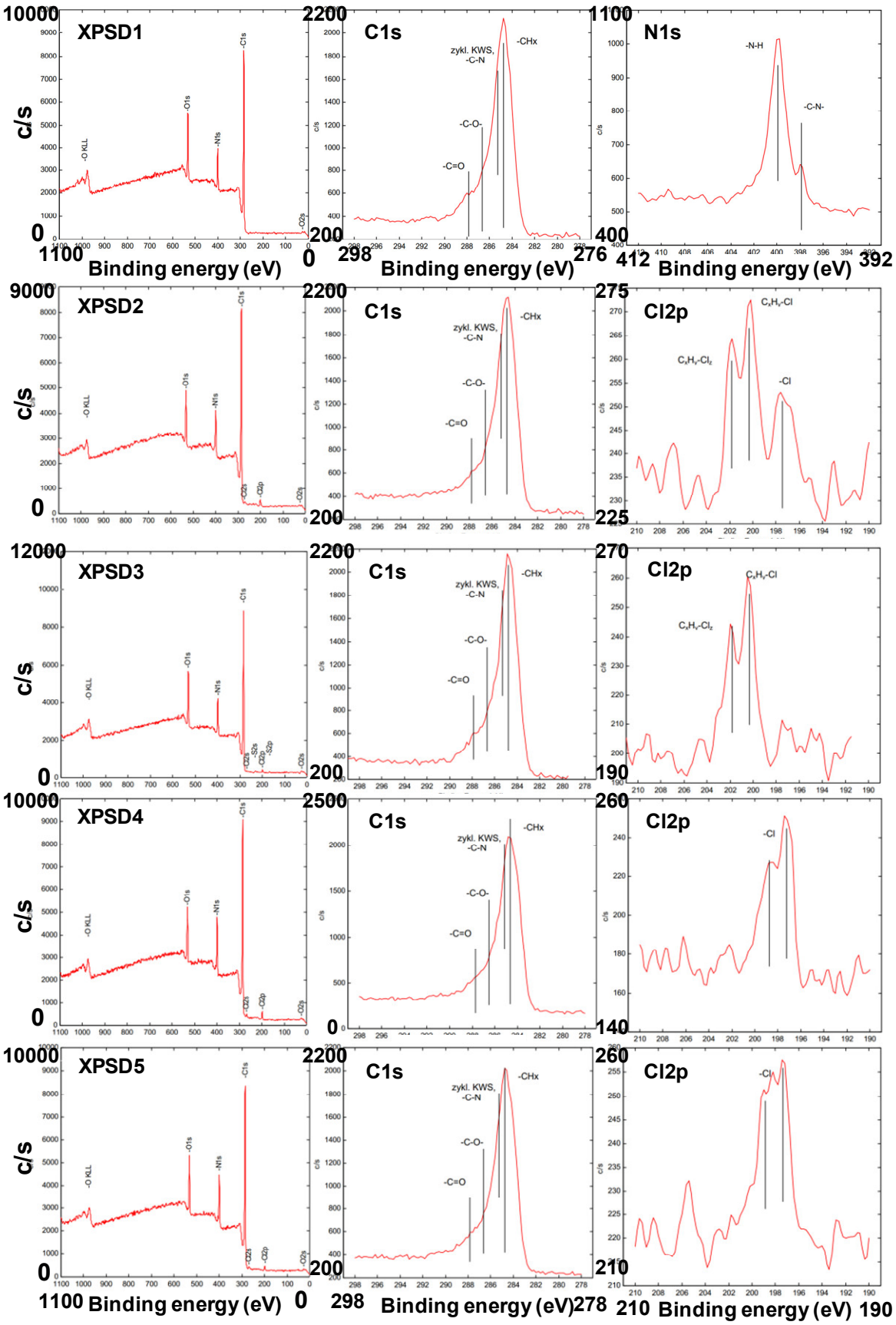

Fig. 68: XPS spectra of XPSD1—5, C1s spectra of XPSD1–5, N1s spectrum of XPSD1, and Cl2p spectra of XPSD2–5.

Peak assignment for samples 3–13 and D4–D3 (Fig. 69), QCM B2 and E3 (Fig. 70), and QCM G1–I4 (Fig. 71):

The peak at ~285 eV could be attributed to C-C bonds in the polymer chain, the peak at ~286 eV to C-N bonds and the peak at ~288 eV could be explained by carbonyl groups [144]. The N1s peaks showed two components, the major peak at ~400 eV, which could be attributed to primary/secondary amine nitrogen (-N-H) [130,131], and a smaller peak at ~399 eV, which could be attributed to tertiary amine nitrogen (=N-), as the shoulder on the low energy side of the peak indicated an electron rich environment [145]. As polypyrrole is usually positively charged if prepared in acid or neutral solutions, there should also appear a peak at ~402 eV, which could be attributed to positively charged amine nitrogen [128,130,146]. The O1s signal consisted of two peaks at ~532 eV and ~533 eV, which could be attributed to C=O and C-O in the polymer backbone or to water or organic contamination [130].

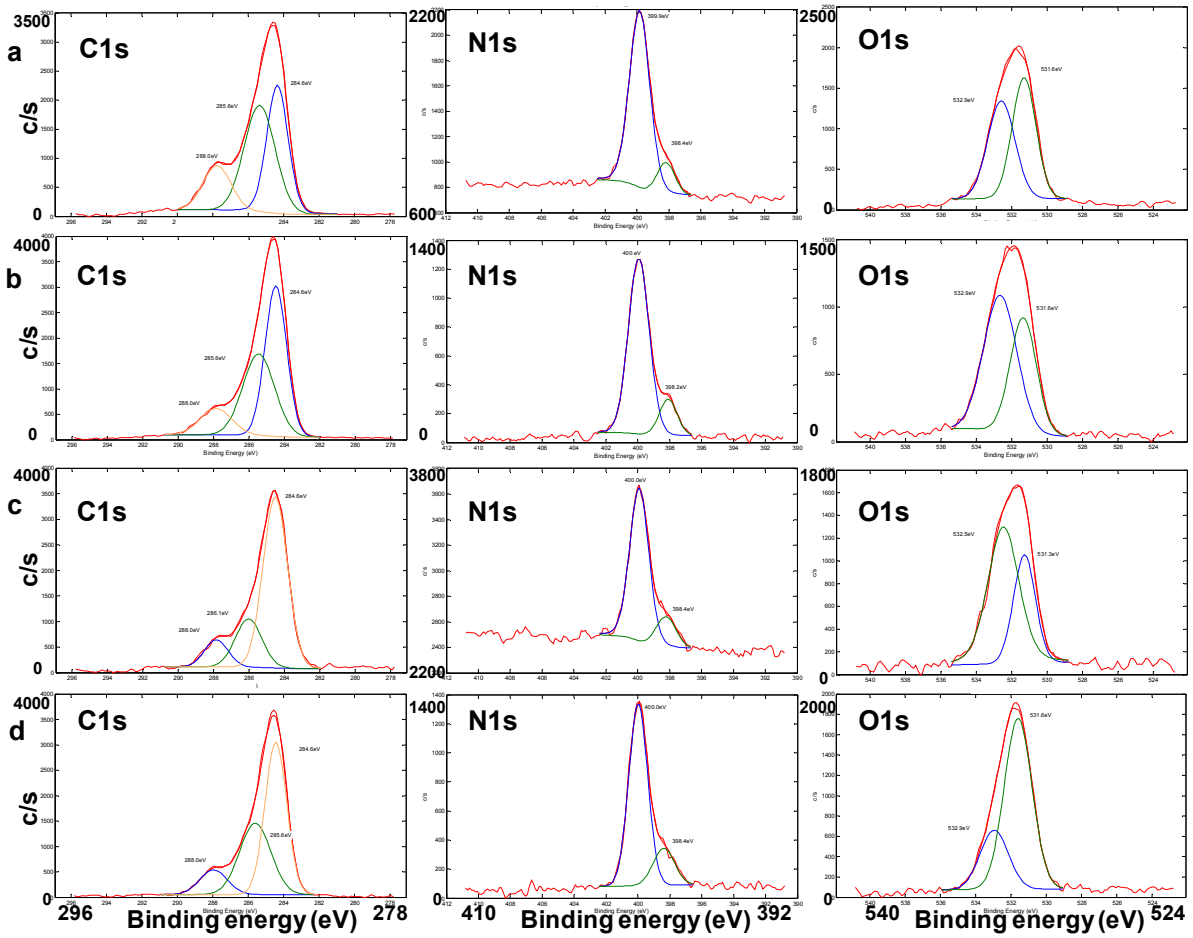

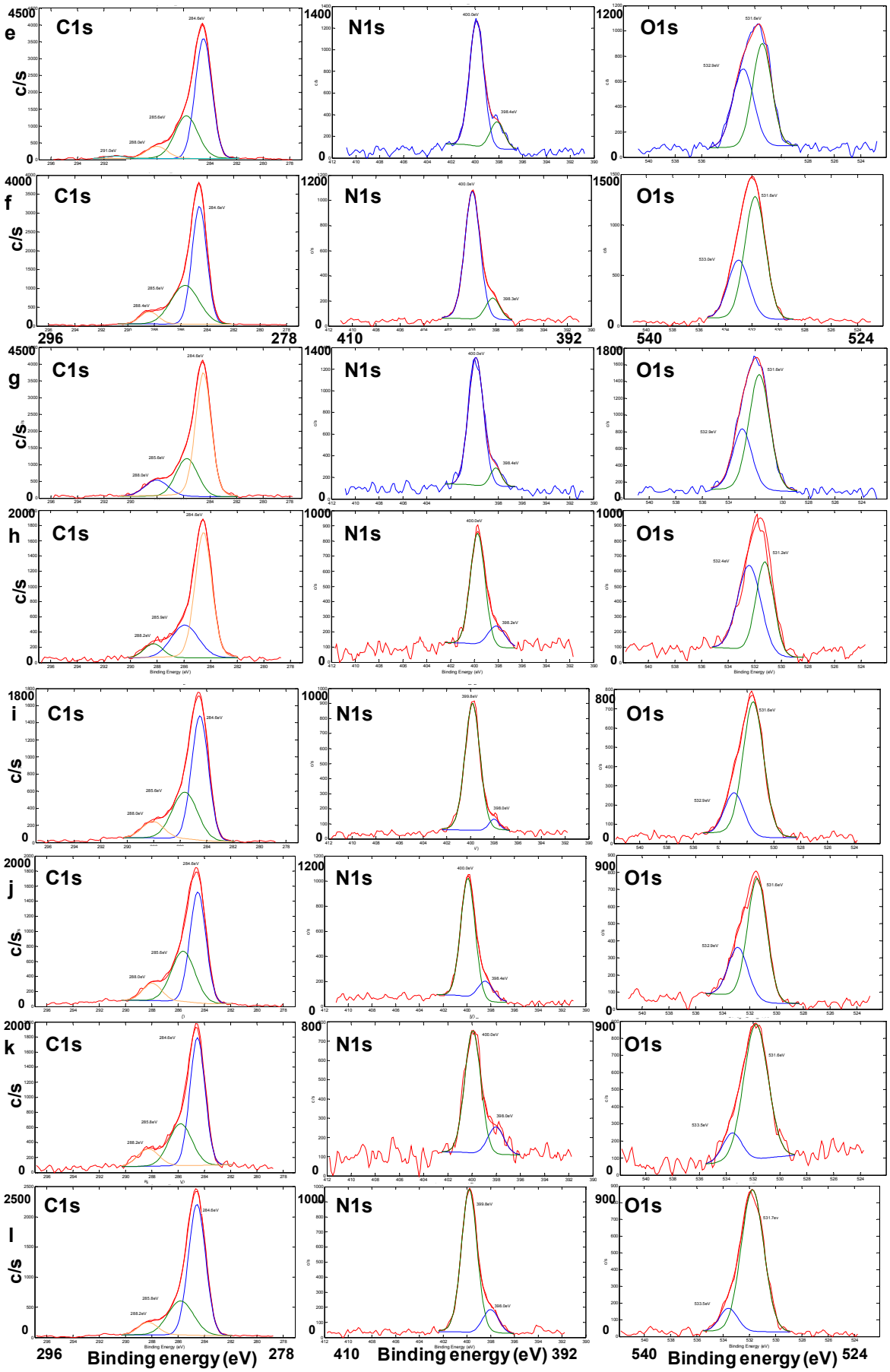

Fig. 69: XPS spectra of (a) #3; (b) #4; (c) #8; (d) #10; (e) #13; (f) D4; (g) D5; (h) C1; (i) C4; (j) D1; (k) D2; (l) D3.

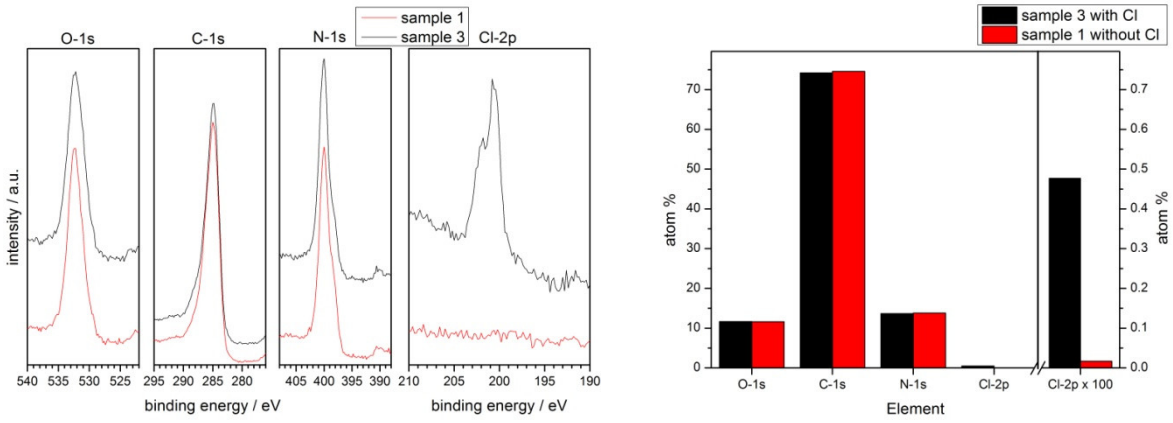

Fig. 70: XPS spectra and atomic concentration of QCM B2 (NIP) and E3 (MIP).

The spectra of samples B2 (NIP) and E3 (MIP) (Fig. 70) (Saarland University) showed peaks for oxygen, carbon, and nitrogen in the same range as the XPS measurements done in Korea and Dresden. Chlorine was found in the imprinted polymer with an amount of 0.48%.

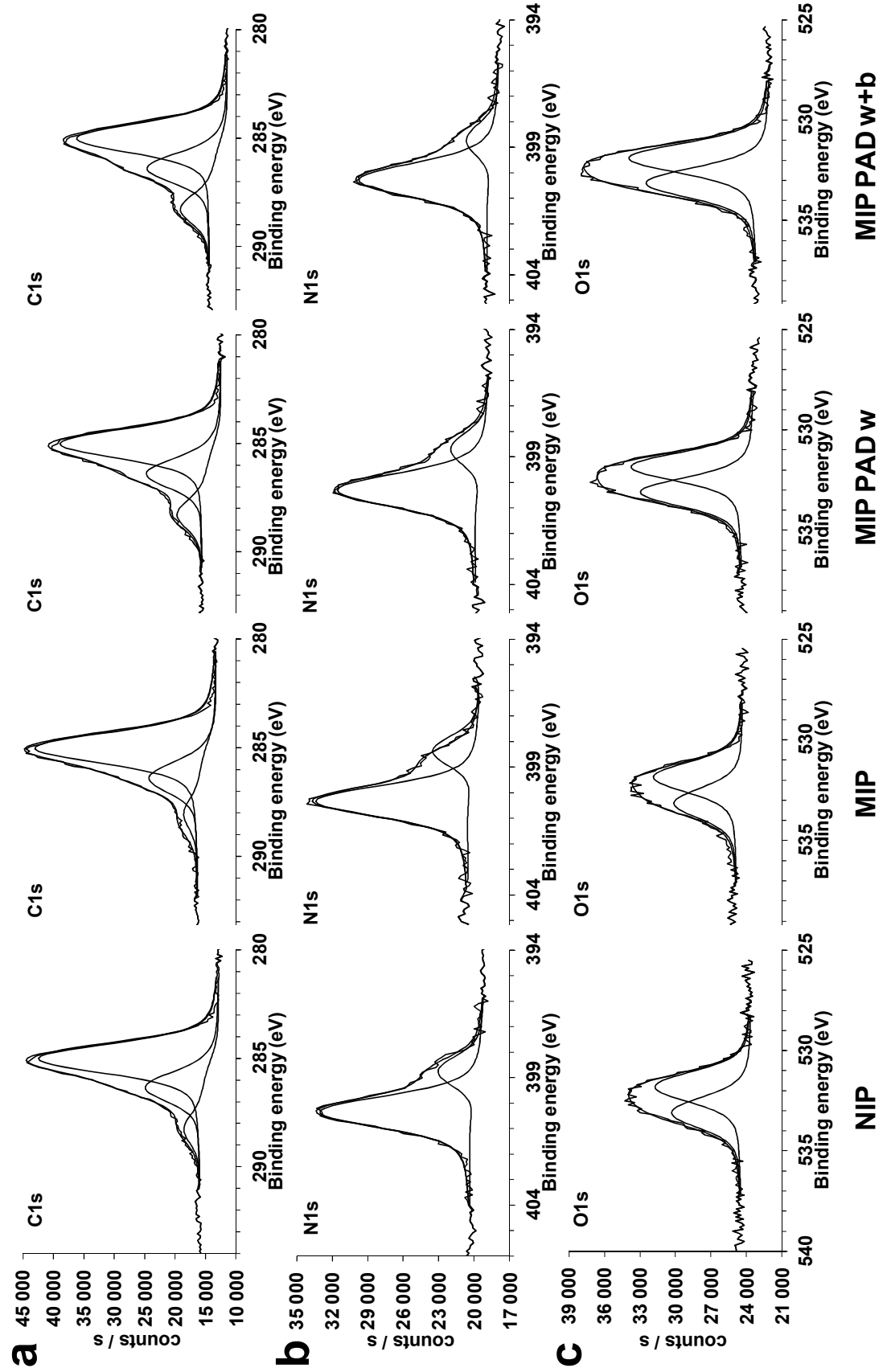

Fig. 71: XPS spectra of NIP and MIP after polymerization, MIP after PAD washing, and MIP after PAD washing and subsequent clofibric acid binding of (a) C1s, (b) N1s, and (c) O1s.

Atomic concentration and element ratio

The atomic concentrations of samples XPSD1–5 were for carbon between 76–79%, for both nitrogen and oxygen 10–13%, and for chlorine 0–1% (Fig. 72). The C/N ratio of an ideal polypyrrole structure would be 4:1. The C/N ratios of samples XPSD1–5 could not be used in this regard because nitrogen containing KNO_3 was used during preparation of the polymers. Defects in the polymer structure due to the max. potential of 900 mV used during polymerization might increase the C/N ratio [131]. Samples washed with acetonitrile have lower C/N ratios than the other samples (Table 14).

Table 14: C/N ratios of samples XPSD1–5 obtained from XPS

	XPSD1	XPSD2	XPSD3	XPSD4	XPSD5
C/N	7.4	8.1	7.2	5.9	6.0

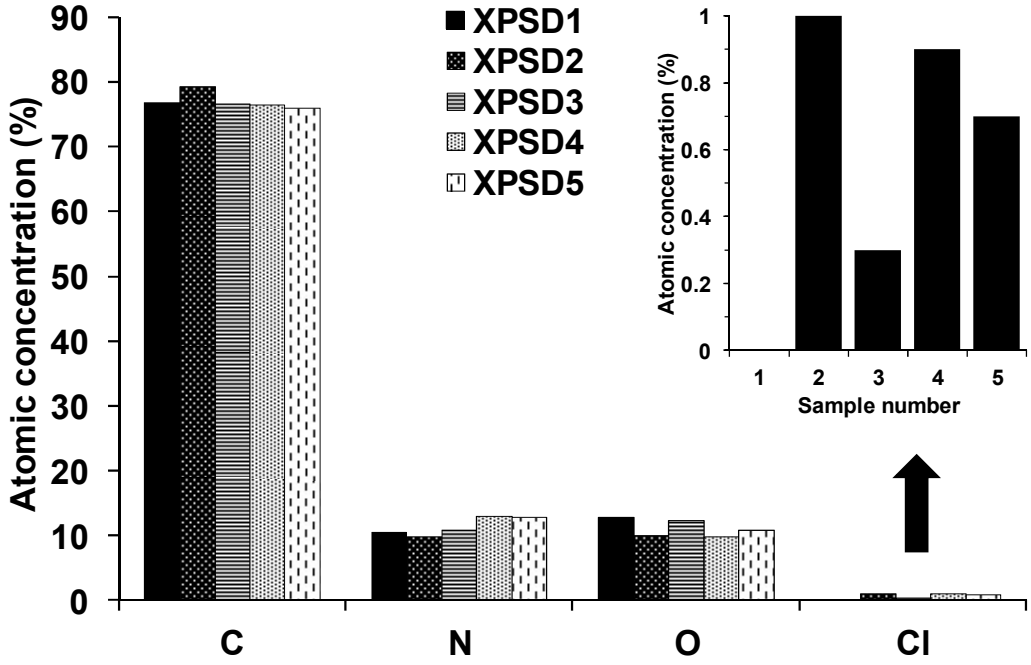

Fig. 72: XPS atomic concentration of XPSD1–5.

For samples 3–13 and QCM D4–D3 (Fig. 73), the fractions of C=O and C-O bonds were very variable and could not be linked to MIP or NIP, cycle number, clofibric acid concentration, or cycling potential. The C/N ratios of the samples (Table 15) showed lower values for most of the MIPs prepared with a max. cycling potential of 800 mV than MIP prepared with a max. potential of 900 mV. For the NIPs, the difference was less pronounced. D4 and D5 were prepared under the same conditions besides the max potential. The C/N ratio of D5 (800 mV) was slightly lower than the ratio of

D4 (900 mV). D3, prepared with 50 cycles and max. 800 mV, had the lowest C/N ratio of a NIP.

Cl2p peaks were only found in samples C4 and D1, which were prepared with 50 cycles. The doping level could be obtained with the Cl/N ratio, which was 0.03 for C4 and 0.02 for C1.

Table 15: C/N ratios of samples 3–13 and D4–D3

	#3	#4	#8	#10	#13		
	NIP	NIP	MIP	MIP	MIP		
C/N	5.2	6.2	6.5	6.1	6.3		
	D4	D5	C1	C4	D1	D2	D3
	NIP	NIP	MIP	MIP	MIP	MIP	NIP
C/N	6.2	5.8	4.8	4.7	4.0	6.1	4.6

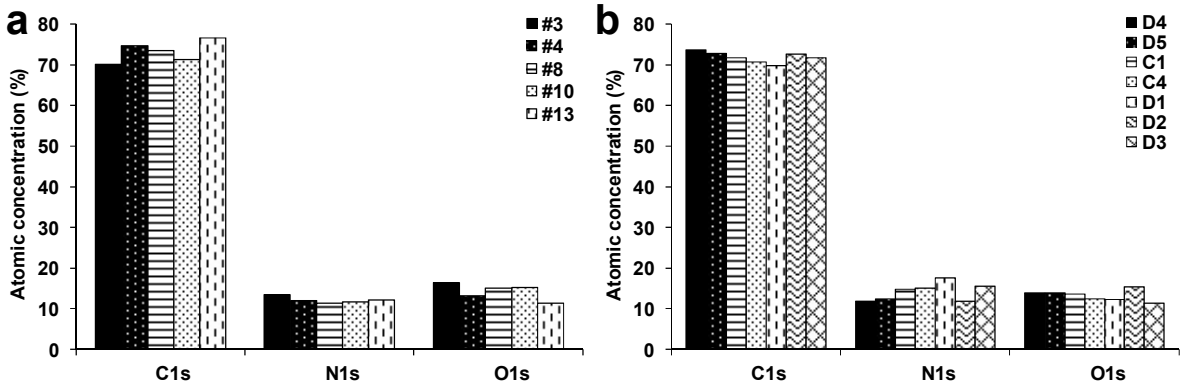

Fig. 73: Atomic concentration of polypyrrole coated glass slides (a) and quartz crystals (b).

Influence of PAD on atomic concentration

The following set of samples was subject to PAD washing and binding experiments and prepared in phosphate buffer solution. Samples which were subject to PAD washing and PAD binding contained a lower fraction of C-H groups and a higher fraction of C=O and C-O groups (Fig. 74). The XPS spectra showed also higher oxygen peaks for these samples (Fig. 71). The repeated potential pulses during the PAD treatment might promote the oxidation of the polymer backbone or the swollen polymer might contain more oxygen from the solvents used during PAD. Dissolved oxygen in the solutions was displaced with nitrogen before electrochemical measurements, but during the time, in which the solutions were pumped into the electrochemical cell and during measurements, the oxygen content might have increased again due to contact with air. The interaction of the polypyrrole with oxygen can lead to the degradation of the polymer [147].

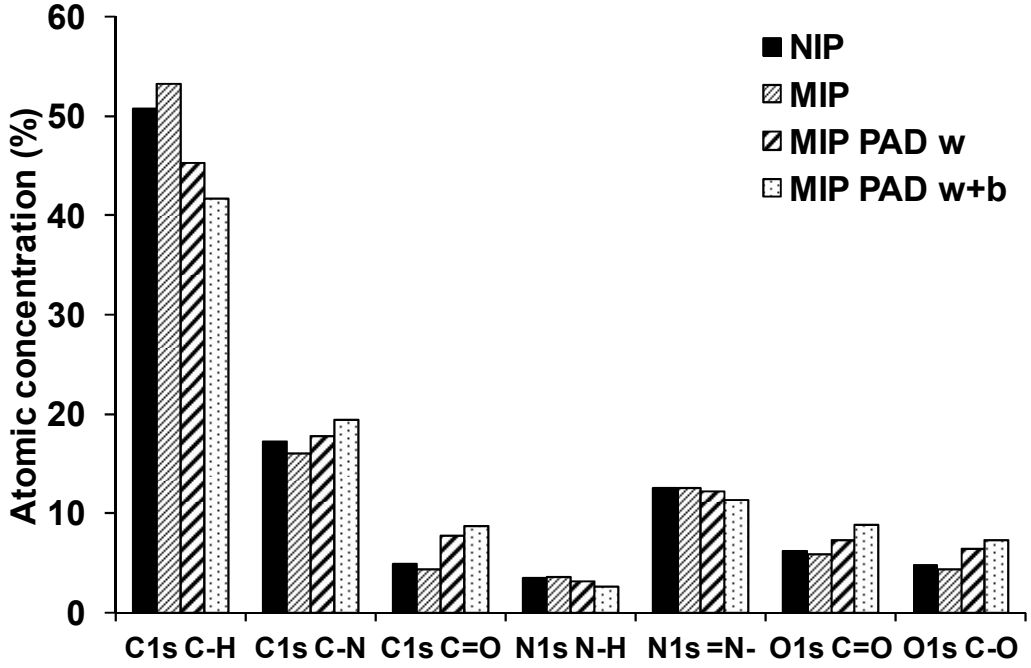

Fig. 74: XPS atomic concentration of C1s, N1s, and O1s components of NIP and MIP after polymerization, and for MIP after PAD washing and after PAD washing and subsequent binding.

XPS spectra of polypyrrole samples showed that O1s, N1s, C1s and Cl2p peaks were independent of the substrate and the use of different instruments at binding energies comparable to literature values. The use of ethanol as washing solvent decreased the amount of chlorine found in XPS measurements compared with water and acetonitrile. Defects in the polymer structure due to the applied potential during polymerization could increase the 4:1 C/N ratio of polypyrrole.

Mostly, C/N ratios were lower for MIPs prepared with a lower potential range than for MIPs prepared with a higher potential range. For NIPs, C/N ratios were less different for different potential ranges.

PAD washing and PAD binding caused changes in the elemental composition of the polymers, which could be observed by a lower fraction of C-H groups and a higher fraction of C=O and C-O groups. This could indicate oxidation of the polymer backbone and might be promoted by PAD treatment, which would support the hypothesis about PAD being the reason for decreased sensor functionality with number of uses (*c.f.* section 5.2.6).

5.3 Polymerization of pyrrole with potential pulses

When a negative potential is applied to polypyrrole, the polymer becomes reduced and ions are expelled. This property was used for the study of polypyrrole-based drug release systems, e.g., for methotrexate, sulfosalicylic acid, salicylate, and risperidone [107,148–150].

5.3.1 Amperometric and potentiometric polymerization

Polypyrrole polymerized by cyclic voltammetry delaminated partly from the gold surface of a QCM sensor when -600 mV were applied (Fig. 75). Therefore, potentiometric (constant current) and amperometric (potential pulses) polymerization were tested to examine the release of clofibric acid from polypyrrole by applying a negative potential (Table 16).

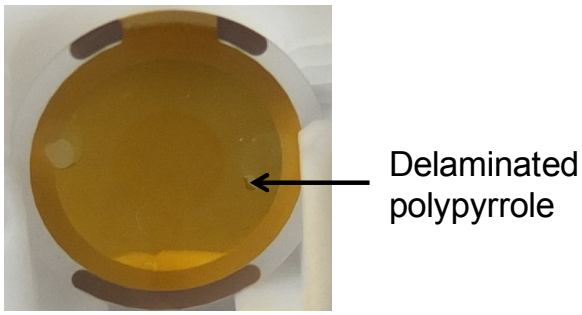

Fig. 75: QCM sensor coated by cyclic voltammetry, 60 mM Pyrrole + 1 mM clofibric acid, 120 cycles, after application of -600 mV for 10 min.

Table 16: Polymerization parameters for release tests

Plate	Coating	Conditions	Solution	Release	Result
1	Potentiometric	2 mA 960 s	200 mM Py, 9 mM Cf, 100 mM Na-pTS in MeOH 70%	-600 mV 30 min	No adherence
2	Potentiometric	2 mA 960 s	200 mM Py, 9 mM Cf, 100 mM Na-pTS in MeOH 70%	-600 mV 15 min	No adherence
3	Amperometric (potential pulses)	0.1 s 700 mV (800 mV, 900 mV) 0.1s -600 mV	200 mM Py, 90 mM Cf in MeOH /PBS 70/30	%	No coating
4	Potentiometric	2 mA 300 s	200 mM Py in MeOH/PBS 70/30 (+ KCl)	%	No adherence
5	Amperometric (potential pulses)	1 s 900 mV 1 s -600 mV (300 s)	200 mM Py in MeOH/PBS 70/30 (+ KCl)	-600 mV (5, 30, 30, 60 min)	Adherence
6	Amperometric (potential pulses)	1 s 900 mV 1 s -600 mV (900 s)	200 mM Py, 9 mM Cf in MeOH/PBS 70/30 (+ KCl)	-600 mV (15, 30, 30, 60 min)	Adherence

Potentiometric polymerization of polypyrrole produced dark, thick films (Fig. 76, plate 1, 2, and 4), but they could be easily removed from the gold surface and did not

adhere to the surface when a potential of -600 mV was applied. Amperometric polymerization did not produce films when the pulse length was 0.1 s (Fig. 76, plate 3). With a pulse length of 1 s, pyrrole could be polymerized on the gold surface (Fig. 76, plate 5). In the presence of clofibric acid, the polymer film was much lighter in appearance (Fig. 76, plate 6). These films did not detach from the surface under negative potential.

Plate 5 (NIP) and 6 (MIP) were used for PAD binding experiments with 30 µM clofibric acid solutions (pH 7). Between the binding experiments, the sensors were washed in buffer solution with -600 mV for 30 min or 60 min.

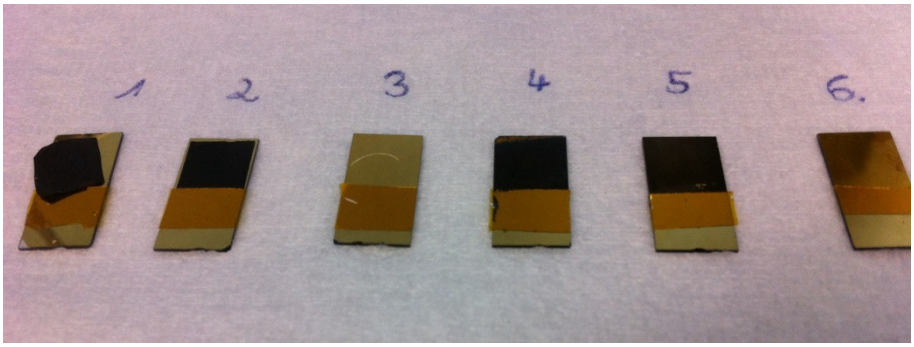

Fig. 76: Gold coated wafers (2 x 1cm), coated with polypyrrole.

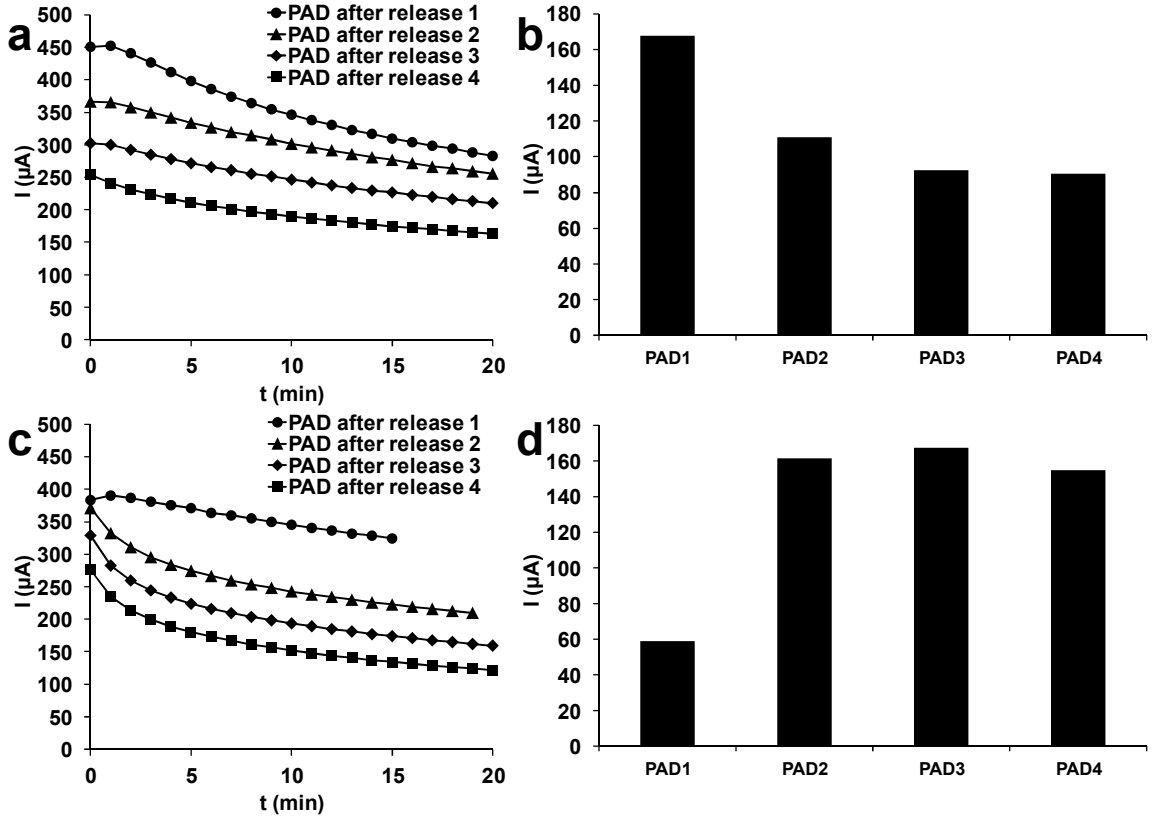

Fig. 77: PAD current response to 30 µM clofibric acid of (a) plate 5 (NIP) and (c) plate 6 (MIP); PAD sensor response of (b) plate 5 (NIP) and (d) plate 6 (MIP).

The response of plate 5 (NIP) to PAD with clofibric acid showed a nearly linear decrease (Fig. 77a), while the response of plate 6 (MIP) showed a more exponential decrease (Fig. 77c). A linear decrease of the response could be attributed to non-specific binding of clofibric acid on the polymer surface [75]. The exponential decay could be attributed to the binding of clofibric acid in the imprinted cavities [93] (*c.f.* Fig. 9, section 2.4). Plate 5 (NIP) and plate 6 (MIP) were not directly comparable because they were made with different polymerization times and treated with different release times. The sensor response of the NIP (Fig. 77b) was the highest after the first release test following polymerization. It decreased with repeated releases from 168 μA to 111 μA. The surface also developed scratches with increasing usage. The sensor response was in the range of 98 ± 11 μA for three consecutive binding experiments with release times of 30 min and 60 min. The sensor response of the MIP (Fig. 77d)after washing with a negative potential, increased from the first PAD measurement to the second (59 μA to 162 μA) when the washing time was increased from 15 min to 30 min. Doubling the washing time to 60 min did not increase the sensor response. The sensor response was in the range of 161 ± 6 μA for three consecutive binding experiments. Compared with the results from PAD washing experiments with acidic ethanol solution (Fig. 53b), where the sensor response decreased steadily during binding experiments, washing with -600 mV seems to be more effective.

5.3.2 Binding tests with polypyrrole prepared by potential pulses

Several more MIP and NIP samples were prepared with potential pulses for PAD binding tests (Table 17).

The potentiometric polymerization of polypyrrole produced inhomogeneous films in ethanolic PBS-KNO_3 solution (Fig. 78, 1–4). Films made in methanolic solution with a higher fraction of organic solvent (70%) produced light and more homogeneous films (Fig. 78, 5–8). Films made in PBS-KCl/MeOH (Fig. 78, 9–12) produced dark films. Films 1–4 detached partly during drying with a stream of nitrogen. The wearing increased with increasing number of releases and binding tests. Films 5–12 did not detach from the surface during drying, but also here the films showed some wearing with usage.

Table 17: Polymerization parameters

Plate	MIP/NIP	Coating Conditions	Solution	Release
1	NIP	1 s 900 mV, 1 s -600 mV, 300 s	120 mM Py in PBS-KNO_3/EtOH (90/10)	-600 mV, 30 min
2	MIP	1 s 900 mV, 1 s -600 mV, 300 s	120 mM Py 1 mM Cf in PBS-KNO_3/EtOH (90/10)	-600 mV, 30 min
3	MIP	1 s 900 mV, 1 s -600 mV, 300 s	120 mM Py 10 mM Cf in PBS PBS-KNO_3/EtOH (90/10)	-600 mV, 30 min
4	MIP	1 s 900 mV, 1 s -600 mV, 300 s	120 mM Py 1 mM Cf in PBS-KNO_3/EtOH (90/10)	-600 mV, 30 min
5	NIP	1 s 900 mV, 1 s -600 mV, 300 s	200 mM Py in PBS-KNO_3/MeOH (30/70)	-600 mV, 30 min
6	NIP	1 s 900 mV, 1 s -600 mV, 900 s	200 mM Py in PBS-KNO_3/MeOH (30/70)	-600 mV, 30 min
7	MIP	1 s 900 mV, 1 s -600 mV, 300 s	200 mM Py 10 mM Cf in PBS-KNO_3/MeOH (30/70)	-600 mV, 30 min
8	MIP	1 s 900 mV, 1 s -600 mV, 900 s	200 mM Py 10 mM Cf in PBS-KNO_3/MeOH (30/70)	-600 mV, 30 min
9	NIP	1 s 900 mV, 1 s -600 mV, 300 s	200 mM Py in PBS-KCl/MeOH (30/70)	-600 mV, 30 min
10	NIP	1 s 900 mV, 1 s -600 mV, 900 s	200 mM Py in PBS- KCl /MeOH (30/70)	-600 mV, 30 min
11	MIP	1 s 900 mV, 1 s -600 mV, 300 s	200 mM Py 10 mM Cf in PBS- KCl /MeOH (30/70)	-600 mV, 30 min
12	MIP	1 s 900 mV, 1 s -600 mV, 900 s	200 mM Py 10 mM Cf in PBS- KCl /MeOH (30/70)	-600 mV, 30 min

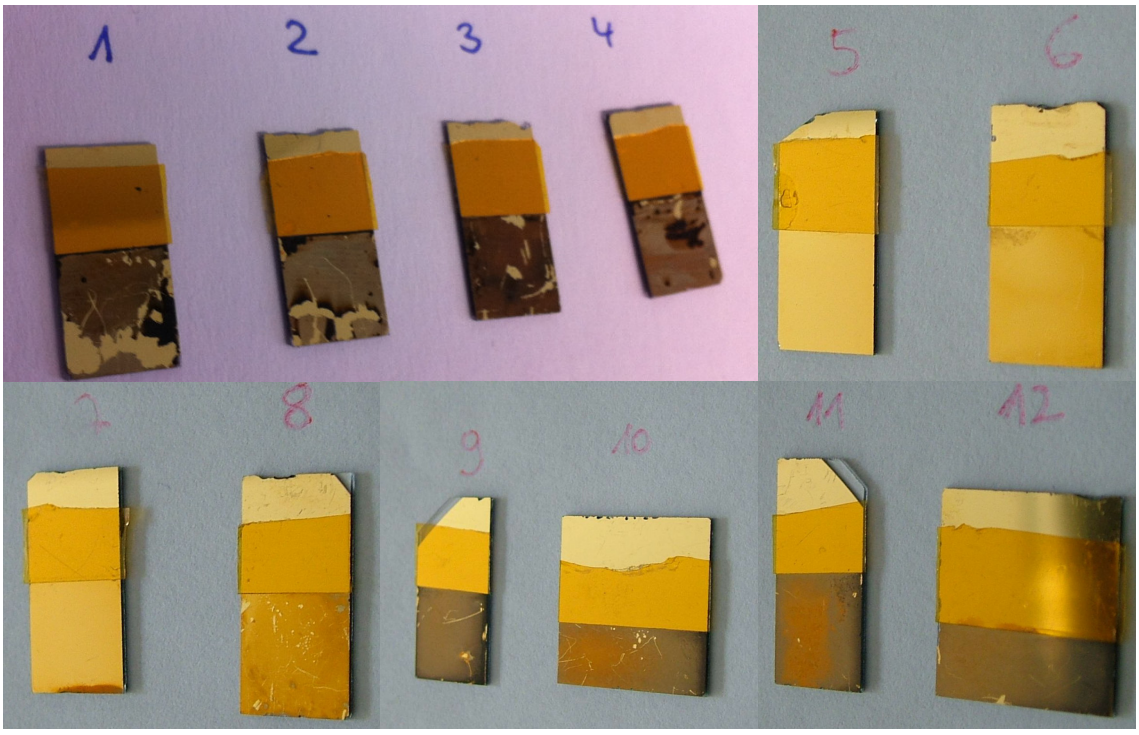

Fig. 78: Polypyrrole samples. 1–4: PBS-KNO_3/EtOH; 5–8: PBS-KNO_3/MeOH; 9–12: PBS-KCl/MeOH.

The PAD current responses of polypyrrole samples made in PBS-KNO_3/EtOH (Fig. 79) were slightly exponential for NIP and MIPs during the first 5 minutes and then continued in a linear way (samples 1–4). Fig. 80 shows the PAD sensor response of samples 1–4 to 30 µM clofibric acid. Sample 2 and 4 (MIPs) were made under the same conditions (1 mM clofibric acid). They showed similar responses in PAD experiments to 30 µM clofibric acid with ΔI values between 60–80 µA comparable to the NIP (Sample 1). Sample 3 was polymerized in a solution containing 10 mM clofibric acid. Here the response was 28 µA higher than for the NIP. Repeated release and binding experiments showed variations in the response between 72–346 µA. As former experiments showed similar responses for repeated binding (Fig. 77) and the polymers adhered better to the surface when sensors had been made in methanolic solution with higher fraction of organic solvent, further samples were prepared in methanolic solution (Plates 5–8).

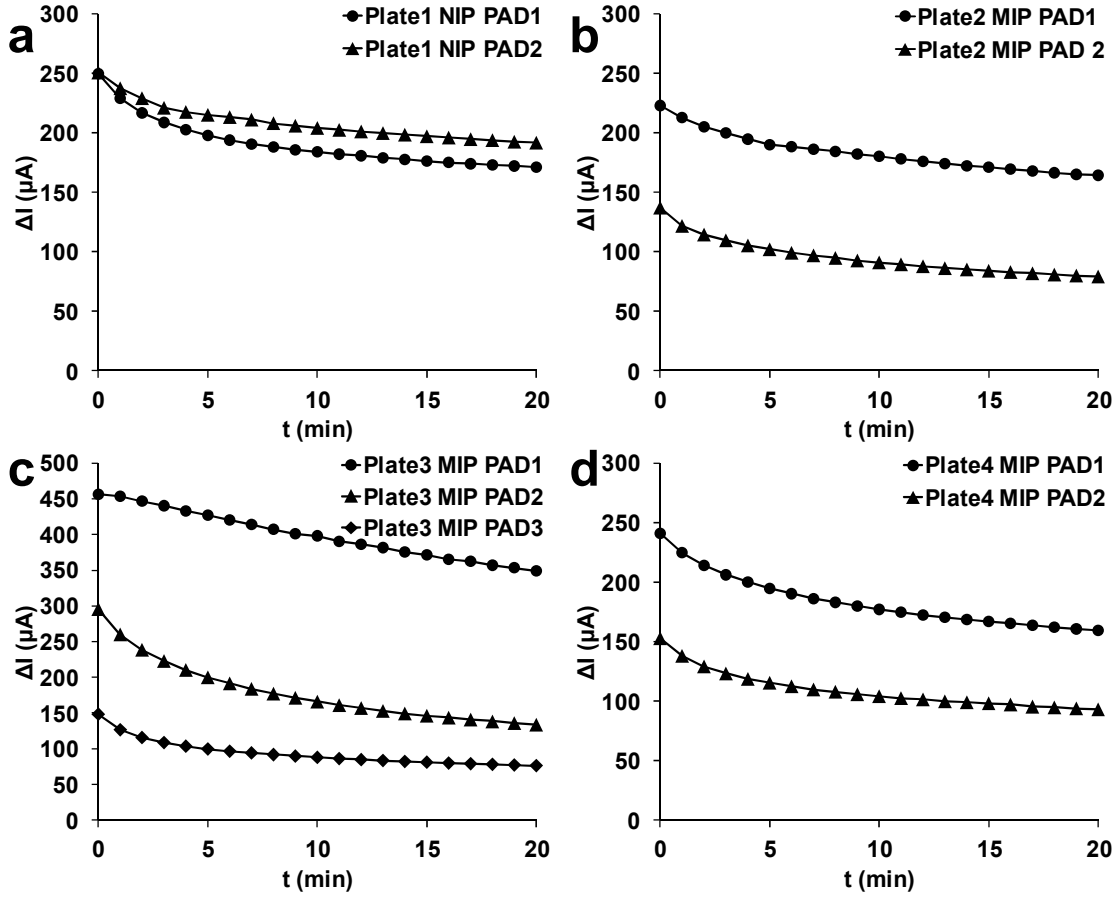

Fig. 79: Current response of polypyrrole samples 1–4 made in PBS-KNO_3/EtOH to 30 µM clofibric acid.

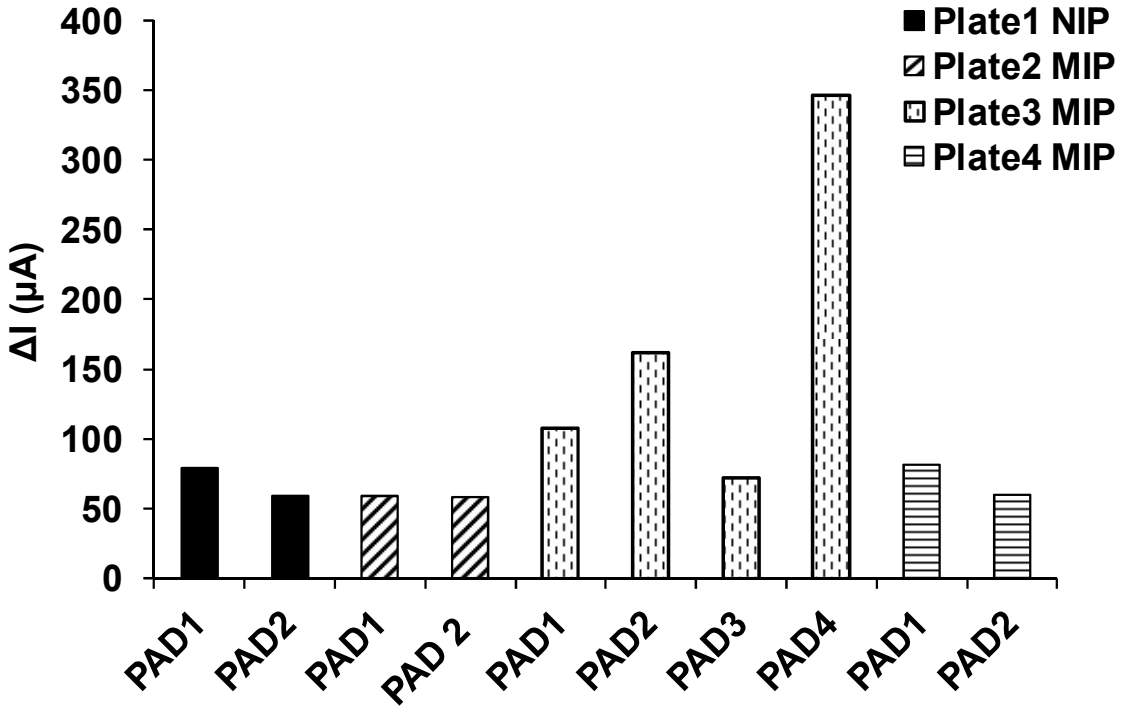

Fig. 80: PAD sensor response of polypyrrole samples 1–4 made in PBS-KNO_3/EtOH to 30 μM clofibric acid.

Fig. 81 shows the current responses of samples 5–8 made in PBS-KNO_3/MeOH. Here, the binding curves obtained after the second and third release reached saturation after ~10 min. MIP and NIP films did not show a difference in PAD sensor response (Fig. 82). Films prepared with a polymerization time of 300 s showed for both MIP and NIP a response of about 50 μA at the first binding, which decreased to ~40 μA at the second binding and increased again at the third binding. Films prepared with a polymerization time of 900 s showed a decrease from ~50 μA to 20 μA from the first to the third binding.

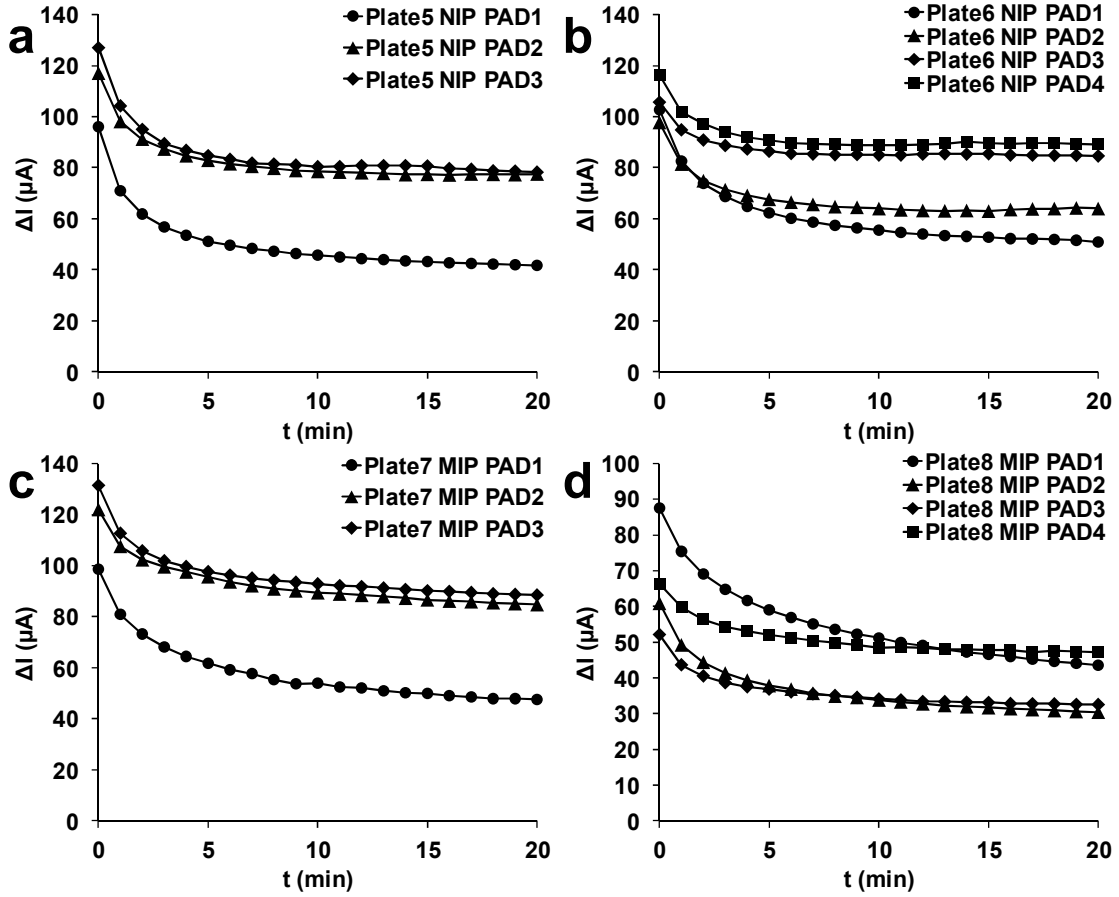

Fig. 81: Current response of polypyrrole samples 5–8 made in PBS-KNO_3/EtOH to 30 μM clofibric acid.

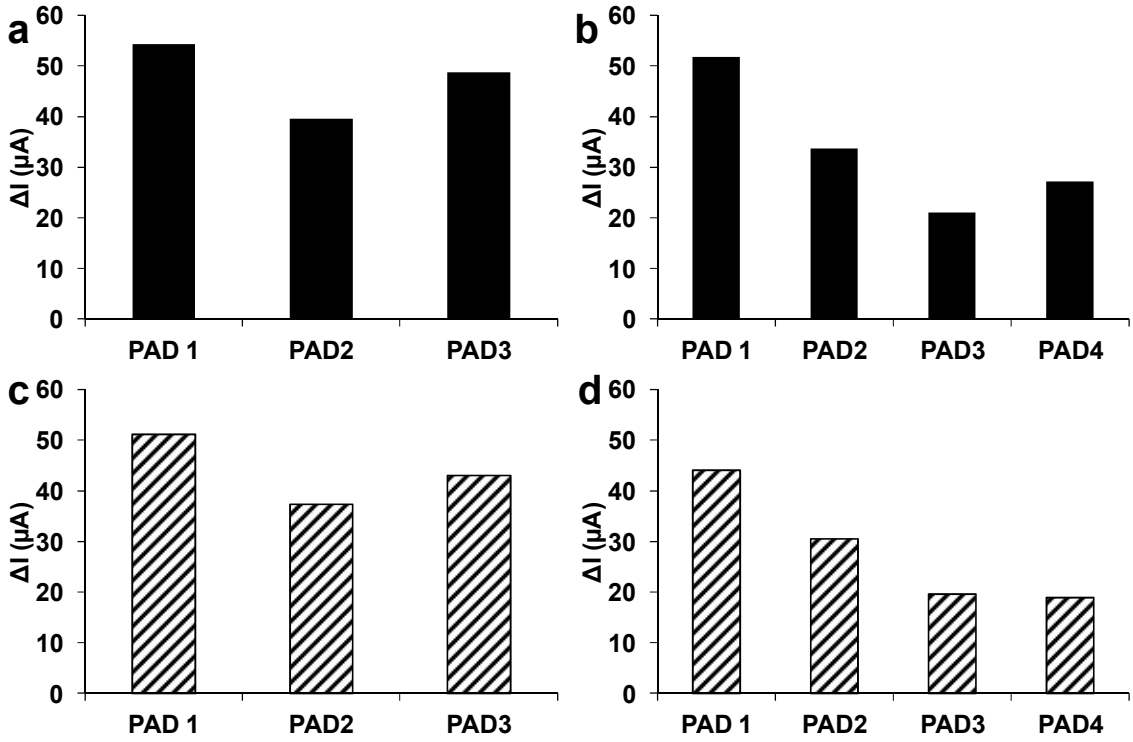

Fig. 82: PAD sensor response of polypyrrole samples made in PBS-KNO_3/MeOH to 30 μM clofibric acid. (a) Plate 5 (NIP); (b) Plate 6 (NIP); (c) Plate 7 (MIP); (d) Plate 8 (MIP).

The PAD current responses of samples 9–12 made in PBS-KCl/MeOH (Fig. 83) showed a linear decrease during the first binding experiment for both of the MIPs and for the NIP with a polymerization time of 300 s. The current response of the NIP with 900 s polymerization time instead increased during the first 5 min of the first binding experiment (Fig. 83b). During the second and third binding tests, the decrease was slightly exponential during the first five min for all samples and then continued in a more linear way.

With KCl, the sensor responses reached values above 1000 µA (Fig. 84). The first binding test resulted in a lower response of NIPs (Plate 9: 377 µA, Plate 10: 142 µA) than of MIPs (Plate 11: 1040 µA, Plate 12:1157 µA) to clofibric acid, but the second binding test showed similar responses for NIP and MIP. At the third binding test, the response of the MIPs was reduced to nearly 50%, while the response of the NIP was at 1008 µA. The addition of KCl produced a difference in the response of NIPs and MIPs for both polymerization times, but only for the first binding experiment.

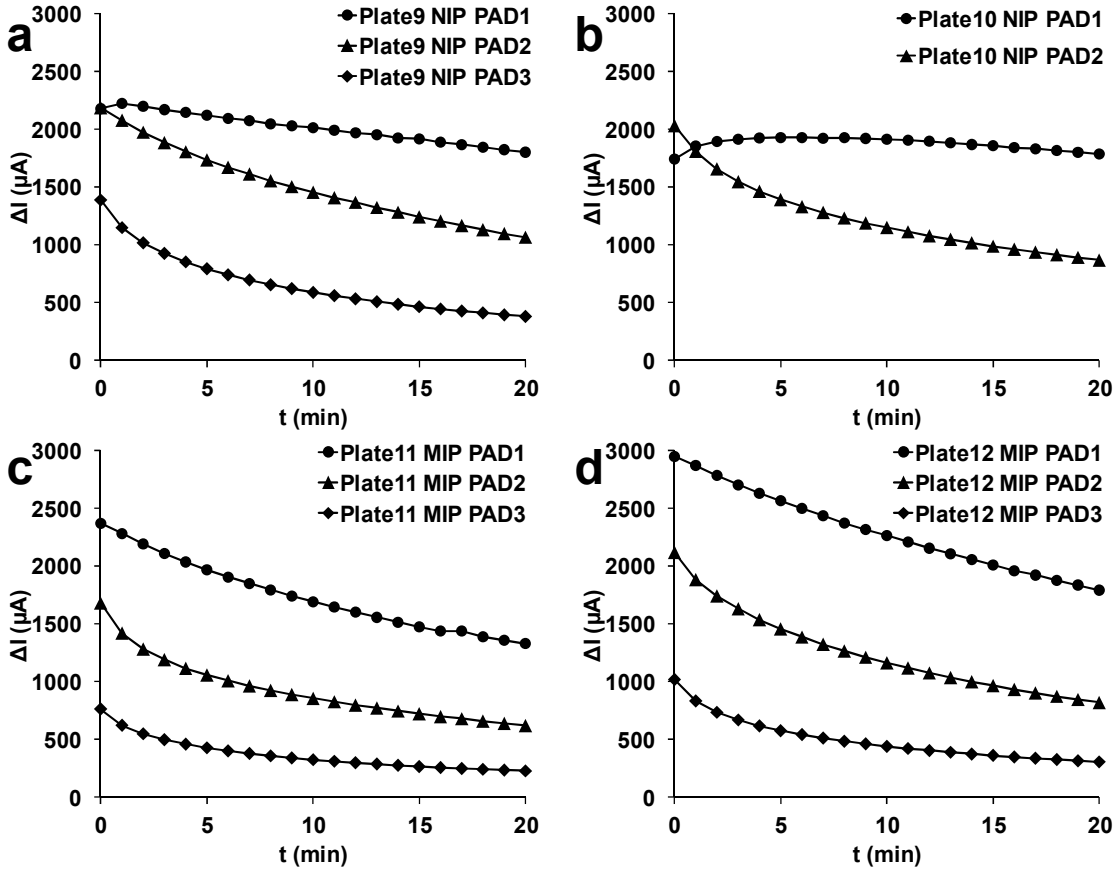

Fig. 83: Current response of polypyrrole samples 9–12 made in PBS-KNO_3/EtOH to 30 µM clofibric acid.

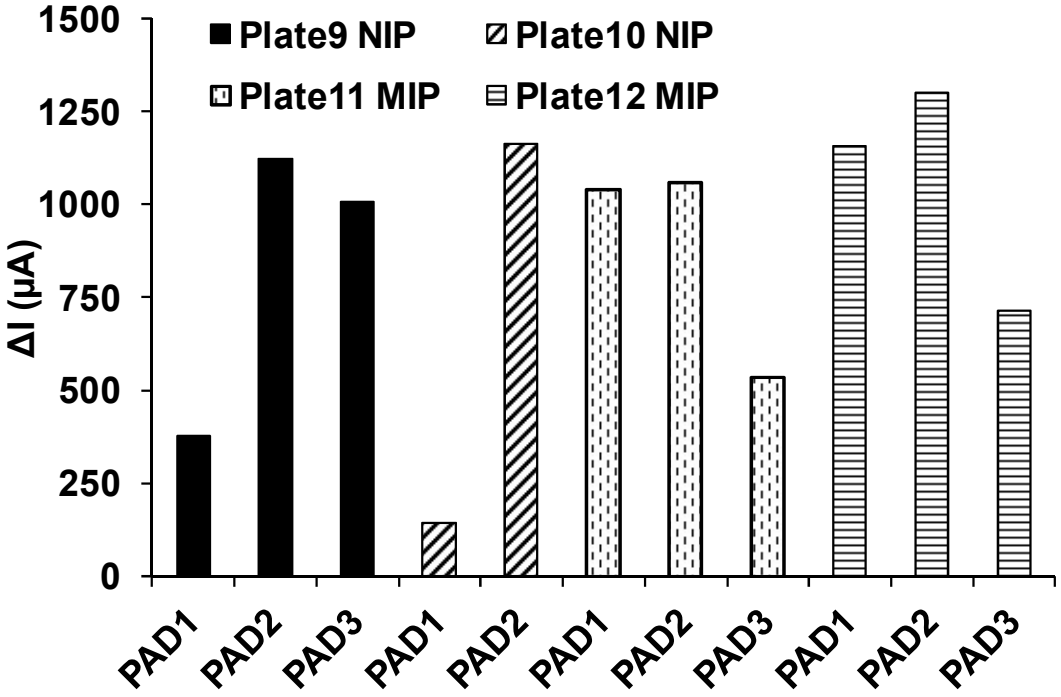

Fig. 84: Sensor response of polypyrrole samples 9–12 made in PBS-KCl/MeOH to 30 μM clofibric acid.

5.3.3 Achievements by potential pulse polymerization

With potential pulses, it is possible to produce adherent films, which do not delaminate during a treatment with negative constant potential. The addition of organic solvent helped to dissolve 10 mM of clofibric acid and an amount of 70% methanol also made the films more homogenous compared to films made with 10% ethanol. A difference between MIP and NIP signals could be obtained in KCl. Still the difference is obtained only for the first use of the sensor.

5.4 Polymerization of pyrrole derivatives

The introduction of functional groups into the polymer could increase the quantity of non-covalent interactions between the template and the polymer. For the imprinting of biomolecules containing amino groups, pyrrole propionic acid (PPA) could be used. As clofibric acid contains a carboxylic acid group, it might be advantageous for imprinting to use a pyrrole derivative such as 2-(1H-pyrrole-1-yl)ethanamine with an amino group, which could build hydrogen bonds with the hydroxyl groups (Fig. 85). Anti-mouse immunoglobulin G (IgG) was entrapped galvanostatically in poly-PPA on glassy carbon electrode for amperometric immunosensing of the antigen, mouse IgG [151]. The same group immobilized anti-mouse IgG on poly-PPA polymerized with cyclic voltammetry on SPR sensors for immunosensing [152]. A multi-walled carbon nanotube modified glassy carbon electrode with poly-PPA coating polymerized with cyclic voltammetry was used for immobilization of anti insulin-like growth factor 1 (IGF1) and the amperometric detection of IGF1 [153].

2-(1H-pyrrole-1-yl)ethanamine was linked to 2,3-dichloronaphthoquinone and chloranil and the resulting monomers were electrochemically polymerized on platinum [154]. In another approach, 2-(1H-pyrrole-1-yl)ethanamine was linked to an alkyl monolayer on silicon substrate and subsequently polymerized by cyclic voltammetry [155]. It was also used to modify oligonucleotides with pyrrole functionality to copolymerize subsequently the nucleotides with pyrrole [156].

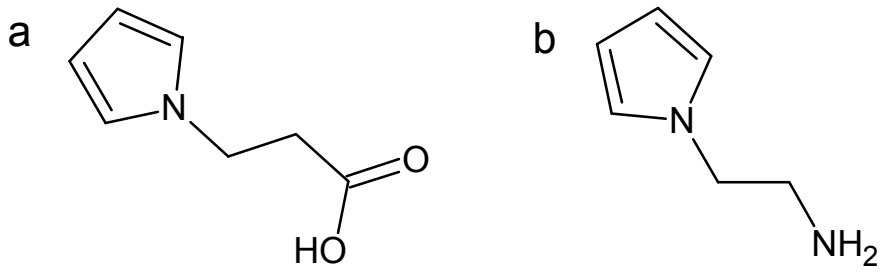

Fig. 85: Molecular structures of (a) pyrrole propionic acid (PPA) and (b) 2-(1H-pyrrole-1-yl)ethanamine.

5.4.1 Polymerization test of PPA in KNO_3-solution

First polymerization tests were done on gold coated glass slides with three potential ranges, but there was no visible film on the samples and cyclic voltammograms in KNO_3 after polymerization had the same shape as before polymerization. The next tests were done on QCM sensors to observe the frequency change during polymerization. In the cyclic voltammogram an oxidation peak appeared at potentials above 0.9 V. The current of the oxidation peak was the highest for the first cycle and

decreased with higher cycle numbers (Fig. 86). The frequency decreased during electropolymerization for NIP (Fig. 87) and MIP (Fig. 88), but when the sensor was washed with KNO_3 solution, the frequency went back to the level it had before polymerization, indicating that the polymer did not adhere to the sensor and was easily washed away.

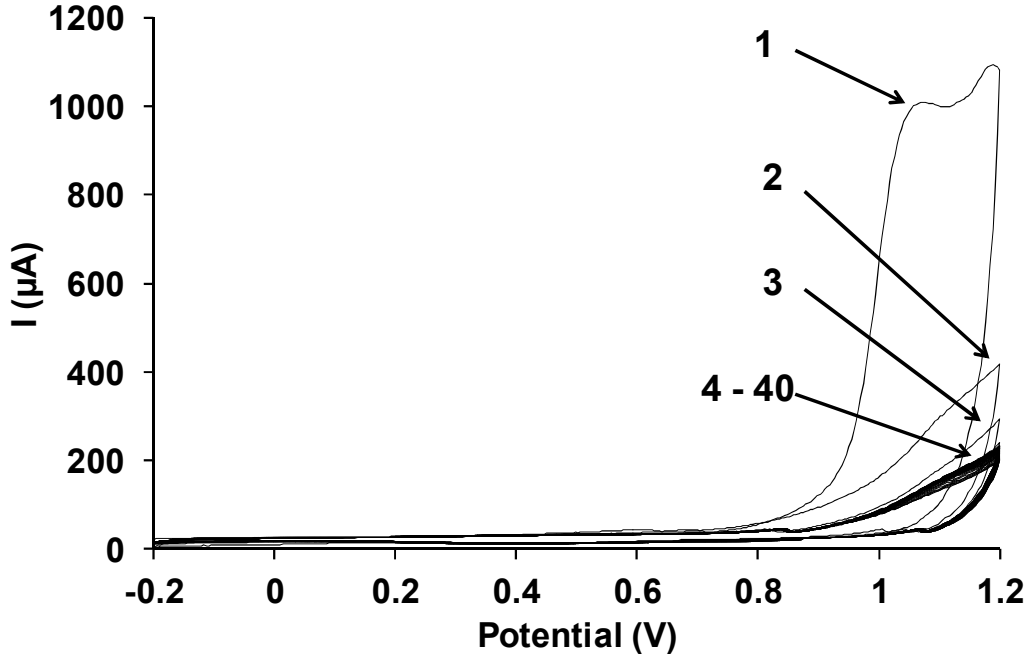

Fig. 86: Polymerization of PPA with cyclic voltammetry.

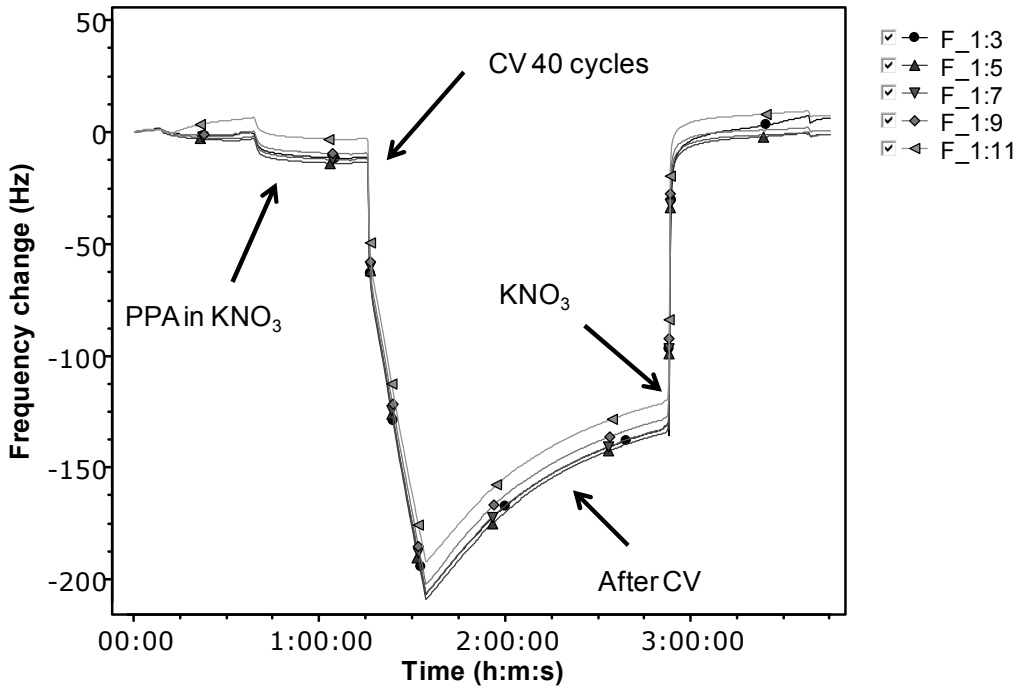

Fig. 87: Frequency change during polymerization experiment with PPA.

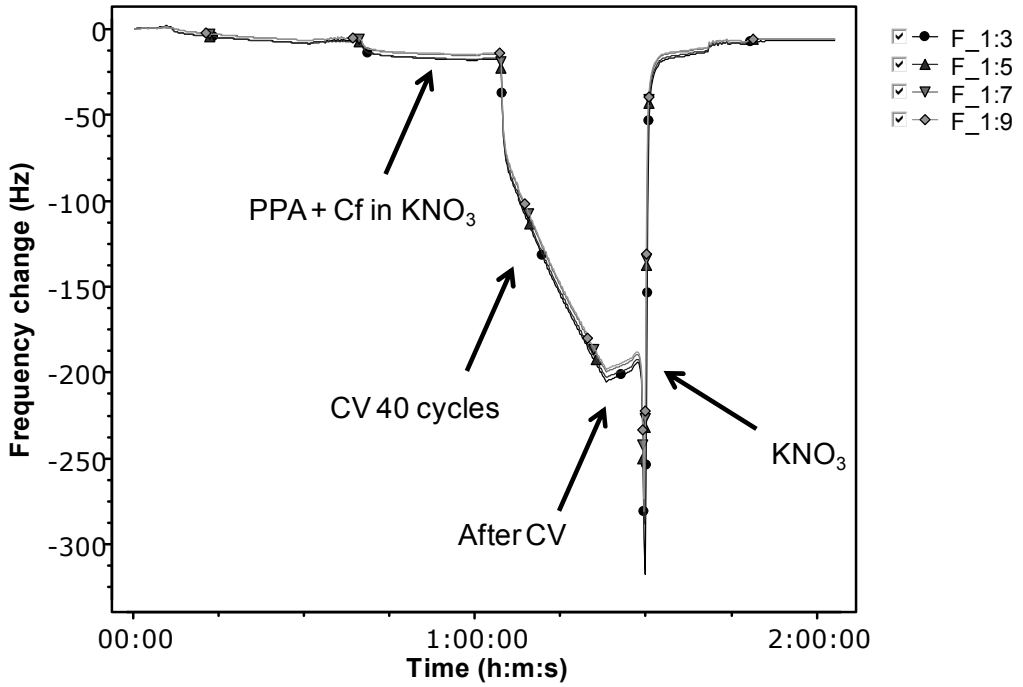

Fig. 88: Frequency change during polymerization experiment with PPA and clofibric acid.

5.4.2 Polymerization test of PPA on polypyrrole layer in KNO_3 solution

In the next experiment, pyrrole was polymerized on a QCM sensor with 5 cycles. In a second step, it was tried to polymerize PPA onto the polypyrrole layer. A drop of frequencies could be observed during potential cycling, but after polymerization the frequencies increased directly when KNO_3 was introduced into the sensor chamber (Fig. 89). A thin film of polypyrrole did not help to attach poly-PPA to the sensor surface.

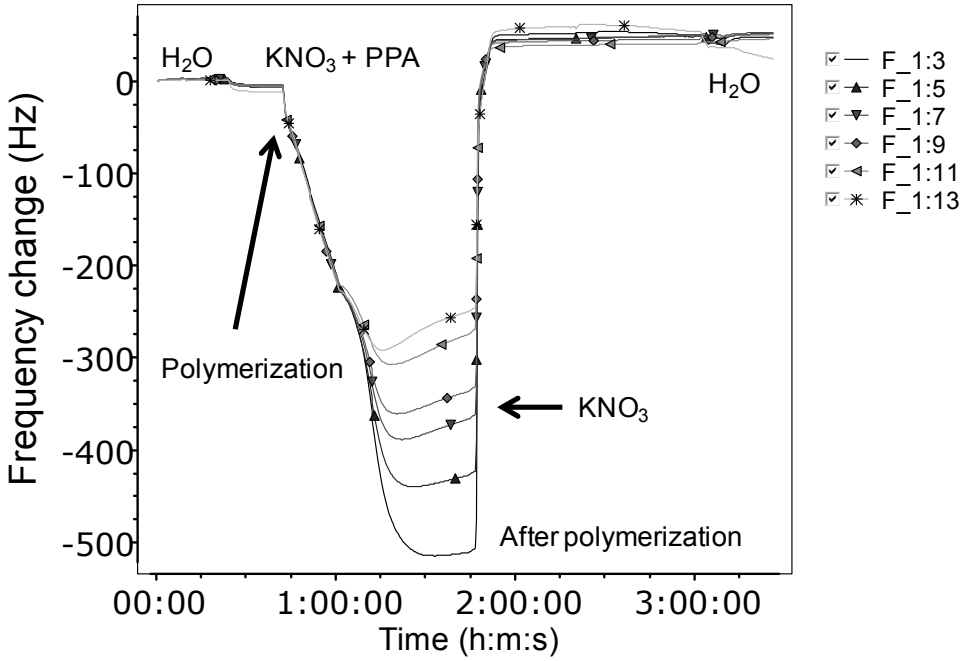

Fig. 89: Frequency change during polymerization experiment with 20 mM PPA and 40 cycles on polypyrrole.

5.4.3 Copolymerization of PPA with pyrrole

Copolymerization was tested with a 1:1 mixture of 20 mM PPA and 20 mM pyrrole. The first oxidation peaks appeared at potentials above 0.8 V in the cyclic voltammograms of MIP and NIP (Fig. 90). The current of the oxidation peak was the highest for the first cycle and decreased with higher cycle numbers.

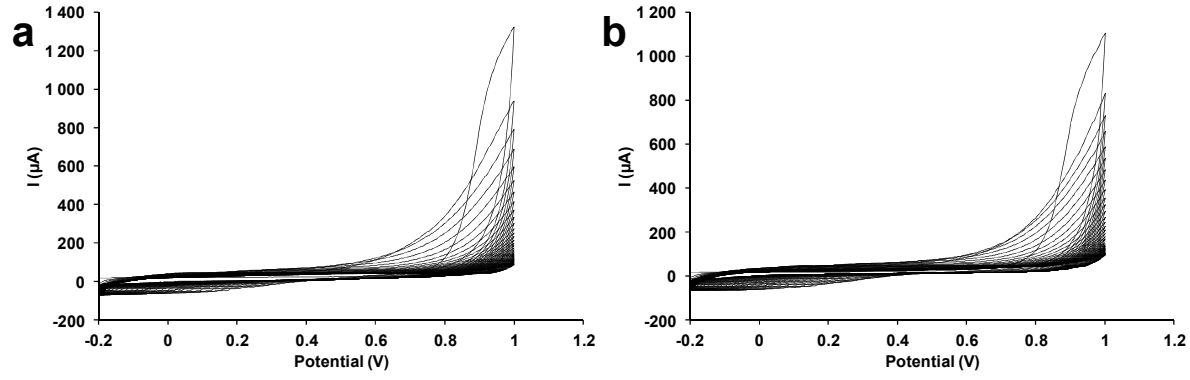

Fig. 90: Cyclic voltammograms of copolymerization of PPA with pyrrole. (a) NIP; (b) MIP.

A frequency drop of about 240 Hz appeared for NIP and MIP during polymerization (Fig. 91, Fig. 92). This drop remained stable after polymerization and during washing with KNO_3 indicated mass deposition on the sensor.

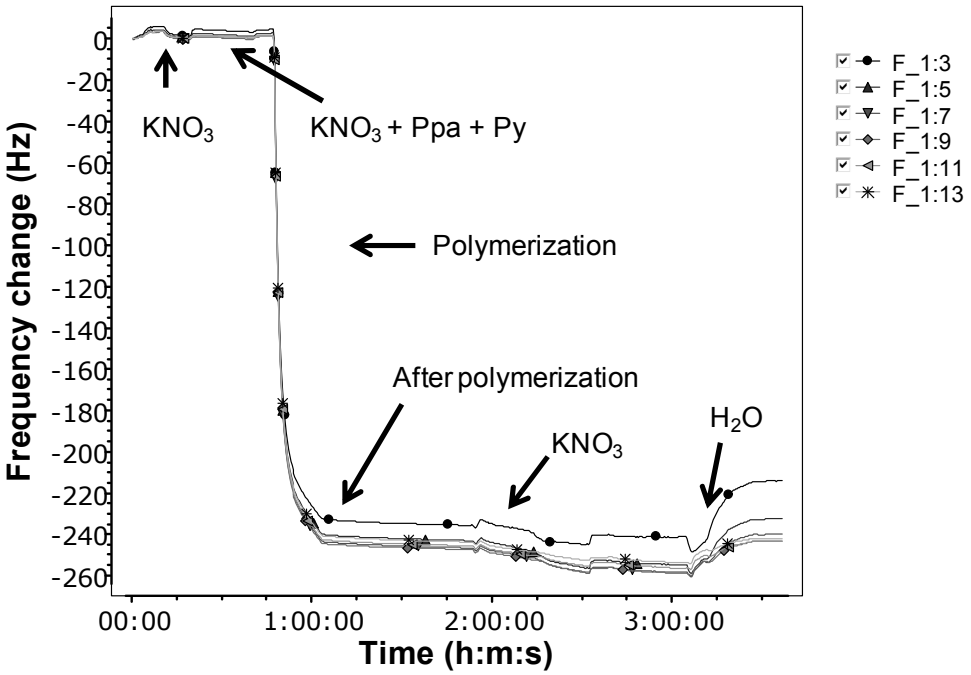

Fig. 91: Frequency change during copolymerization of PPA with pyrrole.

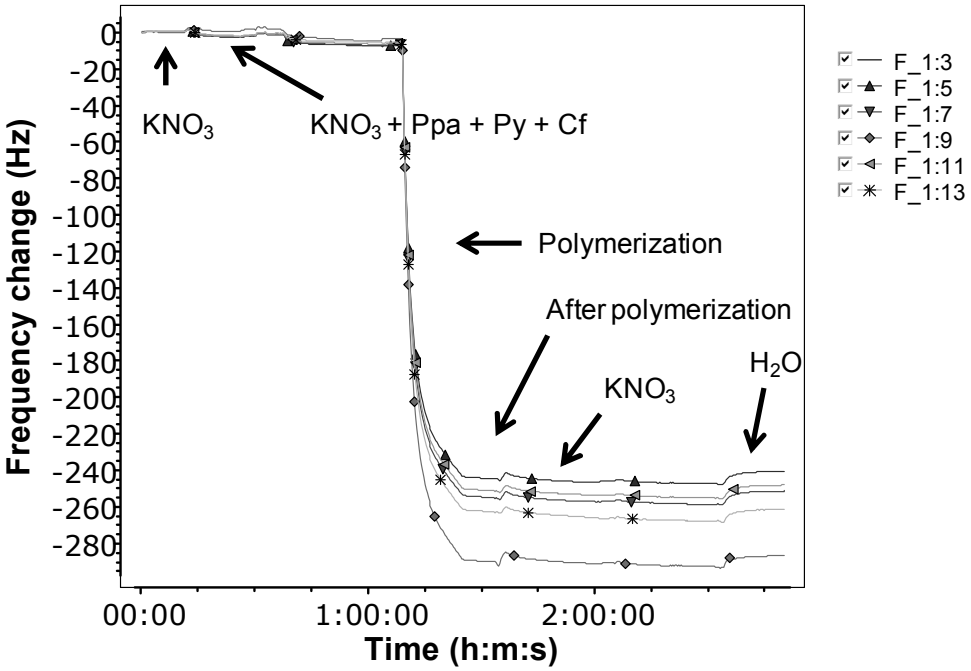

Fig. 92: Frequency change during copolymerization of PPA with pyrrole in the presence of clofibric acid.

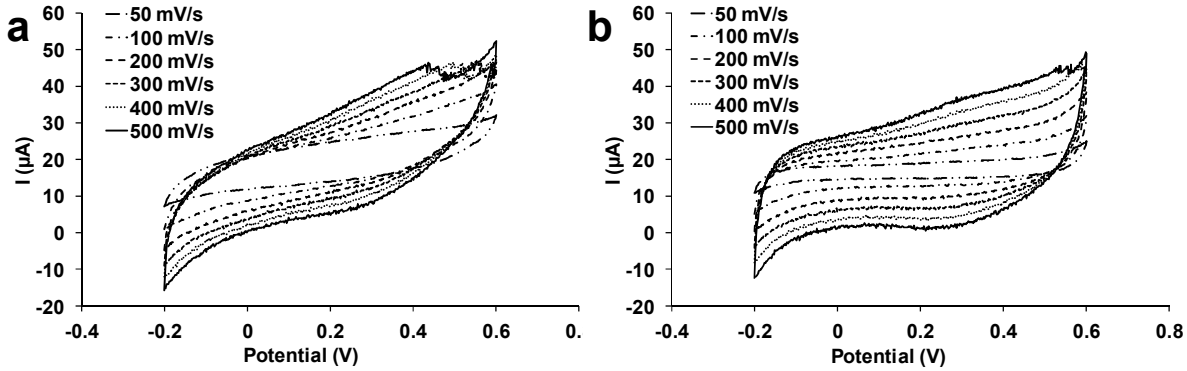

Fig. 93: Cyclic voltammetry of copolymer with scan rates from 50 mV s^{-1}–500 mV s^{-1}. (a) NIP; (b) MIP.

Cyclic voltammograms were recorded in KNO_3 with different scan rates (Fig. 93). The anodic peaks increased for the NIP from 50–200 mV s^{-1}, but with higher scan rates deformation of the peaks occurred. For the MIP, the anodic peaks increased for scan rates between 50–300 mV s^{-1}, while for 400–500 mV s^{-1} peak deformation was observed.

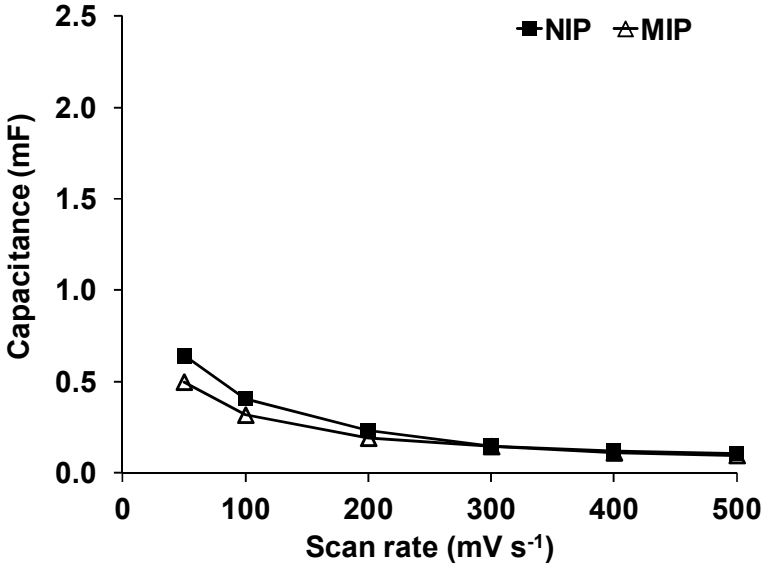

Fig. 94: Capacitance change of NIP and MIP copolymer with scan rate.

The capacitances of the copolymers were calculated dividing the cathodic peak currents by the scan rates (Fig. 94). With a scan rate of 50 mV s^{-1}, capacitances for the NIP copolymer of 0.6 mF and for the MIP copolymer of 0.5 mF were found. They decreased with increasing scan rates to 16% (NIP) and 20% (MIP) of the primary values. Capacitances of ~2 mF were found for polypyrrole prepared with 20 mM pyrrole (Fig. 95, E4 rhomb) at a scan rate of 50 mV^{-s}. With a lower concentration of 5 mM pyrrole, the capacitance of NIP E4 (square) was comparable to the capacitance of the copolymers (0.7 mF).

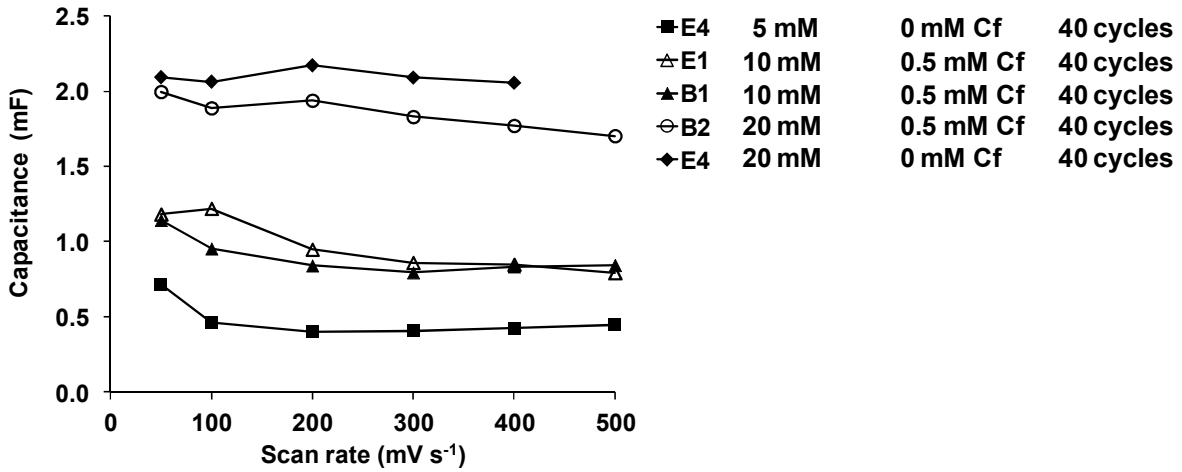

Fig. 95: Capacitance change of polypyrrole NIP and MIP (data obtained from Fig. 35).

The capacitances of the polypyrrole polymers decreased with increasing scan rate, but not lower than to 60% of the primary values (Fig. 96). The capacitance was retained more with increasing pyrrole concentration. With 20 mM pyrrole, the capacity was retained to 98% (E4 rhomb). The presence of clofibric led to a capacitance of 85% (B2 circle).

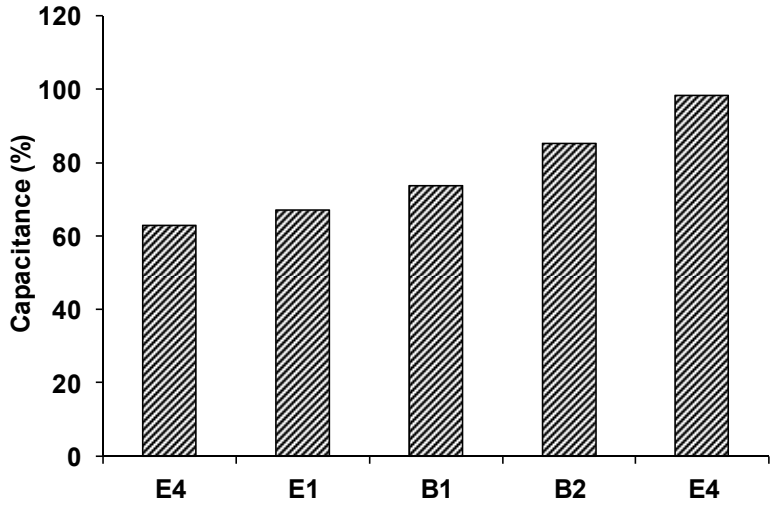

Fig. 96: Capacitance retained at 500 mV^{-s} compared to capacitance at 50 mV^{-s}.

The larger capacitance of thicker films (Table 18) might result from a higher conductivity and that a larger surface area is accessible for ions from the solution [157]. The peak deformation and the low capacitance with higher scan rates could indicate that the polypyrrole-PPA-copolymer is less stable than polypyrrole.

Table 18: Deposited mass of polypyrrole MIPs and NIPs used for scan rate experiments

Sensor	E4	E1	B1	B2	E4
Mass (µg cm^{-2})	2.9	4.9	4.7	10.6	10.2

5.4.4 Copolymerization of pyrrole with 2-(1H-pyrrole-1-yl)ethanamine

The copolymerization of pyrrole and 2-(1H-pyrrole-1-yl)ethanamine with a ratio of 3:1 was done in PBS and Na-pTS.

Table 19: Mass and thickness of copolymers

Sensor	Mass (ng cm^{-2})	Thickness (nm)	Solvent
QCM F1	865	5.8	PBS
QCM F2	1070	7.2	Na-pTS

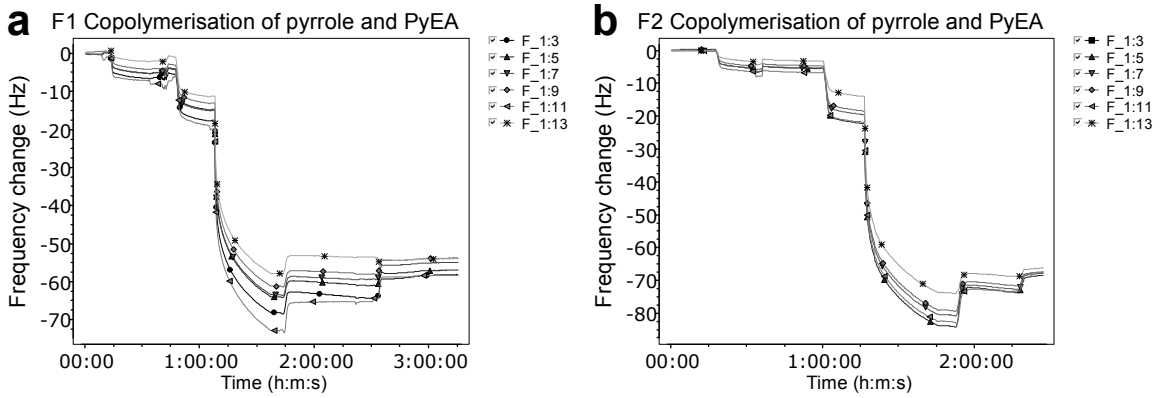

Fig. 97: Frequency change during copolymerization in (a) buffer solution and (b) Na-pTS.

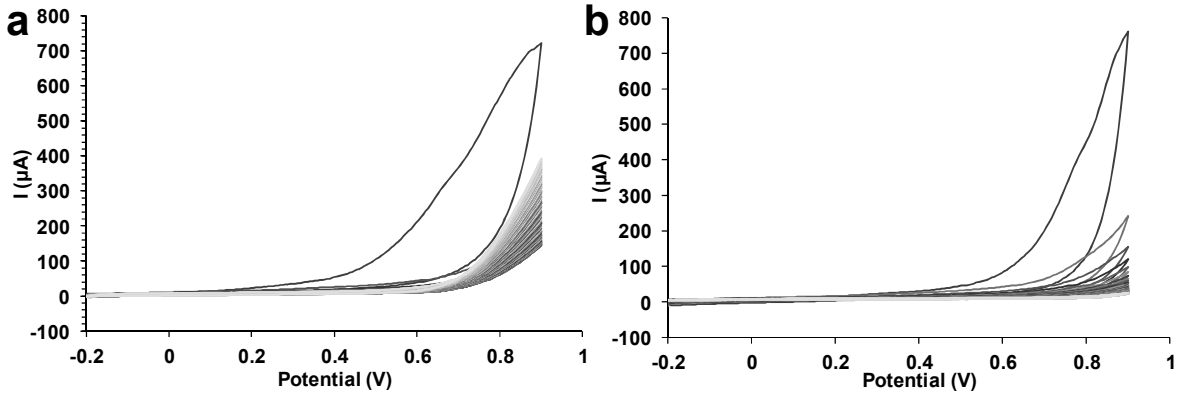

Fig. 98: Voltammograms of copolymerization of pyrrole (100 mM) and 2-(1H-pyrrole-1-yl)ethanamine (33 mM) with 80 cycles in (a) buffer solution and (b) Na-pTS.

Fig. 97 shows a frequency drop between 60–75 Hz for polymerization in buffer solution and between 80–90 Hz for polymerization in Na-pTS. This drop remained stable after polymerization and during washing and indicated mass deposition on the sensor. The mass deposition with 100 mM pyrrole and 33 mM 2-(1H-pyrrole-1-yl)ethanamine (33 mM) with 80 cycles was very low with ~1 µg cm^{-2} (Table 19)

compared to pyrrole polymerization, where 80 mM pyrrole polymerized with 80 cycles resulted in a mass deposition of ~3 μg cm^{-2} (Table 8).
An oxidation peak appeared in the cyclic voltammogram at potentials above 0.7 V. The current of the oxidation peak was the highest for the first cycle and decreased with higher cycle numbers (Fig. 98). The decrease was lower in Na-pTS solution compared with buffer solution.
A PAD binding experiment with 30 μM clofibric acid gave a sensor response of 9 μA. Compared with imprinted polypyrrole (*c.f.* section 5.2.6), where responses between ~15–30 μA were obtained, the response of the copolymer is low.

5.4.5 Achievements by copolymerization

The polymerization of pyrrole derivatives was successful when the derivative was copolymerized with pyrrole. For PPA alone, a drop of QCM frequencies and oxidation peaks could be observed during potential cycling, but the increase of the frequencies after polymerization when KNO_3 was introduced into the sensor chamber indicated that the polymer did not adhere to the sensor surface. Cyclic voltammograms with different scan rates showed that the Py-PPA-copolymer might be less stable in electrochemical measurements than polypyrrole. Optimization of the polymerization parameters, e.g., monomer ratio or polymerization potential, could improve the copolymer characteristics.
The response of an imprinted copolymer of pyrrole and 2-(1H-pyrrole-1-yl)ethanamine to a PAD binding experiment was low compared to imprinted polypyrrole. Here also optimization of the polymerization parameters and the washing conditions might improve the sensor response.

6 Conclusion and outlook

In this work, the development of an electrochemical sensor for clofibric acid based on molecularly imprinted polypyrrole synthesized via electropolymerization was investigated. It was found that polymerization is hindered by the presence of clofibric acid in KNO_3 solutions and phosphate buffer solutions. Mass deposition performed with different sensors under the same polymerization conditions gave reproducible masses with a standard deviation of 6%.

Several solvents were tested for removal of the template. With the use of 70% ethanol, the amount of chlorine found in XPS measurements decreased compared with water and acetonitrile.

Binding experiments with QCM did not result in consistent data. When binding was tested with PAD, it was concluded that the removal of the template after polymerization needed optimization. Washing with solvents under stirring was tested with different washing times. A one hour wash led to reproducible results with PAD binding measurements, but the highest sensor response to clofibric acid could be obtained only after the second wash.

In the next step, washing was also tested under PAD conditions with ethanolic HCl/KCl solution. Binding experiments showed then a higher response of the MIPs to clofibric acid than of the NIPs. The highest sensor response could be obtained after the first wash with PAD washing.

Zeta potential, contact angle, and XPS measurements were done after coating, after PAD washing, and after PAD binding and also revealed differences between MIPs and NIPs. The isoelectric point was lower for MIPs than for NIPs, which might indicate a stronger interaction of clofibric acid with MIP than with NIP. The incorporation of lipophilic clofibric acid molecules could explain why contact angles were higher for MIPs than for NIPs. Samples which were subject to PAD washing and PAD binding contained a lower fraction of C-H groups and a higher fraction of C=O and C-O groups on the surface. The repetition of potential pulses during the PAD treatment might promote the oxidation of the polymer backbone, or dissolved oxygen from the solvents used during PAD might be incorporated into the swollen polymer and might contribute to the degradation of polypyrrole. This oxidation of the polymer structure could explain the conductivity decrease with repeated PAD measurements.

Binding tests with 2,4-D and CBZ showed a pronounced selectivity of the imprinted polymer for clofibric acid *vs.* CBZ with 3.8 for the MIP and 1.4 for the NIP, but the

response to 2,4-D was higher than the response to clofibric acid, presumably due to the structural similarities between the two molecules. The hydrogen atoms in the acetic acid group might allow more hydrogen bonds between 2,4-D and polypyrrole than between clofibric acid and polypyrrole (*c.f.* section 5.2.7, Fig. 61). The high response of MIP and NIP to PES could also be explained by the acetic acid group. The low response of the MIP to CBZ suggests imprinted cavities selective for clofibric acid and closely structurally related molecules; *i.e.*, this and the comparison with the NIP reveals some specificity of the imprinting process.

To be able to apply negative potentials as washing method, potential pulses were tested as polymerization method because films produced by cyclic voltammetry delaminated from the sensor surface when negative potentials were applied for a certain time. Adherent films, which did not detach during the application of -600 mV for 30 min, were produced with methanolic phosphate buffer-KNO_3 or -KCl solution. Films prepared in methanolic phosphate buffer-KNO_3 solution did not show a difference between MIPs and NIPs, but the response of films prepared with a polymerization time of 300 s was different to the response of films prepared with 900 s. The addition of KCl produced a difference in the response of NIPs and MIPs for both polymerization times, but only for the first binding experiment.

AFM measurements of these films could show if the surface roughnesses increased with potential pulses compared to cyclic voltammetry. XPS measurements could show if clofibric acid is released from the polymer by a negative potential when a suitable dopant not containing chlorine could be found. Also the influence of PAD measurements on the structure could be investigated by monitoring the fraction of C=O and C-O groups. Additionally, HPLC or mass spectrometry analysis of the release solution might show the presence of clofibric acid if its concentration is high enough.

Another possibility to make films more adherent could be the roughening of the surface [73]. Overoxidation could then be tested as possibility to obtain a higher fraction of non-covalent binding between polymer and template.

As the introduction of functional groups into the polymer could increase the quantity of non-covalent interactions between the template and the polymer, PPA and 2-(1H-pyrrole-1-yl)ethanamine were tested as monomers. For PPA, a drop of QCM frequencies and oxidation peaks could be observed during potential cycling, but the increase of the frequencies after polymerization when KNO_3 was introduced into the sensor chamber indicated that the polymer did not adhere to the sensor surface.

Only copolymerization of PPA with pyrrole (1:1) resulted in an adherent polymer film. Cyclic voltammetry with different scan rates indicated that the copolymer might be less stable in electrochemical measurements than polypyrrole. Copolymerization of pyrrole with 2-(1H-pyrrole-1-yl)ethanamine (3:1) also gave an adherent film. The mass deposition was low with ~1 µg cm^{-2} compared to pyrrole polymerization, where a lower pyrrole concentration resulted in a mass deposition of ~3 µg cm^{-2}.

The surface and binding properties of pyrrole copolymers could be further investigated and improved by optimization of the polymerization parameters.

The feasibility of sensor fabrication with a combination of molecular imprinting and electrochemical deposition of polypyrrole for the detection of clofibric acid could be demonstrated, but the specificity (response for MIP *vs.* NIP) and selectivity were strongly dependent on preparation and washing conditions.

7 References

1. Marty, J.; Mauzac, M. Molecular imprinting: State of the art and perspectives. In *Microlithography · Molecular Imprinting*; Advances in polymer science; Springer Berlin Heidelberg, 2005; Vol. 172, pp. 1–35.

2. Öpik, A.; Menaker, A.; Reut, J.; Syritski, V. Molecularly imprinted polymers: A new approach to the preparation of functional materials. *Proc. Est. Acad. Sci.* **2009**, *58*, 3–11.

3. Lichtenthaler, F. W. 100 Years "Schlüssel-Schloss-Prinzip": What made Emil Fischer use this analogy? *Angew. Chem. Int. Ed. Engl.* **1995**, *33*, 2364–2374.

4. Pauling, L.; Campbell, D. H.; Pressman, D. The nature of the forces between antigen and antibody and of the precipitation reaction. *Physiol. Rev.* **1943**, *23*, 203–219.

5. Katada, N.; Niwa, M. The re-birth of molecular imprinting on silica. In *Molecular imprinting of polymers*; Piletsky, S.; Turner, A., Eds.; Landes Bioscience, Georgetown, Texas, 2006; pp. 26–40.

6. Wulff, G.; Sarhan, A.; Zabrocki, K. Enzyme-analogue built polymers and their use for the resolution of racemates. *Tetrahedron Lett.* **1973**, 4329–4332.

7. Arshady, R.; Mosbach, K. Synthesis of substrate-selective polymers by host-guest polymerizatioa. *Die Makromol. Chemie* **1981**, *182*, 687–692.

8. Wulff, G. Fourty years of molecular imprinting in synthetic polymers: origin, features and perspectives. *Microchim. Acta* **2013**, *180*, 1359–1370.

9. Mosbach, K.; Ramström, O. The emerging technique of molecular imprinting and its future impact on biotechnology. *Nat. Biotechnol.* **1996**, *14*, 163–170.

10. Alexander, C.; Andersson, H. S.; Andersson, L. I.; Ansell, R. J.; Kirsch, N.; Nicholls, I. A.; O'Mahony, J.; Whitcombe, M. J. Molecular imprinting science and technology: A survey of the literature for the years up to and including 2003. *J. Mol. Recognit.* **2006**, *19*, 106–80.

11. Yan, H.; Row, K. H. Characteristic and synthetic approach of molecularly imprinted polymer. *Int. J. Mol. Sci.* **2006**, *7*, 155–178.

12. Andersson, L. I. Solid-phase extraction on molecularly imprinted polymers: requirements, achievements and future work. In *Molecular imprinting of polymers*; Piletsky, S.; Turner, A., Eds.; Landes Bioscience: Georgetown, Texas, 2006; pp. 140–148.

13. Haupt, K.; Linares, A. V; Bompart, M.; Bui, B. T. S. Molecularly imprinted polymers. *Top. Curr. Chem.* **2012**, *325*, 1–28.

14. Haupt, K.; Dzgoev, A.; Mosbach, K. Assay system for the herbicide 2,4-Dichlorophenoxyacetic Acid using a molecularly imprinted polymer as an artificial recognition element. *Anal. Chem.* **1998**, *70*, 628–631.

15. Caro, E.; Marcé, R. M.; Cormack, P. A. G.; Sherrington, D. C.; Borrull, F. Molecularly imprinted solid-phase extraction of naphthalene sulfonates from water. *J. Chromatogr. A* **2004**, *1047*, 175–180.

16. Biffis, A.; Dvorakova, G.; Falcimaigne-Cordin, A. Physical forms of MIPs. *Top. Curr. Chem.* **2012**, *325*, 29–82.

17. Quaglia, M.; De Lorenzi, E.; Sulitzky, C.; Caccialanza, G.; Sellergren, B. Molecularly imprinted polymer films grafted from porous or nonporous silica: Novel affinity stationary phases in capillary electrochromatography. *Electrophoresis* **2003**, *24*, 952–957.

18. Hosoya, K.; Yoshizako, K.; Shirasu, Y.; Kimata, K.; Araki, T.; Tanaka, N.; Haginaka, J. Molecularly imprinted uniform-size polymer-based stationary phase for high-performance liquid chromatography Structural contribution of cross-linked polymer network on specific molecular recognition. *J. Chromatogr. A* **1996**, *728*, 139–147.

19. Mayes, A. G.; Mosbach, K. Molecularly imprinted polymer beads: Suspension polymerization using a liquid perfluorocarbon as the dispersing phase. *Anal. Chem.* **1996**, *68*, 3769–3774.

20. Sun, H.; Qiao, F.; Liu, G. Characteristic of theophylline imprinted monolithic column and its application for determination of xanthine derivatives caffeine and theophylline in green tea. *J. Chromatogr. A* **2006**, *1134*, 194–200.

21. Lv, Y.-K.; Jia, C.-L.; Zhang, J.-Q.; Li, P.; Sun, H.-W. Preparation and characterization of molecularly imprinted monolithic column for on-line solid-phase extraction coupled with HPLC for determination of the fluoroquinolone residues in honey samples. *J. Liq. Chromatogr. Relat. Technol.* **2013**, *36*, 249–260.

22. Lin, Z.; Yang, F.; He, X.; Zhao, X.; Zhang, Y. Preparation and evaluation of a macroporous molecularly imprinted hybrid silica monolithic column for recognition of proteins by high performance liquid chromatography. *J. Chromatogr. A* **2009**, *1216*, 8612–8622.

23. Qin, L.; He, X.-W.; Jia, M.; Li, W.-Y.; Zhang, Y.-K. A thermosensitive monolithic column as an artificial antibody for the on-line selective separation of the protein. *Chem. – A Eur. J.* **2011**, *17*, 1696–1704.

24. Wang, H.-F.; Zhu, Y.-Z.; Lin, J.-P.; Yan, X.-P. Fabrication of molecularly imprinted hybrid monoliths via a room temperature ionic liquid-mediated nonhydrolytic sol–gel route for chiral separation of zolmitriptan by capillary electrochromatography. *Electrophoresis* **2008**, *29*, 952–959.

25. Trotta, F.; Biasizzo, M.; Caldera, F. Molecularly imprinted membranes. *Membranes (Basel).* **2012**, *2*, 440–477.

26. Ulbricht, M.; Malaisamy, R. Insights into the mechanism of molecular imprinting by immersion precipitation phase inversion of polymer blends via a detailed morphology analysis of porous membranes. *J. Mater. Chem.* **2005**, *15*, 1487–1497.

27. Chen, R.-R.; Qin, L.; Jia, M.; He, X.-W.; Li, W.-Y. Novel surface-modified molecularly imprinted membrane prepared with iniferter for permselective separation of lysozyme. *J. Memb. Sci.* **2010**, *363*, 212–220.

28. Pérez-Moral, N.; Mayes, A. G. MIP formats for analytical applications. In *Molecular imprinting of polymers*; Piletsky, S.; Turner, A., Eds.; Landes Bioscience, Georgetown, Texas, 2006; pp. 1–11.

29. Sellergren, B.; Shea, K. J. Enantioselective ester hydrolysis catalyzed by imprinted polymers. *Tetrahedron: Asymmetry* **1994**, *5*, 1403–1406.

30. Sellergren, B.; Karmalkar, R. N.; Shea, K. J. Enantioselective ester hydrolysis catalyzed by imprinted polymers. 2. *J. Org. Chem.* **2000**, *65*, 4009–4027.

31. Svenson, J.; Nicholls, I. A. On the thermal and chemical stability of molecularly imprinted polymers. *Anal Chim Acta* **2001**, *435*, 19–24.

32. AFFINISEP AFFINIMIP® SPE - Selectives MIP SPE Cartridges http://www.polyintell.com/analytical-products-applications/spe-kit-for-sample-preparation/affinimip-spe---selectives-mip-spe-cartridges/ (accessed May 7, 2015).

33. Biotage AFFINILUTE™ MIP Columns http://www.biotage.com/product-page/affinilute-mip-columns (accessed May 7, 2015).

34. Sigma-Aldrich SupelMIP Molecularly Imprinted Polymer SPE Cartridges http://www.sigmaaldrich.com/analytical-chromatography/sample-preparation/spe/supelmip.html (accessed May 7, 2015).

35. Elschner, A.; Kirchmeyer, S.; Lövenich, W.; Merker, U.; Reuter, K. The discorvery and development of conducting polymers. In *PEDOT Principles and applications of an intrinsically conductive polymer*; CRC Press, Boca Raton, Florida, 2010; pp. 1–20.

36. Scott, J. C. History of conductive polymers. In *Nanostructured conductive polymers*; Eftekhari, A., Ed.; John Wiley & Sons Ltd.: Chichester, United Kingdom, 2010; pp. 1–17.

37. Shirakawa, H.; Louis, J.; Macdiarmid, A. G. Synthesis of electrically conducting organic polymers: Halogene derivatives of polyacetylene, (CH)x. *J. C. S. Chem. Comm* **1977**, 578–580.

38. Miller, J. S. Conducting polymers - materials of commerce. *Adv. Mater.* **1993**, *5*, 587–589.

39. Kumar, N.; Vadera, S. R.; Singh, J.; Das, G.; Negi, S. C.; Aparna, P.; Tuli, A. Conducting polymers: Emerging commercial materials. *Def. Sci. J.* **1996**, *46*, 91–104.

40. Yoon, H. Current trends in sensors based on conducting polymer nanomaterials. *Nanomaterials* **2013**, *3*, 524–549.

41. Ates, M.; Karazehir, T.; Sarac, A. S. Conducting polymers and their applications. *Curr. Phys. Chem.* **2012**, *2*, 224–240.

42. Balint, R.; Cassidy, N. J.; Cartmell, S. H. Conductive polymers: Towards a smart biomaterial for tissue engineering. *Acta Biomater.* **2014**, *10*, 2341–2353.

43. Inzelt, G. Redox transformations and transport processes. In *Conducting polymers*; Scholz, F., Ed.; Springer: Berlin, Heidelberg, 2008; pp. 169–224.

44. Dai, L. Conducting polymers. In *Intelligent macromolecules for smart devices*; Engineering Materials and Processes; Springer London, 2004; pp. 41–80.

45. Heinze, J.; Frontana-Uribe, B. A.; Ludwigs, S. Electrochemistry of conducting polymers-persistent models and new concepts. *Chem. Rev.* **2010**, *110*, 4724–4771.

46. Bredas, J. L.; Street, G. B. Polarons, bipolarons, and solitons in conducting polymers. *Acc. Chem. Res.* **1985**, *1305*, 309–315.

47. Machida, S.; Miyata, S.; Techagumpuch, A. Chemical synthesis of highly electrically conductive polypyrrole. *Synth. Met.* 1989, *31*, 311–318.

48. Ge, Y.; Turner, A. P. F. Too large to fit? Recent developments in macromolecular imprinting. *Trends Biotechnol.* **2008**, *26*, 218–24.

49. Bidan, G. Electropolymerized films of π-conjugated polymers. A tool for surface functionalization: A brief historical evolution and recent trends. In *Electropolymerization: Concepts, Materials and Applications*; Cosnier, S.; Karyakin, A., Eds.; Wiley-VCH Verlag GmbH & Co. KGaA, Weinheim, 2010; pp. 1–26.

50. Pardieu, E.; Cheap, H.; Vedrine, C.; Lazerges, M.; Lattach, Y.; Garnier, F.; Remita, S.; Pernelle, C. Molecularly imprinted conducting polymer based electrochemical sensor for detection of atrazine. *Anal. Chim. Acta* **2009**, *649*, 236–245.

51. Kanazawa, K. K.; Diaz, A. F.; Geiss, R. H.; Gill, W. D.; Kwak, J. F.; Logan, J. A.; Rabolt, J. F.; Street, G. B. "Organic metals": polypyrrole, a stable synthetic "metallic" polymer. *J. Chem. Soc. Chem. Commun.* **1979**, 854–855.

52. Abdulla, H. S.; Abbo, A. I. Optical and electrical properties of thin films of polyaniline and polypyrrole. *Int. J. Electrochem. Sci.* **2012**, *7*, 10666–10678.

53. Vorotyntsev, M. A.; Zinovyeva, V. A.; Konev, D. V Mechanisms of electropolymerization and redox activity: Fundamental aspects. In *Electropolymerization: Concepts, Materials and Applications*; Cosnier, S.; Karyakin, A., Eds.; Wiley-VCH Verlag GmbH & Co. KGaA, Weinheim, 2010; pp. 27–50.

54. Otero, T. F.; De Larreta, E. Electrochemical control of the morphology, adherence, appearance and growth of polypyrrole films. *Synth. Met.* **1988**, *26*, 79–88.

55. Hernández-Pérez, T.; Morales, M.; Batina, N.; Salmón, M. Effect of the electrosynthesis method on the surface morphology of the polypyrrole film An atomic force microscopy study. *J. Electrochem. Soc.* **2001**, *148*, C369–C375.

56. Sadki, S.; Schottland, P.; Brodie, N.; Sabouraud, G. The mechanisms of pyrrole electropolymerization. *Chem. Soc. Rev.* **2000**, *29*, 283–293.

57. Silk, T.; Hong, Q.; Tamm, J.; Compton, R. G. AFM studies of polypyrrole film surface morphology I. The influence of film thickness and dopant nature. *Synth. Met.* **1998**, *93*, 59–64.

58. Iseki, M.; Saito, K.; Kuhara, K.; Mizukami, A. Electrochemical exchange process of dopant anions in polypyrrole. *Synth. Met.* **1991**, *40*, 117–126.

59. Gelmi, A.; Higgins, M. J.; Wallace, G. G. Physical surface and electromechanical properties of doped polypyrrole biomaterials. *Biomaterials* **2010**, *31*, 1974–1983.

60. Kiani, M. S.; Mitchell, G. R. The role of the counter-ion in the preparation of polypyrrole films with enhanced properties using a pulsed electrochemical potential. *Synth. Met.* **1992**, *48*, 203–218.

61. Syritski, V.; Öpik, A.; Forsén, O. Ion transport investigations of polypyrroles doped with different anions by EQCM and CER techniques. *Electrochim. Acta* **2003**, *48*, 1409–1417.

62. Brie, M.; Turcu, R.; Mihut, A. Stability study of conducting polypyrrole films and polyvinylchloride-polypyrrole composites doped with different counterions. *Mater. Chem. Phys.* **1997**, *49*, 174–178.

63. Truong, V.-T.; Ennis, B. C.; Turner, T. G.; Jenden, C. M. Thermal stability of polypyrroles. *Polym. Int.* **1992**, *27*, 187–195.

64. Henne, A. L.; Fox, C. J. Ionization constants of fluorinated acids. *J. Am. Chem. Soc.* **1951**, *73*, 2323–2325.

65. Kuwabata, S.; Nakamura, J.; Yoneyama, H. The effect of basicity of dopant anions on the conductivity of polypyrrole films. *J. Chem. Soc. Chem. Commun.* **1988**, 779–780.

66. Satoh, M.; Kaneto, K.; Yoshino, K. Dependences of electrical and mechanical properties of conducting polypyrrole films on conditions of electrochemical polymerization in an aqueous medium. *Synth. Met.* 1986, *14*, 289–296.

67. Maddison, D. S.; Unsworth, J. Optimization of synthesis conditions of polypyrrole from aqueous solutions. *Synth. Met.* **1989**, *30*, 47–55.

68. Bufon, C. C. B.; Heinzel, T.; Espindola, P.; Heinze, J. Influence of the polymerization potential on the transport properties of polypyrrole films. *J. Phys. Chem. B* **2010**, *114*, 714–718.

69. Patois, T.; Lakard, B.; Monney, S.; Roizard, X.; Fievet, P. Characterization of the surface properties of polypyrrole films: Influence of electrodeposition parameters. *Synth. Met.* **2011**, *161*, 2498–2505.

70. Thompson, B. C.; Moulton, S. E.; Richardson, R. T.; Wallace, G. G. Effect of the dopant anion in polypyrrole on nerve growth and release of a neurotrophic protein. *Biomaterials* **2011**, *32*, 3822–3831.

71. Spurlock, L. D.; Jaramillo, A.; Praserthdam, A.; Lewis, J.; Brajter-Toth, A. Selectivity and sensitivity of ultrathin purine-templated overoxidized polypyrrole film electrodes. *Anal. Chim. Acta* **1996**, *336*, 37–46.

72. Malitesta, C.; Mazzotta, E.; Picca, R. A.; Poma, A.; Chianella, I.; Piletsky, S. A. MIP sensors - the electrochemical approach. *Anal. Bioanal. Chem.* **2012**, *402*, 1827–1846.

73. Tokonami, S.; Shiigi, H.; Nagaoka, T. Molecularly imprinted overoxidized polypyrrole films for sensor applications from enantiorecognition to trace analysis. In *Molecularly imprinted sensors: Overview and applications*; Li, S.; Ge, Y.; Piletsky, S. A.; Lunec, J., Eds.; Elsevier B.V., Oxford, Amsterdam, 2012; pp. 73–89.

74. Ebarvia, B. S.; Cabanilla, S.; Sevilla, F. Biomimetic properties and surface studies of a piezoelectric caffeine sensor based on electrosynthesized polypyrrole. *Talanta* **2005**, *66*, 145–152.

75. Choong, C.-L.; Bendall, J. S.; Milne, W. I. Carbon nanotube array: A new MIP platform. *Biosens. Bioelectron.* **2009**, *25*, 652–656.

76. Choong, C.-L.; Milne, W. I. Dynamic modulation of detection window in conducting polymer based biosensors. *Biosens. Bioelectron.* **2010**, *25*, 2384–2388.

77. Deore, B.; Chen, Z.; Nagaoka, T. Potential-induced enantioselective uptake of amino acid into molecularly imprinted overoxidized polypyrrole. *Anal. Chem.* **2000**, *72*, 3989–3994.

78. Shiigi, H.; Kijima, D.; Ikenaga, Y.; Hori, K.; Fukazawa, S.; Nagaoka, T. Molecular recognition for bile acids using a molecularly imprinted overoxidized polypyrrole film. *J. Electrochem. Soc.* **2005**, *152*, H129–H134.

79. Syritski, V.; Reut, J.; Menaker, A.; Gyurcsányi, R. E.; Öpik, A. Electrosynthesized molecularly imprinted polypyrrole films for enantioselective recognition of l-aspartic acid. *Electrochim. Acta* **2008**, *53*, 2729–2736.

80. Choi, S.-W.; Chang, H.-J.; Lee, N.; Chun, H. S. A surface plasmon resonance sensor for the detection of deoxynivalenol using a molecularly imprinted polymer. *Sensors* **2011**, *11*, 8654–8664.

81. Huang, W.-R.; Chen, Y.-L.; Lee, C.-Y.; Chiu, H.-T. Fabrication of gold/polypyrrole core/shell nanowires on a flexible substrate for molecular imprinted electrochemical sensors. *RSC Adv.* **2014**, *4*, 62393–62398.

82. Maouche, N.; Guergouri, M.; Gam-Derouich, S.; Jouini, M.; Nessark, B.; Chehimi, M. M. Molecularly imprinted polypyrrole films: Some key parameters for electrochemical picomolar detection of dopamine. *J. Electroanal. Chem.* **2012**, *685*, 21–27.

83. Sun, S.; Zhang, M.; Li, Y.; He, X. A molecularly imprinted polymer with incorporated graphene oxide for electrochemical determination of quercetin. *Sensors* **2013**, *13*, 5493–5506.

84. Radi, A.-E.; El-Naggar, A.-E.; Nassef, H. M. Determination of coccidiostat clopidol on an electropolymerized-molecularly imprinted polypyrrole polymer modified screen printed carbon electrode. *Anal. Methods* **2014**, *6*, 7967–7972.

85. Hrichi, H.; Louhaichi, M. R.; Monser, L.; Adhoum, N. Gliclazide voltammetric sensor based on electropolymerized molecularly imprinted polypyrrole film onto glassy carbon electrode. *Sensors Actuators B Chem.* **2014**, *204*, 42–49.

86. Tadi, K. K.; Motghare, R. V.; Ganesh, V. Electrochemical detection of sulfanilamide using pencil graphite electrode based on molecular imprinting technology. *Electroanalysis* **2014**, *26*, 2328–2336.

87. Turco, A.; Corvaglia, S.; Mazzotta, E. Electrochemical sensor for sulfadimethoxine based on molecularly imprinted polypyrrole: Study of imprinting parameters. *Biosens. Bioelectron.* **2015**, *63*, 240–247.

88. Apodaca, D. C.; Pernites, R. B.; Ponnapati, R. R.; Del Mundo, F. R.; Advincula, R. C. Electropolymerized molecularly imprinted polymer films of a bis-terthiophene dendron: folic acid quartz crystal microbalance sensing. *ACS Appl. Mater. Interfaces* **2011**, *3*, 191–203.

89. Kryscio, D. R.; Peppas, N. A. Critical review and perspective of macromolecularly imprinted polymers. *Acta Biomater.* **2012**, *8*, 461–473.

90. Antuña-Jiménez, D.; Díaz-Díaz, G.; Blanco-Lopéz, M. C.; Lobo-Castañón, M. J.; Miranda-Ordieres, A. J.; Tuñón-Blanco, P. Molecularly imprinted electrochemical sensors : Past, present and future. In *Molecularly imprinted sensors: Overview and applications*; Li, S.; Ge, Y.; Piletsky, S. A.; Lunec, J., Eds.; Elsevier, Oxford, 2012; pp. 1 – 34.

91. Ikariyama, Y.; Heineman, W. Polypyrrole electrode as a detector for electroinactive anions by flow injection analysis. *Anal. Chem.* **1986**, *58*, 1803–1806.

92. Ye, J.; Baldwin, R. Flow-injection analysis for electroinactive anions at a polyaniline electrode. *Anal. Chem.* **1988**, *60*, 1979–1982.

93. Ramanaviciene, A.; Finkelsteinas, A.; Ramanavicius, A. Molecularly imprinted polypyrrole for sensor design. *Mater. Sci.* **2004**, *10*, 18–23.

94. Ramanaviciene, A.; Ramanavicius, A. Molecularly imprinted polypyrrole-based synthetic receptor for direct detection of bovine leukemia virus glycoproteins. *Biosens. Bioelectron.* **2004**, *20*, 1076–1082.

95. Sauerbrey, G. Verwendung von Schwingquarzen zur Wägung dünner Schichten und zur Mikrowägung. *Zeitschrift für Phys.* **1959**, *155*, 206–222.

96. Cooper, M. A.; Singleton, V. T. A survey of the 2001 to 2005 quartz crystal microbalance biosensor literature: Applications of acoustic physics to the analysis of biomolecular interactions. *J. Mol. Recognit.* **2007**, *20*, 154–184.

97. Marx, K. A. Quartz crystal microbalance: A useful tool for studying thin polymer films and complex biomolecular systems at the solution-surface interface. *Biomacromolecules* **2003**, *4*, 1099–1120.

98. Mujahid, A.; Dickert, F. L. Molecularly imprinted polymers for sensors: Comparison of optical and mass-sensitive detection. In *Molecularly imprinted sensors: Overview and*

applications; Li, S.; Ge, Y.; Piletsky, S. A.; Lunec, J., Eds.; Elsevier B.V., Oxford, 2012; pp. 125–159.

99. Derry, C. J.; Derry, S.; Moore, R. A. Caffeine as an analgesic adjuvant for acute pain in adults. *Cochrane Database Syst. Rev.* **2014**, 1–62.

100. Buerge, I. J.; Poiger, T.; Müller, M. D.; Buser, H. R. Combined sewer overflows to surface waters detected by the anthropogenic marker caffeine. *Environ. Sci. Technol.* **2006**, *40*, 4096–4102.

101. Hillebrand, O.; Nödler, K.; Licha, T.; Sauter, M.; Geyer, T. Caffeine as an indicator for the quantification of untreated wastewater in karst systems. *Water Res.* **2012**, *46*, 395–402.

102. Švorc, L. Determination of caffeine: A comprehensive review on electrochemical methods. *Int. J. Electrochem. Sci.* **2013**, *8*, 5755–5773.

103. Jin, Y.; Row, K. H. Solid-phase extraction of caffeine and catechin compounds from green tea by caffeine molecular imprinted polymer. *Bull. Korean Chem. Soc.* **2007**, *28*, 276–280.

104. Farrington, K.; Magner, E.; Regan, F. Predicting the performance of molecularly imprinted polymers: Selective extraction of caffeine by molecularly imprinted solid phase extraction. *Anal. Chim. Acta* **2006**, *566*, 60–68.

105. Silvestri, D.; Barbani, N.; Cristallini, C.; Giusti, P.; Ciardelli, G. Molecularly imprinted membranes for an improved recognition of biomolecules in aqueous medium. *J. Memb. Sci.* **2006**, *282*, 284–295.

106. Liang, C.; Peng, H.; Bao, X.; Nie, L.; Yao, S. Study of a molecular imprinting polymer coated BAW bio-mimic sensor and its application to the determination of caffeine in human serum and urine. *Analyst* **1999**, *124*, 1781–1785.

107. Alizadeh, N.; Shamaeli, E. Electrochemically controlled release of anticancer drug methotrexate using nanostructured polypyrrole modified with cetylpyridinium: Release kinetics investigation. *Electrochim. Acta* **2014**, *130*, 488–496.

108. Ternes, T. A. Occurrence of drugs in German sewage treatment plants and rivers. *Water Res.* **1998**, *32*, 3245–3260.

109. Weigel, S.; Kuhlmann, J.; Hühnerfuss, H. Drugs and personal care products as ubiquitous pollutants: Occurrence and distribution of clofibric acid, caffeine and DEET in the North Sea. *Sci. Total Environ.* **2002**, *295*, 131–141.

110. Duan, Y.-P.; Meng, X.-Z.; Wen, Z.-H.; Ke, R.-H.; Chen, L. Multi-phase partitioning, ecological risk and fate of acidic pharmaceuticals in a wastewater receiving river: The role of colloids. *Sci. Total Environ.* **2013**, *447*, 267–273.

111. Emudianughe, T.; Caldwell, J.; Sinclair, K.; Smith, R. Species differences in the metabolic conjugation of clofibric acid and clofibrate in laboratory animals and man. *Drug Metab. Dispos.* **1983**, *11*, 97–102.

112. Zhang, Y.; Liu, Y.; Dai, C.; Zhou, X.; Liu, S. Adsorption of clofibric acid from aqueous solution by graphene oxide and the effect of environmental factors. *Water, Air, Soil Pollut.* **2014**, *225*, 2064.

113. Huang, D.-L.; Wang, R.-Z.; Liu, Y.-G.; Zeng, G.-M.; Lai, C.; Xu, P.; Lu, B.-A.; Xu, J.-J.; Wang, C.; Huang, C. Application of molecularly imprinted polymers in wastewater treatment: A review. *Environ. Sci. Pollut. Res. Int.* **2015**, *22*, 963–977.

114. Dai, C.-M.; Zhang, J.; Zhang, Y.-L.; Zhou, X.-F.; Duan, Y.-P.; Liu, S.-G. Selective removal of acidic pharmaceuticals from contaminated lake water using multi-templates molecularly imprinted polymer. *Chem. Eng. J.* **2012**, *211-212*, 302–309.

115. Dai, C.; Zhang, J.; Zhang, Y.; Zhou, X.; Liu, S. Application of molecularly imprinted polymers to selective removal of clofibric acid from water. *PLoS One* **2013**, *8*, e78167.

116. Dai, C.; Zhang, J.; Zhang, Y.; Zhou, X.; Duan, Y.; Liu, S. Removal of carbamazepine and clofibric acid from water using double templates-molecularly imprinted polymers. *Environ. Sci. Pollut. Res. Int.* **2013**, *20*, 5492–5501.

117. Zorita, S.; Boyd, B.; Jönsson, S.; Yilmaz, E.; Svensson, C.; Mathiasson, L.; Bergström, S. Selective determination of acidic pharmaceuticals in wastewater using molecularly imprinted solid-phase extraction. *Anal. Chim. Acta* **2008**, *626*, 147–154.

118. Ambrosi, A.; Antiochia, R.; Campanella, L.; Dragone, R.; Lavagnini, I. Electrochemical determination of pharmaceuticals in spiked water samples. *J. Hazard. Mater.* **2005**, *122*, 219–225.

119. Campanella, L.; Ambrosi, A.; Bellanti, F.; Tomassetti, M. Comparison between voltammetric and spectrophotometric methods for drug analysis. *Curr. Anal. Chem.* **2006**, *2*, 229–241.

120. Verma, H. R. X-Ray Photoelectron Spectroscopy. In *Atomic and Nuclear Analytical Methods*; Springer Berlin Heidelberg, 2007; pp. 213–241.

121. Yuan, Y.; Lee, T. R. Contact angle and wetting properties. In *Surface Science Techniques*; Bracco, G.; Holst, B., Eds.; Springer Series in Surface Sciences; Springer Berlin Heidelberg, 2013; Vol. 51, pp. 3–34.

122. Elimelech, M.; Chen, W.; Waypa, J. Measuring the zeta (electrokinetic) potential of reverse osmosis membranes by a streaming potential analyzer. *Desalination* **1994**, *95*, 269–286.

123. Werner, C.; Körber, H.; Zimmermann, R.; Dukhin, S.; Jacobasch, H.-J. Extended electrokinetic characterization of flat solid surfaces. *J. Colloid Interface Sci.* **1998**, *208*, 329–346.

124. Ebarvia, B. S.; Binag, C. A.; Sevilla, F. Biomimetic piezoelectric quartz sensor for caffeine based on a molecularly imprinted polymer. *Anal. Bioanal. Chem.* **2004**, *378*, 1331–1337.

125. Higgins, M. J.; McGovern, S. T.; Wallace, G. G. Visualizing dynamic actuation of ultrathin polypyrrole films. *Langmuir* **2009**, *25*, 3627–3633.

126. Luo, Y.; Guo, W.; Ngo, H. H.; Nghiem, L. D.; Hai, F. I.; Zhang, J.; Liang, S. A review on the occurrence of micropollutants in the aquatic environment and their fate and removal during wastewater treatment. *Sci. Total Environ.* **2014**, *473-474*, 619–641.

127. *QTools Quick Start Guide*; Q-Sense, Biolin Scientific AB, 2006.

128. Zaid, B.; Aeiyach, S.; Lacaze, P. C. Electropolymerization of pyrrole in propylene carbonate on zinc electrodes modified by heteropolyanions. *Synth. Met.* **1994**, *65*, 27–34.

129. Struzzi, C.; Erbahar, D.; Scardamaglia, M.; Amati, M.; Gregoratti, L.; Lagos, M. J.; Van Tendeloo, G.; Snyders, R.; Ewels, C.; Bittencourt, C. Selective decoration of isolated carbon nanotubes by potassium evaporation: Scanning photoemission microscopy and density functional theory. *J. Mater. Chem. C* **2015**, *3*, 2518–2527.

130. Idla, K.; Talo, A.; Niemi, H.; Forsén, O.; Yläsaari, S. An XPS and AFM study of polypyrrole coating on mild steel. *Surf. Interface Anal.* **1997**, *25*, 837–854.

131. Atanasoska, L.; Naoi, K.; Smyrl, W. H. XPS studies on conducting polymers: Polypyrrole films doped with perchlorate and polymeric anions. *Chem. Mater.* **1992**, *4*, 988–994.

132. Bose, C.; Basak, S.; Rajeshwar, K. Electrochemistry of poly(pyrrole chloride) films: A study of polymerization efficiency, ion transport during redox and doping level assay by electrochemical quartz crystal microgravimetry, pH, and ion-selective electrode measurements. *J. Phys. Chem.* **1992**, *96*, 9899–9906.

133. Nabid, M. R.; Entezami, A. A. A novel method for synthesis of water-soluble polypyrrole with horseradish peroxidase enzyme. *J. Appl. Polym. Sci.* **2004**, *94*, 254–258.

134. Löffler, D.; Römbke, J.; Meller, M.; Ternes, T. A. Environmental fate of pharmaceuticals in water/sediment systems. *Environ. Sci. Technol.* **2005**, *39*, 5209–5218.

135. Scheytt, T.; Mersmann, P.; Lindstädt, R.; Heberer, T. 1-Octanol/water partition coefficients of 5 pharmaceuticals from human medical care: carbamazepine, clofibric acid, diclofenac, ibuprofen, and propyphenazone. *Water. Air. Soil Pollut.* **2005**, *165*, 3–11.

136. Ryan, E. M.; Breslin, C. B.; Moulton, S. E.; Wallace, G. G. The effect of dopant pKa and the solubility of corresponding acid on the electropolymerisation of pyrrole. *Electrochim. Acta* **2013**, *92*, 276–284.

137. Dwivedi, P.; Matz, L. M.; Atkinson, D. A.; Hill, H. H. Electrospray ionization-ion mobility spectrometry: A rapid analytical method for aqueous nitrate and nitrite analysis. *Analyst* **2004**, *129*, 139–144.

138. Ratautaite, V.; Plausinaitis, D.; Baleviciute, I.; Mikoliunaite, L.; Ramanaviciene, A.; Ramanavicius, A. Characterization of caffeine-imprinted polypyrrole by a quartz crystal microbalance and electrochemical impedance spectroscopy. *Sensors Actuators B Chem.* **2015**, *212*, 63–71.

139. Özcan, L.; Şahin, Y. Determination of paracetamol based on electropolymerized-molecularly imprinted polypyrrole modified pencil graphite electrode. *Sensors Actuators B Chem.* **2007**, *127*, 362–369.

140. Gelmi, A.; Higgins, M. J.; Wallace, G. G. Physical surface and electromechanical properties of doped polypyrrole biomaterials. *Biomaterials* **2010**, *31*, 1974–1983.

141. Pernites, R.; Ponnapati, R.; Felipe, M. J.; Advincula, R. Electropolymerization molecularly imprinted polymer (E-MIP) SPR sensing of drug molecules: pre-polymerization complexed terthiophene and carbazole electroactive monomers. *Biosens. Bioelectron.* **2011**, *26*, 2766–71.

142. Apodaca, D. C.; Pernites, R. B.; Ponnapati, R.; Del Mundo, F. R.; Advincula, R. C. Electropolymerized molecularly imprinted polymer film: EIS sensing of bisphenol A. *Macromolecules* **2011**, *44*, 6669–6682.

143. Zhang, X.; Bai, R. Surface electric properties of polypyrrole in aqueous solutions. *Langmuir* **2003**, *19*, 10703–10709.

144. Zaid, B.; Aeiyach, S.; Lacaze, P. Electropolymerization of pyrrole in propylene carbonate on zinc electrodes modified by heteropolyanions. *Synth. Met.* **1994**, *65*, 27–34.

145. Inganäs, O.; Erlandsson, R.; Nylander, C.; Lundström, I. Proton modification of conducting polypyrrole. *J. Phys. Chem. Solids* **1984**, *45*, 427–432.

146. Skotheim, T. A.; Florit, M. I.; Melo, A.; O'Grady, W. E. Ultrahigh-vacuum in situ electrochemistry with solid polymer electrolyte and x-ray photoelectron spectroscopy studies of polypyrrole. *Phys. Rev. B* **1984**, *30*, 4846–4849.

147. Maksymiuk, K. Chemical reactivity of polypyrrole and its relevance to polypyrrole based electrochemical sensors. *Electroanalysis* **2006**, *18*, 1537–1551.

148. Ge, D.; Tian, X.; Qi, R.; Huang, S.; Mu, J.; Hong, S.; Ye, S.; Zhang, X.; Li, D.; Shi, W. A polypyrrole-based microchip for controlled drug release. *Electrochim. Acta* **2009**, *55*, 271–275.

149. Shamaeli, E.; Alizadeh, N. Kinetic studies of electrochemically controlled release of salicylate from nanostructure conducting molecularly imprinted polymer. *Electrochim. Acta* **2013**, *114*, 409–415.

150. Svirskis, D.; Wright, B. E.; Travas-Sejdic, J.; Rodgers, A.; Garg, S. Evaluation of physical properties and performance over time of an actuating polypyrrole based drug delivery system. *Sensors Actuators B Chem.* **2010**, *151*, 97–102.

151. Dong, H.; Li, C. M.; Chen, W.; Zhou, Q.; Zeng, Z. X.; Luong, J. H. T. Sensitive amperometric immunosensing using polypyrrolepropylic acid films for biomolecule immobilization. *Anal. Chem.* **2006**, *78*, 7424–7431.

152. Dong, H.; Cao, X.; Li, C. M.; Hu, W. An in situ electrochemical surface plasmon resonance immunosensor with polypyrrole propylic acid film: Comparison between SPR and

electrochemical responses from polymer formation to protein immunosensing. *Biosens. Bioelectron.* **2008**, *23*, 1055–1062.

153. Serafín, V.; Agüí, L.; Yáñez-Sedeño, P.; Pingarrón, J. M. Electrochemical immunosensor for the determination of insulin-like growth factor-1 using electrodes modified with carbon nanotubes-poly(pyrrole propionic acid) hybrids. *Biosens. Bioelectron.* **2014**, *52*, 98–104.

154. Grimshaw, J.; Perara, S. D. Redox behaviour of polypyrrole films containing naphthoquinone and benzoquinone groups. *J. Electroanal. Chem. Interfacial Electrochem.* **1990**, *281*, 125–132.

155. Fabre, B.; Ababou-Girard, S.; Solal, F. Covalent integration of pyrrolyl units with modified monocrystalline silicon surfaces for macroscale and sub-200 nm-scale localized electropolymerization reactions. *J. Mater. Chem.* **2005**, *15*, 2575–2582.

156. Livache, T.; Roget, A.; Dejean, E.; Barthet, C.; Bidan, G.; Téoule, R. Preparation of a DNA matrix via an electrochemically directed copolymerization of pyrrole and oligonucleotides bearing a pyrrole group. *Nucleic Acids Res.* **1994**, *22*, 2915–2921.

157. Fatnassi, M.; Es-Souni, M. Nanoscale phase separation in laponite-polypyrrole nanocomposites. Application to electrodes for energy storage. *RSC Adv.* **2015**, *5*, 21550–21557.

8 Appendix

8.1 List of abbreviations

2,4-D	2,4-dichlorophenoxyacetic acid
IGF1	Anti insulin-like growth factor 1
IgG	Anti-mouse immunoglobulin G
AFM	Atomic force microscopy
gp51	Bovine leukemia virus glycoproteine
CBZ	Carbamazepine
CS	Chondroitin sulfate A
Cf	Clofibric acid
CYV	Cyclic voltammetry
CV	Cyclic voltammogram
C	Cyclovoltammetric cycles
Da	Dalton
DPV	Differential pulse voltammetry
DMSO	Dimethylsulfoxide
DBS	Dodecylbenzenesulfonate
EtOH	Ethanol
Fig.	Figure
F	Harmonics
HA	Hyaluronic acid
HCl	Hydrochloric acid
$FeCl_3$	Iron(III) chloride
LSP	Linear scanning polarography
$LiClO_4$	Lithium perchlorate
MeOH	Methanol
min	Minute
MIP	Molecularly imprinted polymer
NIP	Non-imprinted polymer
PES	Phenoxyacetic acid
PBS	Phosphate buffer solution
PMAS	Poly(2-methoxyaniline-5-sulfonic acid)
PTFE	Polytetrafluoroethylene

PSS	Poly(4-styrenesulfonate)
KCl	Potassium chloride
KNO_3	Potassium nitrate
PAD	Pulsed amperometric detection
Py	Pyrrole
PPA	Pyrrole propionic acid
QCM	Quartz crystal microbalance
rms	Root mean square
SEM	Scanning electron microscope
Ag	Silver
$AgNO_3$	Silvernitrate
Na-pTS	Sodium p-toluenesulfonate
pTS	p-Toluenesulfonate
XPS	X-ray photoelectron spectroscopy

8.2 List of figures

8.3 List of tables

8.4 Supplementary data

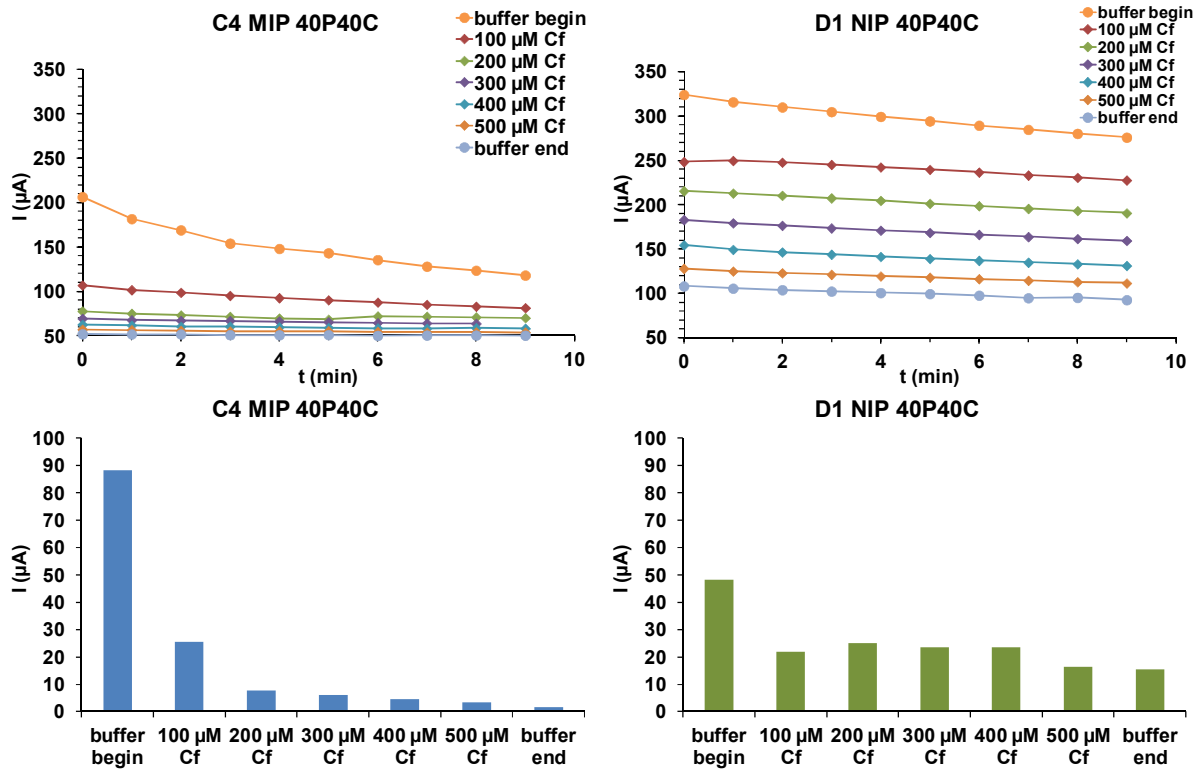

Fig. S 1: PAD current response and sensor response of MIP and NIP prepared with 40 mM pyrrole and 40 cycles to 100–500 µM clofibric acid solutions.

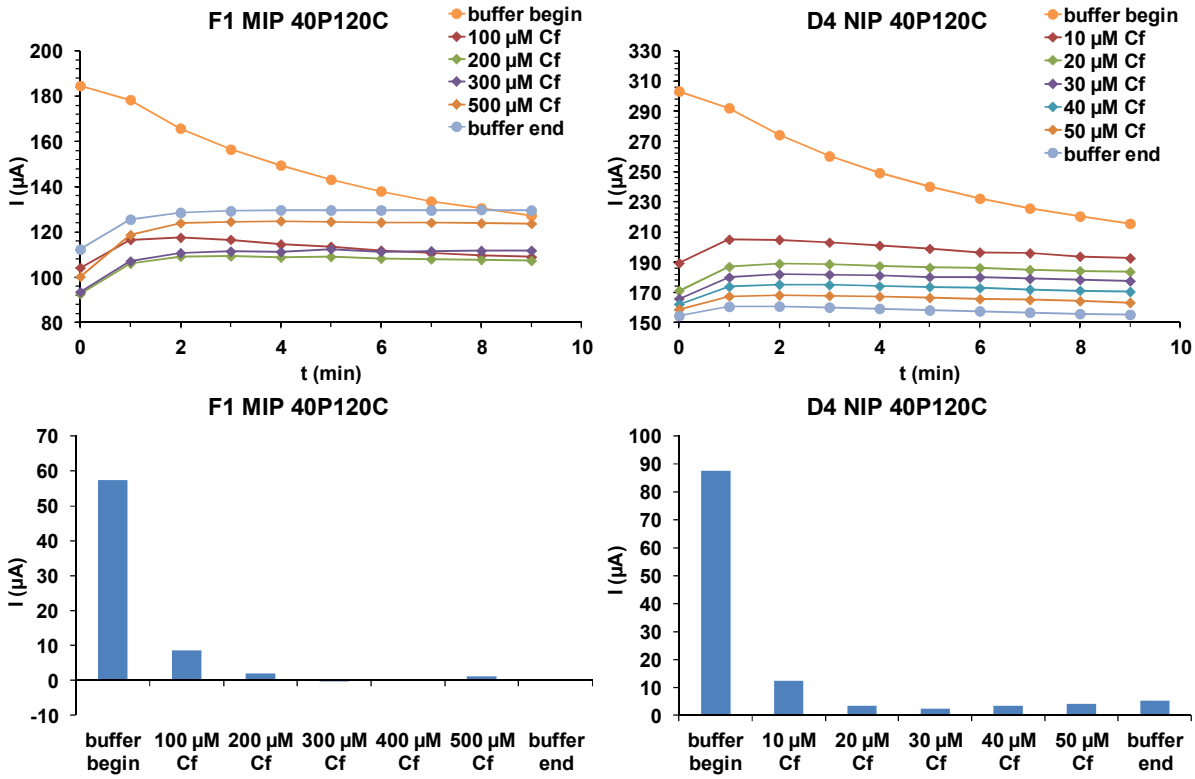

Fig. S 2: PAD current response and sensor response of MIP and NIP prepared with 40 mM pyrrole and 120 cycles to 100–500 µM clofibric acid (MIP) and 10–50 µM clofibric acid (NIP).

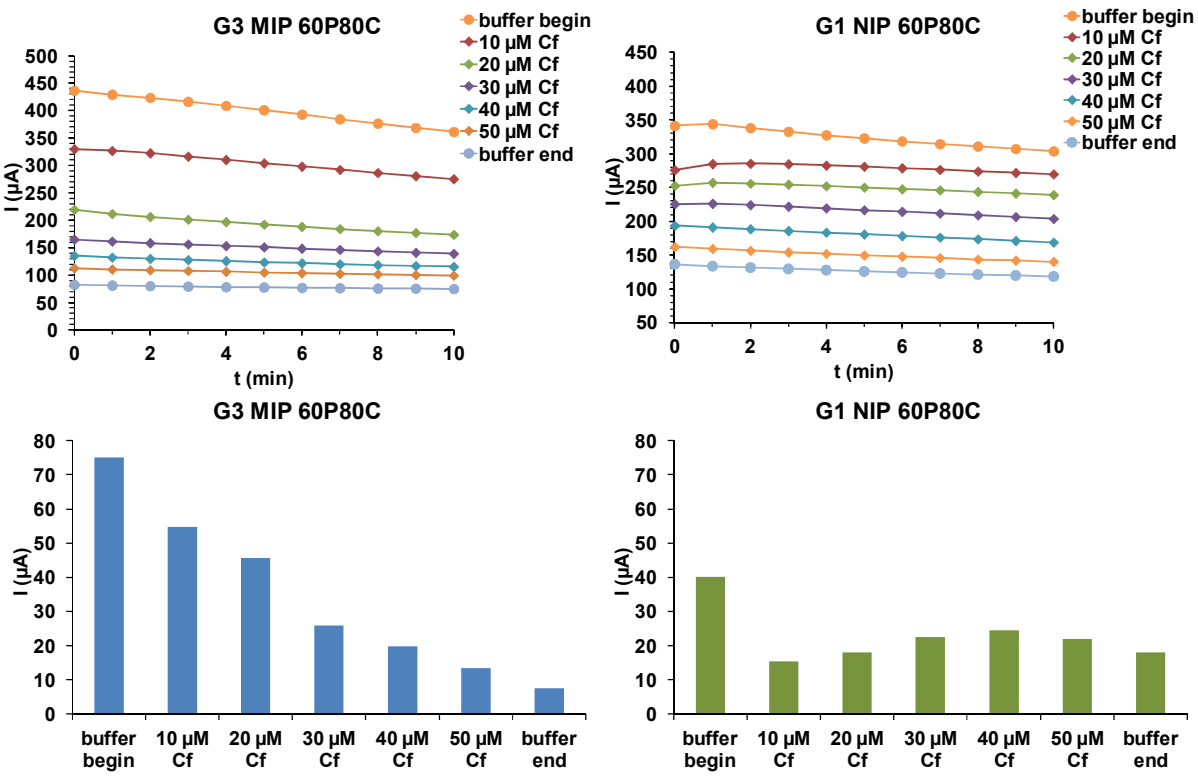

Fig. S 3: PAD current response and sensor response of MIP and NIP prepared with 60 mM pyrrole and 80 cycles to 10–50 µM clofibric acid solutions.

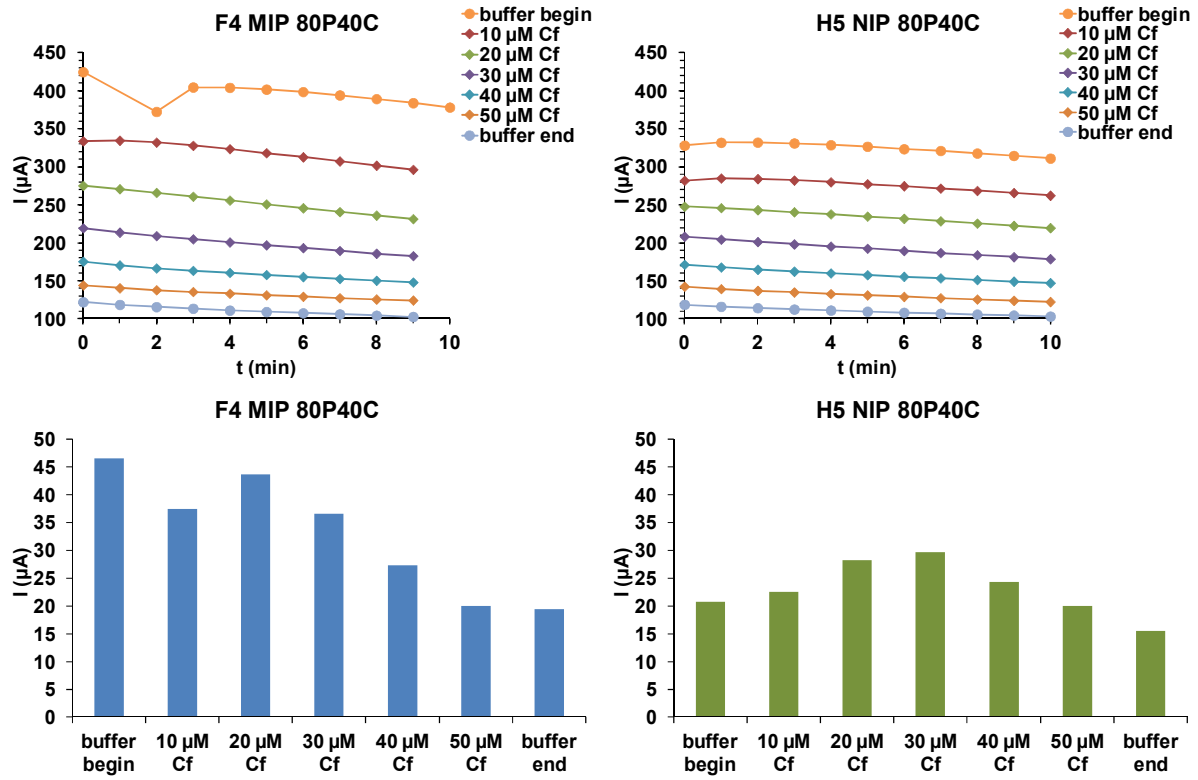

Fig. S 4: PAD current response and sensor response of MIP and NIP prepared with 80 mM pyrrole and 40 cycles to 10–50 µM clofibric acid solutions.

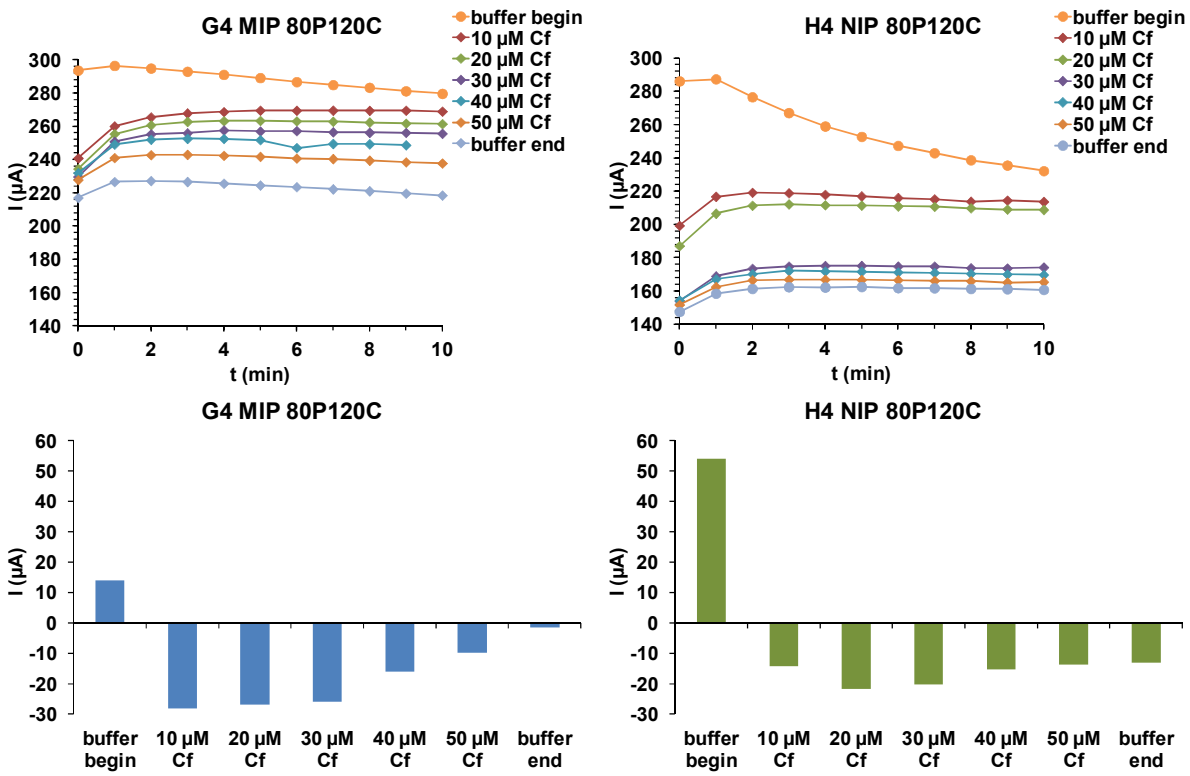

Fig. S 5:PAD current response and sensor response of MIP and NIP prepared with 80 mM pyrrole and 120 cycles to 10–50 µM clofibric acid solutions.

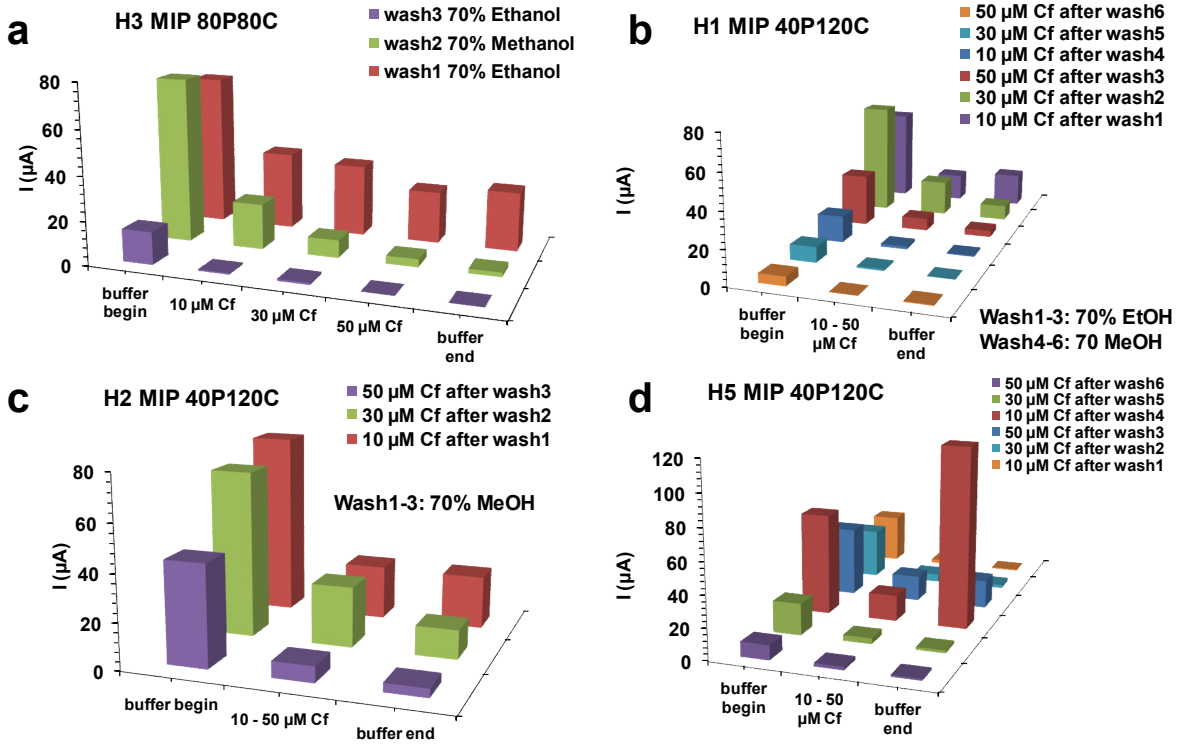

Fig. S 6: (a) PAD sensor response of sensor H3 (MIP 80P 80C) after washing with 70% ethanol and 70% methanol (30 min); (b) H1 (MIP 40P 120C) after washing with 70% ethanol and 70% methanol (30 min); (c) H2 (MIP 40P 120C) after washing with 70% methanol (30 min); (d) H5 (MIP 40P 120C) after washing with 70% ethanol (10 min).

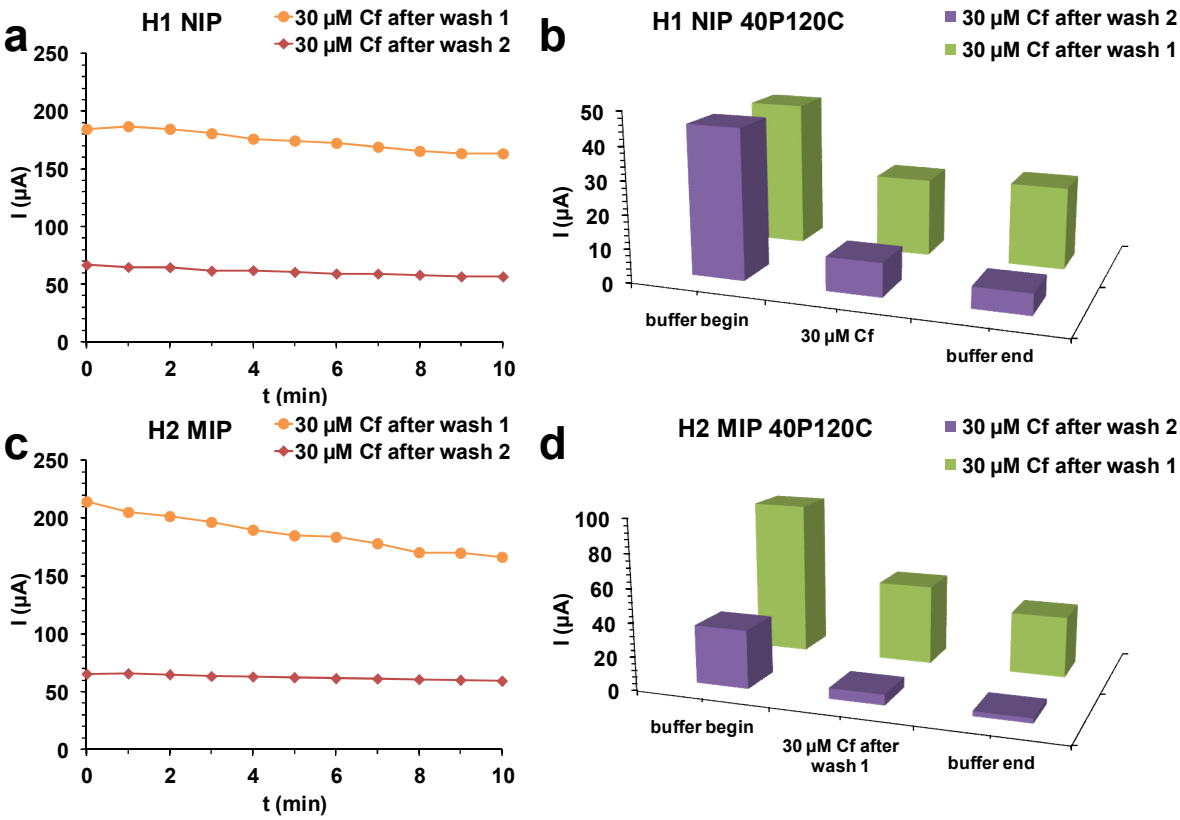

Fig. S 7: I values (a),(c) and PAD sensor response (b),(d) after PAD wash of MIP H2 and NIP H1.

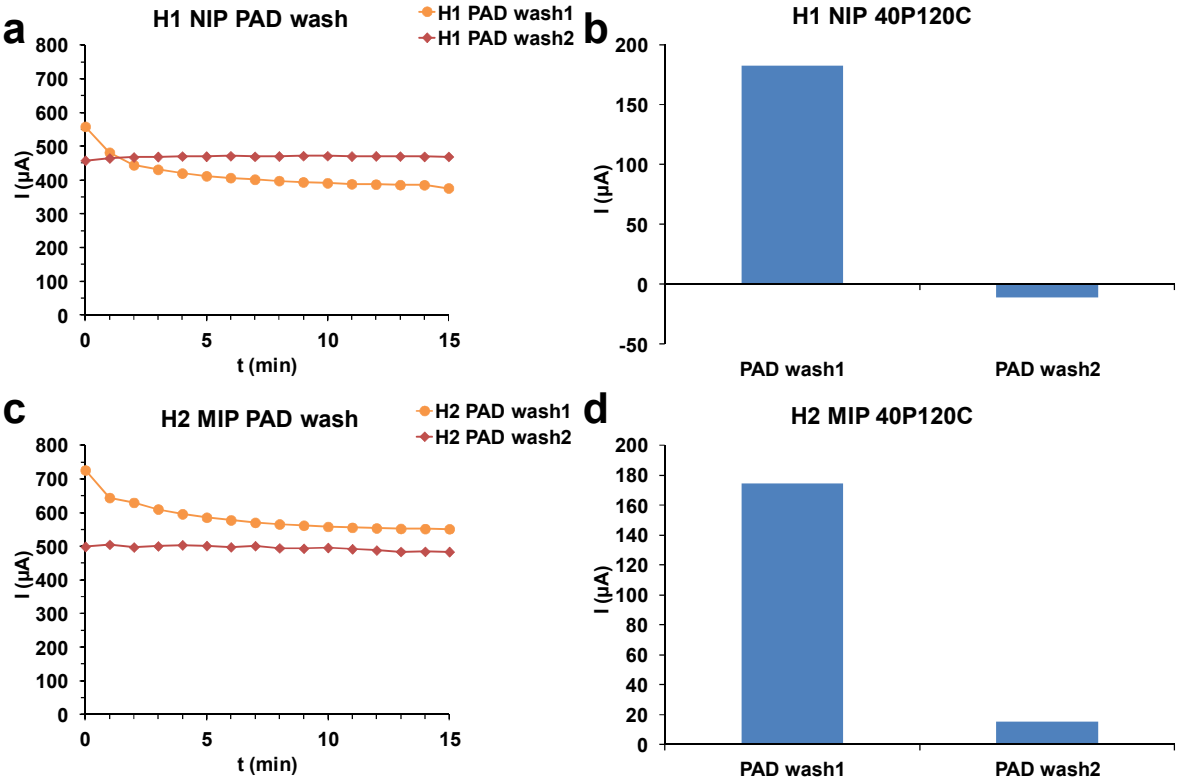

Fig. S 8: PAD washing of NIP H1 and MIP H2 (pulse time 1 s).

8.5 Publications

8.5.1 Refereed publications

Parts of this thesis had been published in:

- Schweiger, B, Kim, J., Kim, Y.J., Ulbricht, M. Electropolymerized molecularly imprinted polypyrrole film for sensing of clofibric acid, *Sensors*, **2015**, *15*, 4870-4889.

Publications from previous works:

- Krause, H., Schweiger, B., Prinz, E., Kim, J., Steinfeld, U. Degradation of persistent pharmaceuticals in aqueous solutions by a positive dielectric barrier discharge treatment, *Journal of Electrostatics*, ***2011***, *69*, 333–338.

- Krause, H., Schweiger, B., Schuhmacher, J., Scholl, S., Steinfeld, U. Degradation of the endocrine disrupting chemicals (EDCs) carbamazepine, clofibric acid, and iopromide by corona discharge over water, *Chemosphere*, **2009**, *75*, 163-168.

- Schweiger, B., Hansen, H.P., Bange, H.W. A time series of hydroxylamine (NH_2OH) in the southwestern Baltic Sea, *Geophysical Research. Letters,* **2007**, *34*, L24608.

8.5.2 Conference proceedings

- Schweiger, B., Bahnweg, L., Palm, B., Steinfeld, U. Development of molecular imprinted polymers (MIPs) for the selective removal of carbamazepine from aqueous solution, *Proceedings of the World Academy of Science, Engineering and Technology* **2009**, *54*, 661-666.

8.6 Lebenslauf

Der Lebenslauf ist in der Online-Version aus Gründen des Datenschutzes nicht enthalten.

8.7 Erklärung (Declaration)

Hiermit versichere ich, dass ich die vorliegende Arbeit mit dem Titel

„Molecular imprinting of polypyrrole for electrochemical sensing of clofibric acid"

selbst verfasst und keine außer den angegebenen Hilfsmitteln und Quellen benutzt habe, und dass die Arbeit in dieser oder ähnlicher Form noch bei keiner anderen Universität eingereicht wurde.

Saarbrücken, im Oktober 2015

8.8 Acknowledgements

First and foremost, I want to thank Prof. Dr. Mathias Ulbricht for his willingness to supervise this work. His dedicated support and the continuous encouragement with many helpful discussions contributed to the completion of this dissertation.

I want to thank Prof. Dr. Torsten C. Schmidt for accepting the position of second reviewer.

I gratefully thank KIST Europe and Prof. Dr. Kwang Ho Kim, Prof. Dr. Ho Seong Lee, Dr. Kuiwon Choi, and Prof. Dr. Andreas Manz for their financial and technical support which made this work possible. Especially I want to thank Dr. Jungtae Kim for his support in devising and conducting the project as well as Dr. Chang Hoon Nam, Dr. Myung Hee Jung, Dr. Sanghun Kim, and Dr. Young Jun Kim for supporting the continuation of this work and for the provision of funds.

Special thanks go to the people of the Department of Technical Chemistry II of the University of Duisburg-Essen, who supported me during my stay there, especially Inge Danielzik, Tobias Kallweit, Claudia Schenk, and Roswitha Nordmann-Silberg for their always friendly organizational and technical support, Mathias Quilitzsch for the introduction to the contact angle device and ellipsometry, Anne Vaterrodt and Ibrahim Elsherbiny for sharing their zeta potential measurement time, and Hanna Thierfeld, Sarah Walter, and Dr. Alexandra Wittmar for sharing their office with me.

I want to thank Dr. Jae Pyoung Ahn of the Advanced Analysis Center of KIST (Seoul), Dr. Michael Bruns of the Karlsruhe Nano Micro Facility (Forschungszentrum Karlsruhe, Institute for Applied Materials), and Dr. Frank Müller of the Department of Experimental Physics of the Saarland University for XPS measurements and Klaus Pärschke of the Department of Physics of the University Duisburg-Essen for ellipsometry measurements.

Many thanks go to the members of KIST Europe, especially to my colleagues Ruth Eggers, Dr. Nuriye Korkmaz, Holger Krause, Michael Müller, Carsten Brill, Neha Agarwal, Ralf Wilhelm, Andre-René Blaudszun, Michelle Seif, and Daniela Vanni-Strassner for the technical and instrumental support, fruitful discussions, and the friendly working atmosphere.

감사합니다 to Jang Mi, Sun Woo Moon, Yohan Yu and all choir members for the pleasant memories and the insight into korean language and culture.

Last but not least, I want to thank my friends and my family for their support and understanding.